General Disclaimer

One or more of the Following Statements may affect this Document

- This document has been reproduced from the best copy furnished by the organizational source. It is being released in the interest of making available as much information as possible.

- This document may contain data, which exceeds the sheet parameters. It was furnished in this condition by the organizational source and is the best copy available.

- This document may contain tone-on-tone or color graphs, charts and/or pictures, which have been reproduced in black and white.

- This document is paginated as submitted by the original source.

- Portions of this document are not fully legible due to the historical nature of some of the material. However, it is the best reproduction available from the original submission.

Nasa-CR-167893

CONTRACT NO. NAS3-22139

(NASA-CR-167893) HIGH ACCURACY FUEL FLOWMETER, PHASE 1 Final Report (General Electric Co.) 156 p HC A08/MF A01 CSCL 14B

N83-21314

Unclas

G3/35 03162

HIGH ACCURACY FUEL FLOWMETER

PHASE I – FINAL REPORT

Prepared For
National Aeronautics & Space Administration
Lewis Research Center
21,000 Brookpark Road Cleveland, OH 44135

GENERAL ELECTRIC

AIRCRAFT INSTRUMENTS DEPARTMENT

WILMINGTON, MA 01887

1. Report No. CR 167893	2. Government Accession No.	3. Recipient's Catalog No.
4. Title and Subtitle High Accuracy Fuel Flowmeter		5. Report Date MARCH 1983 6. Performing Organization Code
7. Author(s) Christopher Mayer, Len Rose, Alan Chan, Bock Chin, William Gregory		8. Performing Organization Report No. 10. Work Unit No.
9. Performing Organization Name and Address General Electric Co., AID 50 Fordham Road, Wilmington, MA		11. Contract or Grant No. NAS3-22139
12. Sponsoring Agency Name and Address National Aeronautics and Space Administration Washington, D.C. 20546		13. Type of Report and Period Covered CONTRACTOR REPORT 14. Sponsoring Agency Code 505-31-54

15. Supplementary Notes

Final Report, Phase I, Project Manager, Howard F. Hobart, NASA Lewis Research Center, Cleveland, OH 44135

16. Abstract Technology related to aircraft fuel mass - flowmeters was comprehensively reviewed to determine what flowmeter types could provide 0.25%-of-point accuracy over a 50 to one range in flowrates. Three types were selected and were further analyzed to determine what problem areas prevented them from meeting the high accuracy requirement, and what the further development needs were for each. A dual-turbine volumetric flowmeter with densi-viscometer and microprocessor compensation was selected for its relative simplicity and fast response time.

An angular momentum type with a motor-driven, spring-restrained turbine and viscosity shroud was selected for its direct mass-flow output. This concept also employed a turbine for fast response and a microcomputer for accurate viscosity compensation.

The third concept employed a vortex precession volumetric flowmeter and was selected for its unobtrusive design. Like the turbine flowmeter, it uses a densi-viscometer and microprocessor for density correction and accurate viscosity compensation.

17. Key Words (Suggested by Author(s))	18. Distribution Statement
High Accuracy, Fuel Flowmeter Turbine, Angular Momentum, Vortex Precession, Densitometer, Viscometer, Microcomputer	Unclassified - Unlimited

19. Security Classif. (of this report)	20. Security Classif. (of this page)	21. No. of Pages	22. Price*
Unclassified	Unclassified	147	

* For sale by the National Technical Information Service, Springfield, Virginia 22161

FOREWARD

The authors wish to acknowledge the technical contributions of W. B. Giles of the General Electric Corporate Research and Development laboratory in Schenectady, New York, relative to operation of the vortex precession flow meter.

S. W. Tehon of the General Electric Electronics laboratory in Syracuse, New York, provided the technical analysis of ultrasonic flow measurement techniques.

R. A. Pfuntner provided the technical analysis of the closed loop angular momentum flow measurement technique.

Optical techniques of flow measurement were analyzed by J. W. Wyler of the Aircraft Instrument Department of General Electric.

Professors A. Ferron and W. Durgin of the Alden Hydraulic Laboratory in Holden, Massachusetts provided technical inputs on flow measurement techniques in general, as did K. Benson of the National Bureau of Standards in Washington, D. C.

TABLE OF CONTENTS

TABLE OF CONTENTS

LIST OF FIGURES

LIST OF FIGURES

LIST OF FIGURES

LIST OF TABLES

1.0 SUMMARY

This report concludes the Phase I effort of NASA contract NAS3-22139 to develop a high accuracy fuel flowmeter. The following tasks were completed:

- o Study and selection of methods of flow measurement.
- o Preliminary analysis of all flight worthy methods.
- o Rating of methods.
- o Review and selection of most promising methods.
- o Detailed analysis of three selected methods.
- o Preliminary conceptual designs of three selected methods.

The study and selection of methods of flow measurement consisted of comprehensive patent and literature searches, consultation with experts and brainstorming sessions. Over 1000 abstracts and over 750 patents were reviewed. Preliminary analysis of all methods indicated that the following concepts might be viable in an aircraft environment:

- Closed Loop Angular Momentum
- Open Loop Angular Momentum
- Double Turbine with Densitometer/Viscometer
- Vortex Precession with Densitometer/Viscometer

These four concepts were then subjected to a comprehensive rating. Nineteen parameters of performance were evaluated on a zero-to-ten scale, weighted and summed. The four concepts rated 596, 693, 805, 748 in the order listed above. The closed-loop angular momentum concept had the lowest rating and was dropped from further consideration.

The detailed performance analysis of the three selected methods concentrated on accuracy, time response, pressure drop and package size with the objective of defining problem areas which need further investigation (Phase II work). Since the double turbine and vortex precession flowmeters are volumetric and require density and viscosity compensation, a complete analysis was conducted on an oscillatory type densitometer/viscometer. All three flowmeters require a microcomputer for compensation of temperature sensitivity (except angular momentum) and Reynolds number dependence. Conceptual designs of each flowmeter are presented which identify initial selections of materials, sensors and part sizes.

Separate sections of this report summarize the expected uncertainy of each of the flowmeter systems and explain the sources of error. The following RSS estimates were obtained (% of flow rate):

- Angular Momentum ±0.23
- Double Turbine ±0.18 to ±0.28
- Vortex Precession ±0.23

These estimates exclude calibration stand errors which at this time are unknown.

And finally, the problem areas uncovered in the analysis and conceptual design tasks that may prevent the flowmeter from meeting the design specifications are summarized for each flowmeter system. Investigation of these problem areas is to be continued in Phase II of the development contract.

2.0 INTRODUCTION

Precision flight-type fuel flowmeters are needed to make accurate measurements of engine fuel consumption under flight conditions. At the present time much effort is being focused on improving engine and airframe components which have a direct effect on fuel consumption. Component improvements that result in fuel consumption improvements of only a few tenths of a percent, although costly to implement, have been shown to produce significant net savings over engine and/or airframe life cycles. However, the ability to accurately measure such small changes in fuel consumption during short duration flight tests is presently beyond the state of the art.

Precision fuel flowmeters also have application in computerized systems for minimizing fuel consumption during a given flight mission. In additon, future engine control systems can potentially be improved by the direct and precise measurement of fuel mass flow rate.

To a lesser degree there is a need to improve the accuracy of determination of fuel mass remaining in order to reach a desired gross weight at a particular point in a flight mission. Totalizing is also required for center-of-gravity adjustments in flight. Near real-time data processing is a requirement for the last two applications.

The work statement consisted of eight separate tasks, providing a methodical and controlled approach to the development of a high accuracy flowmeter. In brief, the tasks were as follows:

Task 1 - Study And Selection Of Methods - Study the methods of measuring the mass flow rates of fuels and compile a list of potential methods that are suited for in flight use. The approach included a literature search of flow measuring instrumentation including commercially available equipment, devising conceptual ideas that lend themselves to the development of a prototype meter and consulation with recognized authorities in the field of flow measurement.

Task 2 - Preliminary Analysis Of All Methods - Perform a preliminary analysis of the methods selected in Task 1 with consideration of potential accuracy, size, weight, response time, vibration and attitude sensitivity, safety and cost.

Task 3 - Rating Of Methods - Devise a rating system and apply it to the flowmeters analyzed in Task 2. Applied weighting coefficients to performance parameters of each concept to indicate those having the greatest potential for development and for meeting the design criteria.

Task 4 - Review And Selection Of Most Promising Methods - Conduct a review at NASA facilities of Tasks 1, 2 and 3 and in conjunction with NASA, select three methods of flow measurement for further analysis and design (Tasks 5 and 6).

Task 5 - Detailed Analysis Of Selected Methods - Perform detailed analyses of the three methods selected in Task 4. The primary considerations in the analysis are accuracy, definition of problems in meeting requirements and definition of experiments to rectify the problems.

Task 6 - Preliminary Designs Based On Selected Methods - Prepare preliminary designs of the three selected methods, including drawings, materials, weight, input power requirements, output signals, special piping sections and wiring diagrams.

Task 7 - Briefing - Conducted a one day oral briefing at NASA facilities with detailed discussions of Tasks 5 and 6.

Task 8 - Reporting Requirements - Technical financial and schedular reporting, including this report were required.

Tasks 1, 2 and 3 are covered in Section 3.0 of this report while Tasks 5 and 6 are covered in Sections 4.0 through 8.0.

Each of the three methods studied in detail is evaluated for accuracy on a common basis: the value of each contributing error source is an estimate of two standard deviations of the random error only; no bias is included in the estimate. Biases and random error between the calibration stand and true flow rate are not included.

The various interface electronics needed to drive turbine speed pick-offs, vortex sensors, spring windup sensors and temperature sensors are presented in one section and provide a basis for initial estimates of input power, package volume and overall feasibility.

A unique approach is presented whereby both precise density and approximate viscosity data are obtained from a single sensor element. Theory and expectations of the densitometer/viscometer are explored via equivalent electric circuit analysis.

All three systems require a microcomputer to compensate for Reynolds number dependencies and temperature effects, and to calculate density and mass flow rate where a densitometer is involved. The microcomputer is naturally suited to the job since most inputs are of time-based origin (i.e., frequency or time difference). A preliminary microcomputer design is presented, along with details of custom interface circuits, power requirements and package volume estimates.

3.0 STUDY AND SELECTION OF MOST PROMISING METHODS

This section is a brief review of the survey, preliminary analysis and rating method of flowmeter technologies and leads to the selection of the three concepts which are then studied in detail in sections 4 through 7.

3.1 Technology Survey -

General Electric conducted a comprehensive study of methods for measuring mass flow rates of fuels and compiled a list of those methods having potential for flight use. Table 1 details all of the sources of information encompassed by the investigation: literature and patent searches; brainstorming sessions; consultation with experts.

Determination of the potential of a particular technology for flight use was based on the criteria set forth in the design guidelines and specifications which are summarized in Table 2 and included in full in Appendix 10.1. The main goal of the program is to achieve accuracy within $\pm$ 0.25% of rate over a 50:1 flow range.

The flowmeter concepts considered for flight use are listed in Appendix 10.2 and are catagorized into either "true" mass flowmeters or volumetric flowmeters, the latter type being differentiated by the need for independent density measurement to obtain mass flow rate. Because there are a considerable number of volumetric technologies, densitometer concepts were subjected to the same rigorous survey and evaluation and are listed separately. Furthermore, many of the true mass and volumetric flowmeters exhibit calibration characteristics that are a regular function of Reynolds number. To achieve the desired accuracy, these flowmeters require a viscosity measurement from which Reynolds number and compensation can be calculated. Therefore, viscosity measurement concepts are also covered in appendix 10.2.

TABLE 1

INFORMATION SOURCES

1. Literature Search
   General Electric Electronics Park Library
   Syracuse, New York

   Search of Data Bases (Commercial)

   a. NTIS - Government Research Reports
   b. Compendex - Engineering Index
   c. Inspec - Scientific Abstracts

   Approximately 1500 Abstracts on Flow, Density, Viscosity

   100 Applicable - Ordered

2. Alden Flow Laboratories, Worcester, Mass.

   a. Library Use
   b. Consultation

3. National Bureau of Standards - Consultation

4. Massachusetts Institute of Technology-Engineering Library

5. Patent Search (Total 750 Patents)

   a. Pre 1968 True Mass Flow
   b. 1968 - Present: Mass and Volumetric, Densitometry

6. Internal Expertise

   a. 6 Formal "Brainstorming" Sessions
   b. Over 20 Informal Sessions

7. General Electric Corporate Research and Development Center

   1 Week Consulting from Vortex Flow Expert

8. General Electric Electronics Laboratory, Syracuse, New York

   3 Weeks Consulting, Expert in Ultrasonics

TABLE 2

SUMMARY OF DESIGN GUIDELINES AND SPECIFICATIONS

Accuracy	±0.25% of mass flow rate uncertainty
Response	25 msec time constant (for 63% response to step flow change)
Flow Range	9091 kg/hr to 182 kg/hr (20,000 PPH to 400 PPH) 1364 kg/hr to 27 kg/hr (3,000 PPH to 60 PPH) (alternate)
Resolution	±0.25% of min. flow rate
Output	Digital, voltage or frequency
Pressure Drop	68 kPa (10 psi) maximum
Static Pressure	7000 kPa (1000 psi operating 10,500 kPa (1500 psi) burst
Temperature	-55°C to +130°C (ambient & fuel) -55°C to 71°C (electronics)
Vibration	±1.2 mm 5 to 14 Hz ±1 g 14 to 23 Hz ±.045 mm 23 to 90 Hz ±15 g 90 to 2000 Hz
Size	3.8 cm (1 1/2") nominal pipe dia. 30.5 cm (12") long max. 11 x 8 x 3 cm (4.5" L x 3"H x 1/1/8" W) side protrusion 1000cc (61 cu. in.) electronics package volume
Weight	5 kg (11 pounds)
Power	28 Vdc

3.2 Preliminary Analysis -

Many technologies for flow measurement were eliminated at the first pass based on gross defficiencies in meeting the requirements of this program. Others required more detailed investigations of various depths before it became apparent that they were unsuited for the task. In some cases, performance objectives could be met but only with an aircraft full of computers: these too were screened out as impractical. Appendix 10.2 also addresses this initial screening process by describing briefly the "modus operandi" and then listing the main reasons for rejecting or accepting the flowmeter type for further scrutiny.

Most of the flowmeter types encountered proved to be unsatisfactory when compared to the design guidelines and specifications, except that four methods were found to have potential. These are two angular momentum "true" mass flow devices and two volumetric devices with densitometers. Analysis of all other methods was terminated at this time while the four viable types were subjected to more comprehensive rating.

3.3 Description of Four Methods -

3.3.1 Closed Loop Angular Momentum - See Figure 1. This technique is basically a two element angular momentum flowmeter. Flow enters the flowmeter and is given a known angular velocity in a constant speed motor driven impeller. The angular momentum of the flow is then reduced to zero in a fixed turbine. The turbine remains stationary, restrained by an electromagnetic torquer. Variations in flow result in a small deflection of the turbine from its null position, which creates an error signal. A closed loop feedback network adjusts the current in the torquer to restore the turbine to its null position. Ratioing torquer current and impeller speed of rotation provides a direct measurement of mass flow.

In order to meet the accuracy requirements, correction for Reynolds number and torquer temperature characteristics will be required. These are provided by the viscosity shroud and a resistance temperature detector (RTD) coupled with table look-up data stored within a dedicated microcomputer. Relative rotation between the motor driven impeller and the shroud which it drives through a spring is a function of viscosity and speed of rotation. Deflection of the shroud is sensed by the time difference between a reference pickoff on the drive shaft and a pickoff on the shroud.

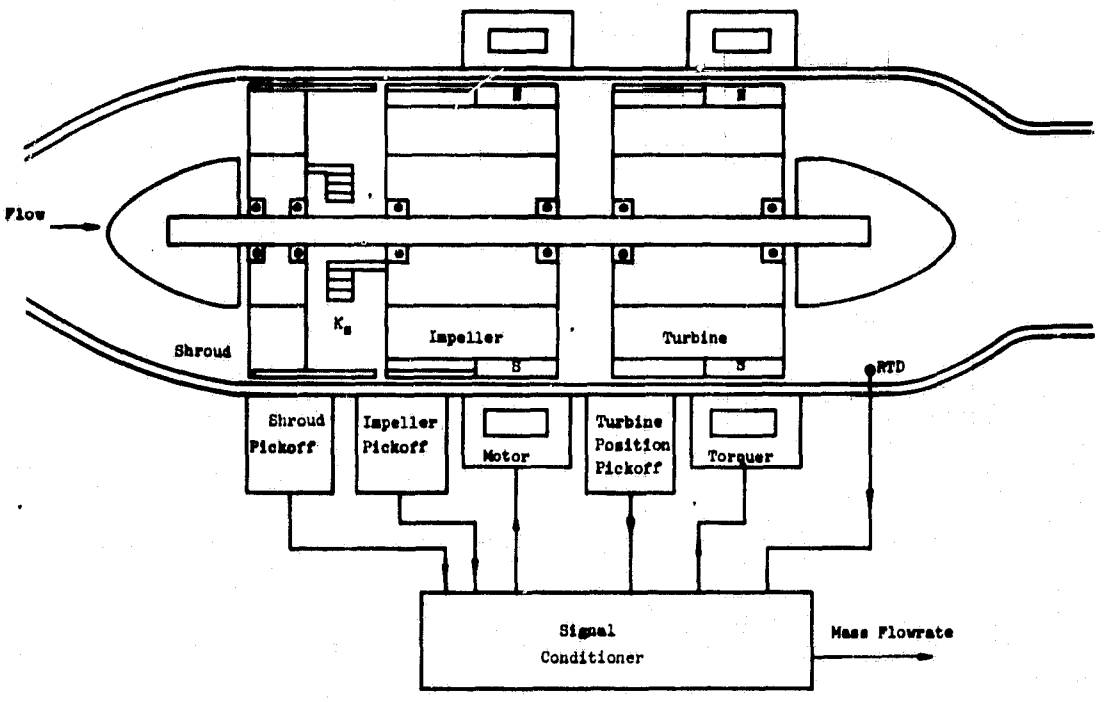

FIGURE 1 CLOSED LOOP MOMENTUM FLOWMETER

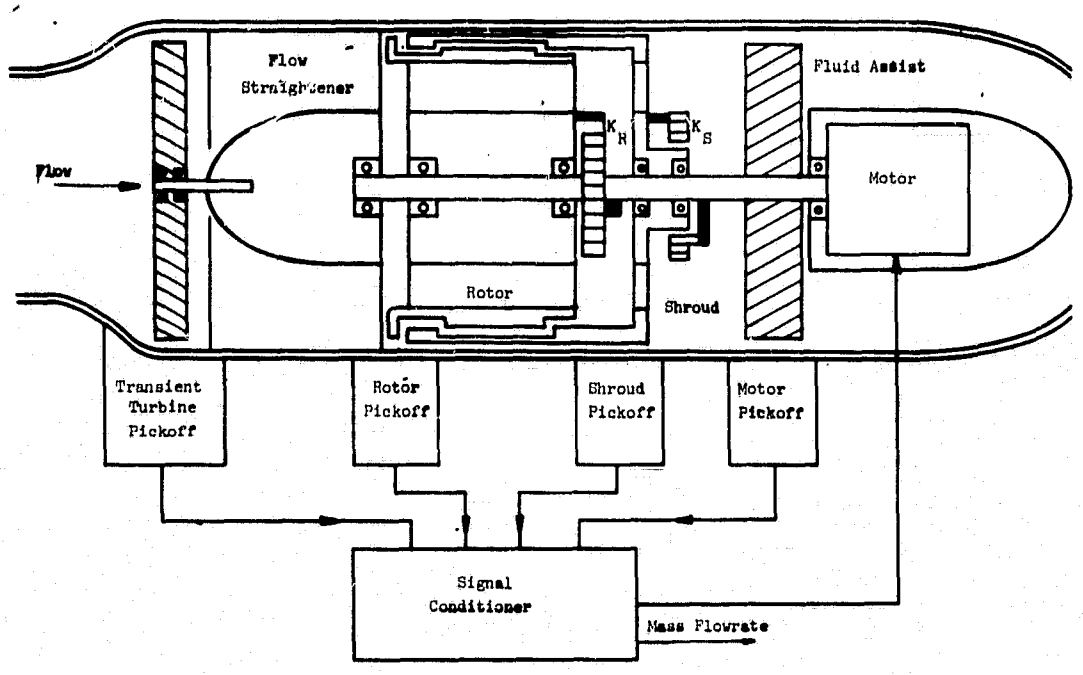

FIGURE 2 OPEN LOOP MOMENTUM FLOWMETER

3.3.2 Open-Loop Angular Momentum Flowmeter - See Figure 2. This is essentially a single element angular momentum flowmeter. Straightened flow enters the long straight passages of a motor driven rotor where the entire flow achieves the same rotational speed. The torque required to accelerate the flow to this rotational speed is proportional to the product of the mass rate of flow and the rotor speed. This torque turns the rotor relative to its drive shaft until balanced by the torque of the rotor spring. This angle, which is proportional to the product of mass flow and rotor speed, is measured by the time difference between the passage of a reference point on the drive shaft and a similar point on the rotor. The two reference points are aligned at zero flow. Since the time required for the rotor to traverse the deflection angle is proportional to that angle divided by the rotor speed, the speed term cancels from the equation, and the time difference is directly proportional to mass flow. A viscosity shroud rotating with the rotor prevents viscous drag from introducing an error into the time delay. By driving the viscosity shroud through a precision spring similar to that driving the rotor and measuring its deflection relative to the same reference on the drive shaft viscosity can be measured. Viscous drag between the outer diameter of the shroud and the housing deflects the shroud spring resulting in a time based signal analagous to that for mass flow. A Reynolds number correction can be performed by the microcomputer, greatly improving the accuracy of the measurement over that currently achieved.

Since the response time of the spring-mass system described is high (approximately 1 second), a free spinning turbine element is added upstream of the flowmeter. The fast response rate of the turbine is combined with the overall accuracy of the mass flowmeter to meet the requirements of the specification.

3.3.3 Turbine-Densitometer - See Figure 3. A particularly simple mass flowmeter can be achieved by combining a turbine volumetric meter with a precision densitometer. The problems associated with standard turbine meters of sensitivity to upstream swirl, bearing friction/wear, limited range, and viscosity sensitivity are mitigated by the addition of a second free counter-rotating turbine element immediately downstream of the first. The second turbine has only a fraction, say 10%, of the main turbine pitch (and, therefore, free rotational speed). The speed of each is measured and sum of speeds used as the volumetric flow signal. An analysis of the flow vectors entering and leaving each turbine shows that this sum of speeds (as measured by blade passing frequency) is nearly independent of upstream swirl content and of bearing or viscosity induced drag on the main (high speed) turbine. Furthermore, by measuring the ratio of the two speeds the flowmeter can monitor the health of its own bearings.

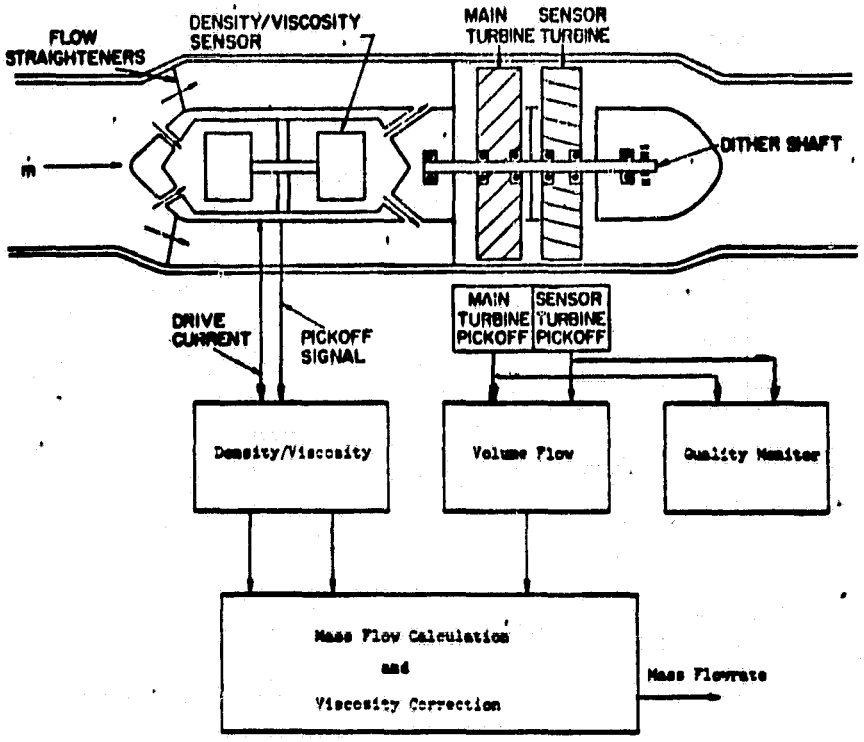

FIGURE 3 TURBINE-DENSITOMETER MASS FLOW

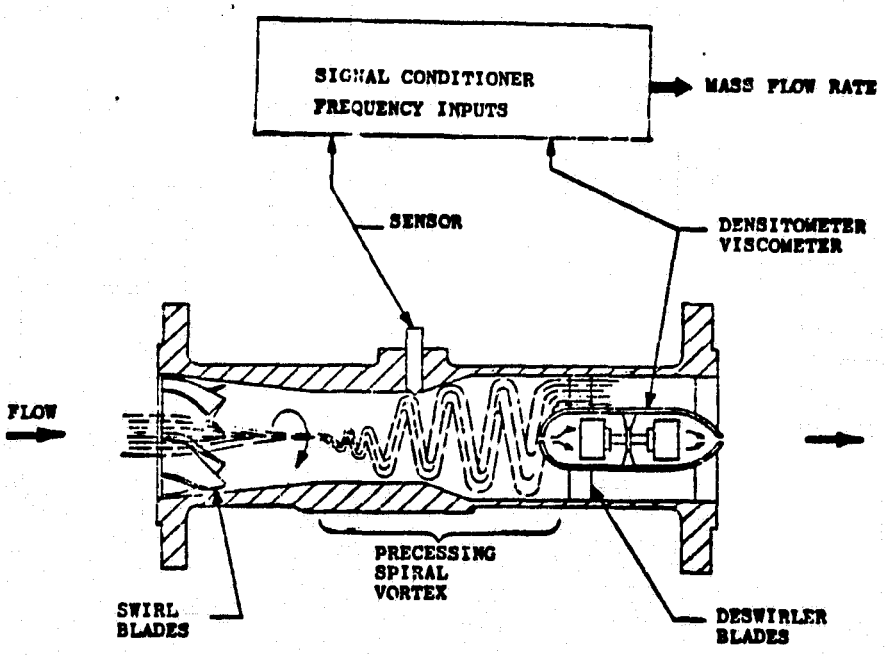

FIGURE 4 VORTEX PRECESSION FLOWMETER

As described later in the Densitometer section, the densitometer also provides a time based signal from which may be derived viscosity. It will thus be possible to perform the Reynolds number corrections needed to ensure system accuracy over the required range of flow, temperature, and fluid properties.

3.3.4 Vortex Precession/Densitometer - See Figure 4. An essentially non-intrusive (from the standpoint of having no moving parts in the flow stream) flowmeter is the precessing vortex meter. Flow enters a set of fixed-vane swirlers which impart a fixed proportion of swirl-to-axial flow to the fluid. The swirling jet which leaves the throat of the nozzle remains coherent, attaches to a wall of the downstream section and precesses rapidly about the flowmeter axis at a frequency proportional to volumetric flow rate. A sensor, which may be acoustic, thermal, force, or pressure sensing, placed at the nozzle exit provides a time based volumetric flow signal. This signal is combined with density information from a precision densitometer to enable an accurate output of mass flow. Again a Reynolds number correction is needed and is provided using the viscosity information from the densitometer.

3.4 Rating And Selection Of The Four Methods - Nineteen parameters were evaluated on a scale from zero to ten for each of the four systems described above. Each parameter was assigned a weighting factor by concensus of G.E. expert opinion. For each parameter a weighted value was obtained by multiplying value by weight. All nineteen figures for one meter type were summed to obtain totals. The results are shown in Table 3.

Selection -

The closed loop angular momentum type rated lowest of the four and subsequently was dropped from further consideration in the program. This is due to estimated poor performance in the following areas:

Size
Attitude Sensitivity
Wiring
Remote Electronics (Amount)
Power Consumption

The remaining three methods were selected by General Electric and NASA for further analysis and design. Since there is only one angular momentum concept being considered further the "open-loop" identifier is now dropped and the concept hereinafter is referred to simply as Angular Momentum.

TABLE 3

FLOWMETER SYSTEM RATING

PARAMETER	WT'G FACTOR	FLOWMETER SYSTEM TYPE: CLOSED LOOP MOMENTUM VALUE	CLOSED LOOP MOMENTUM WT'D VALUE	OPEN LOOP MOMENTUM VALUE	OPEN LOOP MOMENTUM WT'D VALUE	TURBINE METER + DENSITOMETER VALUE	TURBINE METER + DENSITOMETER WT'D VALUE	VORTEX PRECESSION VALUE	VORTEX PRECESSION WT'D VALUE
SAFETY	8	7	56	7	56	8	64	10	80
ACCURACY	9	8	72	8	72	7	63	6	54
REPEATABILITY	9	7	63	6	54	8	72	9	81
RANGE	7	7	49	7	49	6	42	6	42
WEIGHT	2	5	10	7	14	9	18	10	20
COST	1	4	4	5	5	8	8	10	10
RELIABILITY	4	4	16	5	20	6	24	8	32
WIRING	2	4	8	7	14	7	14	8	16
SIGNAL TYPE	8	10	80	10	80	10	80	10	80
REMOTE ELECTRONICS AMOUNT	1	3	3	7	7	5	5	6	6
EXCITATION	2	3	6	5	10	7	14	6	12
POWER CONSUMPTION	2	3	6	4	8	7	14	8	16
RESPONSE TIME	7	7	49	7	49	8	56	6	42
PRESSURE DROP	5	7	35	7	35	9	45	6	30
VIBRATION RESISTANCE	5	6	30	6	30	8	40	10	50
ATTITUDE SENSITIVITY	5	4	20	8	40	8	40	8	40
SIZE	7	3	21	8	56	10	70	10	70
RISK	9	4	36	6	54	8	72	3	27
DEVELOPMENT SCHEDULE	8	4	32	5	40	8	64	5	40
	TOTALS		596		693		805		748

4.0 ANGULAR MOMENTUM FUEL FLOWMETER

The detailed descriptions contained in the following paragraphs apply to the angular momentum High Accuracy Fuel Flowmeter designed to meet NASA requirements. The proposed flowmeter will ultilize established and new design concepts to eliminate or circumvent the majority of error sources which are inherent in current designs. Although high accuracy is the main goal, the design does not sacrifice other secondary system parameters such as reliability, size and weight.

4.1 Principle Of Operation -

The mass flowmeter described herein operates on the principle of rate of change of angular momentum. The design combines some of the most desirable features of flowmeters presently in production and microprocessor compensation techniques. The following description covers the operating principles involved.

The most important elements of the angular momentum mass flowmeter as shown in Figure 5 are:

1. A free spinning transient turbine wheel mounted on bearings and containing multiple short flow channels at a specified pitch angle.

2. A cylindrical, free spinning rotor, mounted on bearings and containing multiple axial flow channels for passage of fluid.

3. A spiral restraining spring attached to the rotor at one end and to the rotating shaft at the other end. The restraining spring controls the angle of deflection of the rotor and its wind up is a measure of fluid torque.

4. A viscosity shroud mounted on bearings and having a large area with fluid in contact with the outer surface of the rotor and the inner surface of the housing.

5. A spiral restraining spring attached to the viscosity shroud at one end and to the rotating shaft at the other end. The restraining spring controls the angle of deflection of the viscosity shroud, and its wind-up is a measure of fluid viscosity.

6. A fluid-assist turbine fixed to the rotating shaft. The pitch angle of its short passages helps to minimize the required motor torque, and reduce motor size.

7. A synchronous motor generates constant angular speed for the rotor, viscosity shroud and fluid-assist.

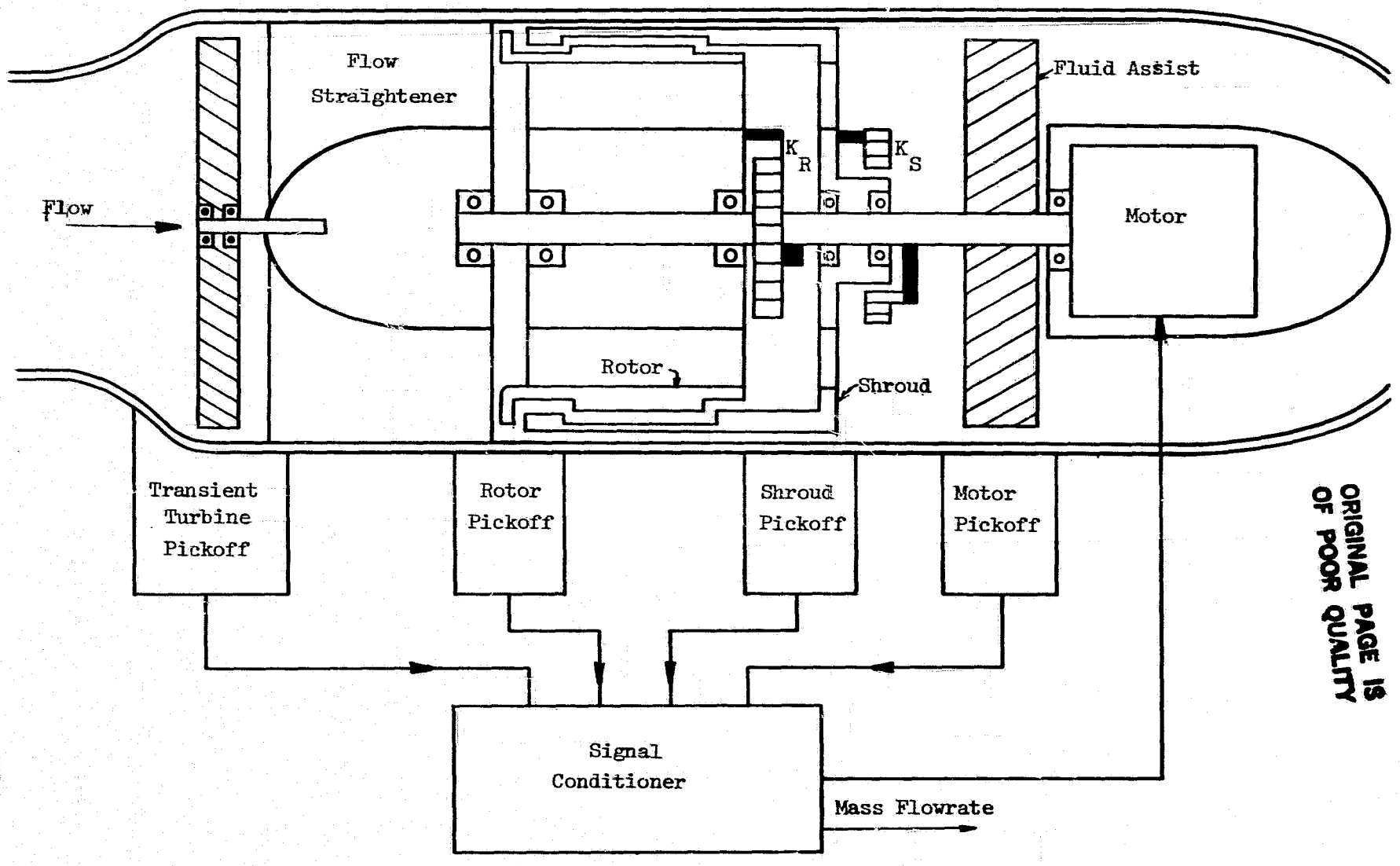

FIGURE 5 PICTORIAL REPRESENTATION OF OPERATION OF ANGULAR MOMENTUM FLOWMETER

8. A modulated frequency pick-off measures the angular speed of transient turbine.

9. A pick-off at the fluid-assist turbine generates an electrical signal when a magnet on one of the turbine blades passes a predetermined point on the main housing (reference pulse).

10. A rotor pick-off generates an electrical signal when a magnet on the rotor passes a predetermined point on the main housing (rotor pulse).

11. A viscosity shroud pick-off generates an electrical signal when a magnet on the viscosity shroud passes a predetermined point on the main housing (viscosity pulse).

12. A signal conditioner houses the necessary electronics and microcomputer to provide the necessary power input and signal compensation. Its output will indicate the mass flow rate.

4.1.1 Angular Momentum Generation and Torque Balance - This meter will require power input to generate the necessary fluid angular momentum. This is accomplished by a synchronous motor which by means of a reduction gear-head, turns the rotor at a fixed angular speed. As fluid enters the rotor passages, it is accelerated to rotor speed which requires torque. This fluid torque is given by: (refer to Section 4.6 for a complete nomenclature listing):

$$\tau_f = \omega\left(\frac{r_{ID}^2 + r_{OD}^2}{2}\right)\dot{m} = \omega \bar{r}_R^2 \dot{m} \qquad (4\text{-}1)$$

where τ_f = fluid torque

ω = angular speed of rotor

r_{ID} = Inner radius of rotor flow passage

r_{OD} = outer radius of rotor flow passage

$\bar{r}_R$ = average radius of gyration of rotor flow passage

$\dot{m}$ = mass flow rate

The torque is balanced by the spiral rotor spring. The rotor, which is spring restrained, deflects through some angle θ_R where the spring torque equals the fluid torque. The spring torque is given by:

$$\tau_{SR} = K_R \theta_R \qquad (4\text{-}2)$$

where τ_{sR} = torque of rotor spring

K_R = spring constant of rotor spring

Θ_R = angle of deflection of rotor spring

A balance of torques on the rotor leads to

$$\tau_f = \tau_{sR} \tag{4-3}$$

and substituting equations (4-1) and (4-2) into equation (4-3) yields the mass flow rate.

$$\dot{m} = \frac{K_R \Theta_R}{\omega \bar{r}_R^2} \tag{4-4}$$

4.1.2 Viscosity Measurement - The NASA high accuracy flowmeter is able to provide viscosity information which compensates the mass flow rate over the temperature range. The viscosity shroud works on the principle of Couette Flow between concentric cylinders. When the motor turns the shroud at a fixed angular speed ω , the viscous drag developed between the inner wall of the main housing and the outer surface of the shroud is given by:

$$\tau_\mu = K_\mu \mu \omega \tag{4-5}$$

where τ_μ = torque due to viscous drag

K_μ = viscosity proportional constant

μ = absolute viscosity

ω = angular speed of shroud (same as rotor)

and this viscous torque is balanced by the spiral spring mounted on the shroud. The shroud spring deflected through some angle θ_S where the spring torque equals the viscous torque. The spring torque is given by:

$$\tau_{ss} = k_s \theta_s \qquad (4\text{-}6)$$

where τ_{ss} = torque of shroud spring

k_s = constant of shroud spring

θ_s = angle of deflection of shroud spring

A balance of torques on the shroud leads to:

$$\tau_M = \tau_{ss} \qquad (4\text{-}7)$$

and substituting equation (4-5) and (4-6) into equation (4-7) yields the viscosity

$$\mu = \frac{k_s \theta_s}{k_M \omega} \qquad (4\text{-}8)$$

4.1.3 Time Base Signal Generation - The essence of the angular momentum signal generation is that instead of measuring the spring angle directly, the receiver measures the time that it takes for a point on the rotor or shroud to move through the angles θ_R and θ_S respectively measured relative to a reference point on the fluid assist. Then

$$\theta_R = \omega \Delta t_R \qquad (4\text{-}9)$$

and

$$\theta_S = \omega \Delta t_S \qquad (4\text{-}10)$$

where Δt_R = time signal from rotor.

Δt_s = time signal from shroud.

Substituting equations (4-9) and (4-10) into equations (4-4) and (4-8) respectively, results in:

$$\dot{m} = \frac{K_R}{r_R^2} \Delta t_R \qquad (4\text{-}11)$$

$$\mu = \frac{K_s}{K_\mu} \Delta t_s \qquad (4\text{-}12)$$

These equations show that mass flow rate and viscosity are directly proportional to their respective time differences relative to the reference point, and are independent of the angular speed. The angular momentum flowmeter provides output signals of the form shown in Figure 6. The signals are generated by passing a magnet by the pole piece of a coil as shown in Figure 7. The changing flux level in the core generates a signal pulse. The reference signal is a pulse generated by the fluid-assist turbine when a reference point on the turbine passes a fixed reference point on housing. The rotor signal is a pulse generated by the rotor when a reference point on the rotor passes through the same housing reference point. Under no flow conditions, the reference points on the fluid-assist and rotor are the same so the output from both signal coils coincide and the time difference is equal zero. The shroud signal is generated in the same manner.

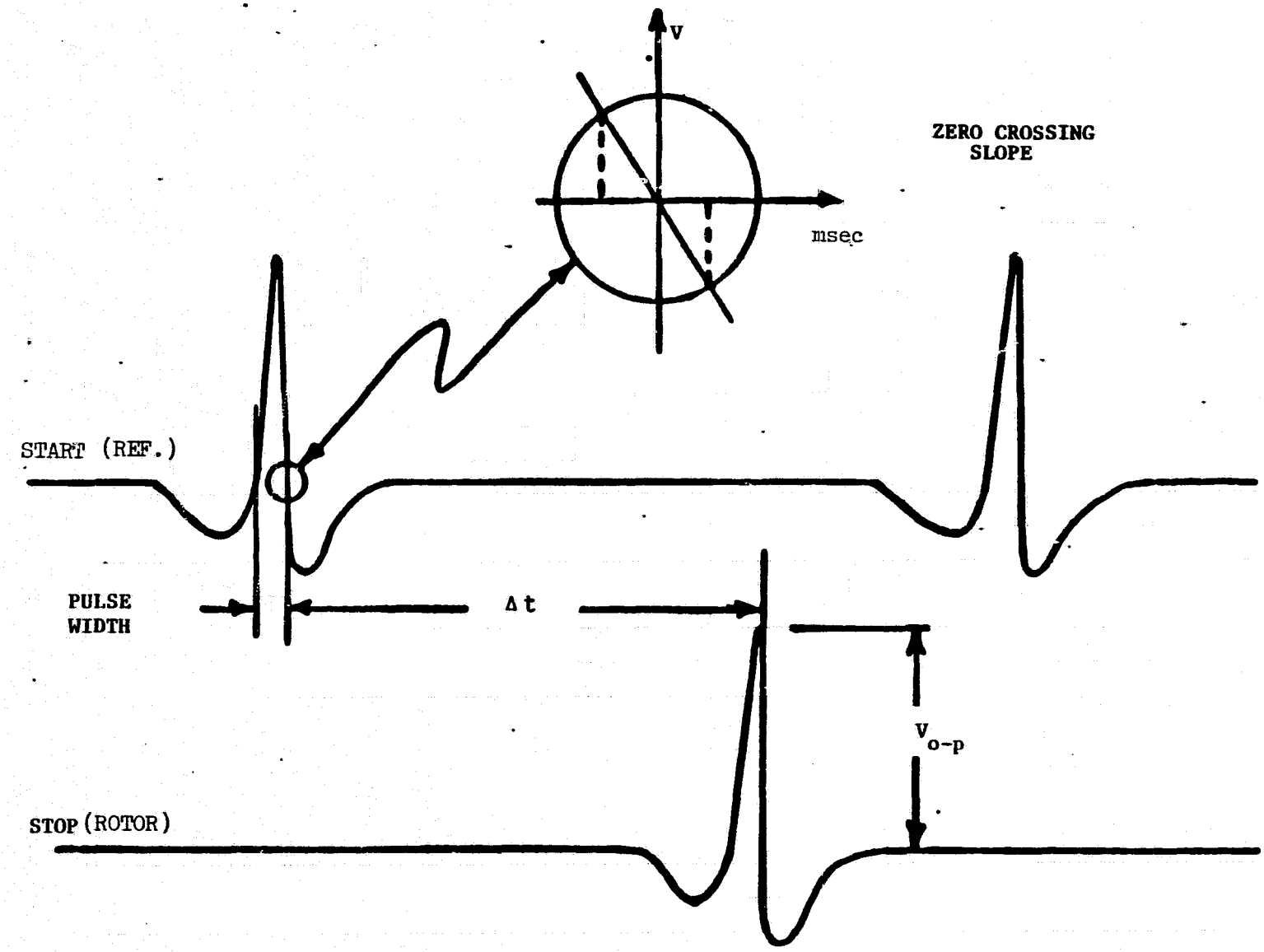

Figure 6 Output Signal Characteristics of Angular Momentum Flowmeter

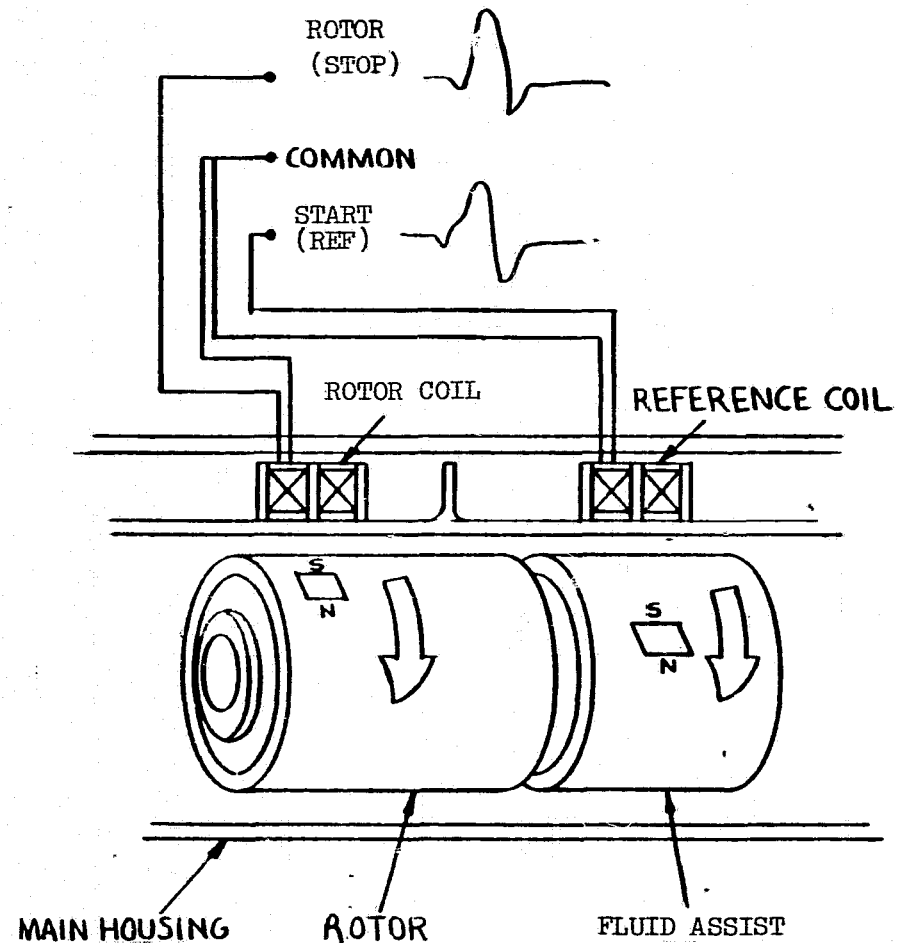

Figure 7 Pictorial Representation of Signal Generation of Angular Momentum Flowmeter

The actual method of determining the time difference between the reference signal and rotor or shroud signal is to measure the time interval from the negative going zero crossing of each pulse after a predetermined signal level is exceeded (Figure 6).

4.1.4 Accuracy - Typical flowmeter accuracy and NASA system specification and goal are shown in Figure 8.

4.1.5 Time Response - Typical angular momentum flowmeter response is in the order of 0.5 to one second and is shown in Figure 9.

4.2 High Accuracy Concept -

The NASA high accuracy flowmeter will combine conventional flowmeter technologies and innovative concepts in order to meet the high accuracy requirement. A cross sectional drawing of all various components is shown in Figure 10. The functional description of major components will be covered in the following description.

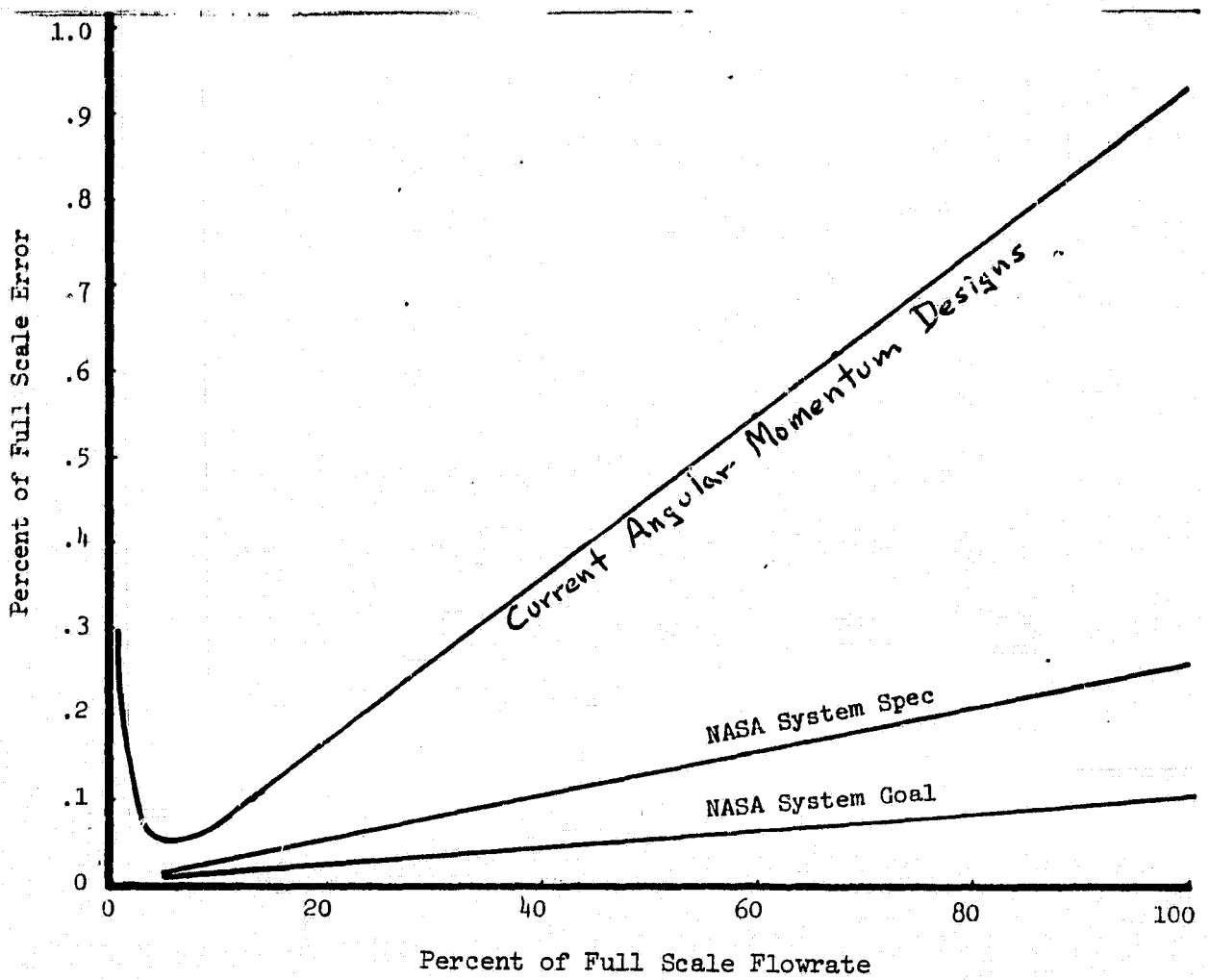

FIGURE 8 SYSTEM ACCURACY OF TYPICAL ANGULAR MOMENTUM FLOWMETERS

TYPICAL MOMENTUM FLOWMETER RESPONSE

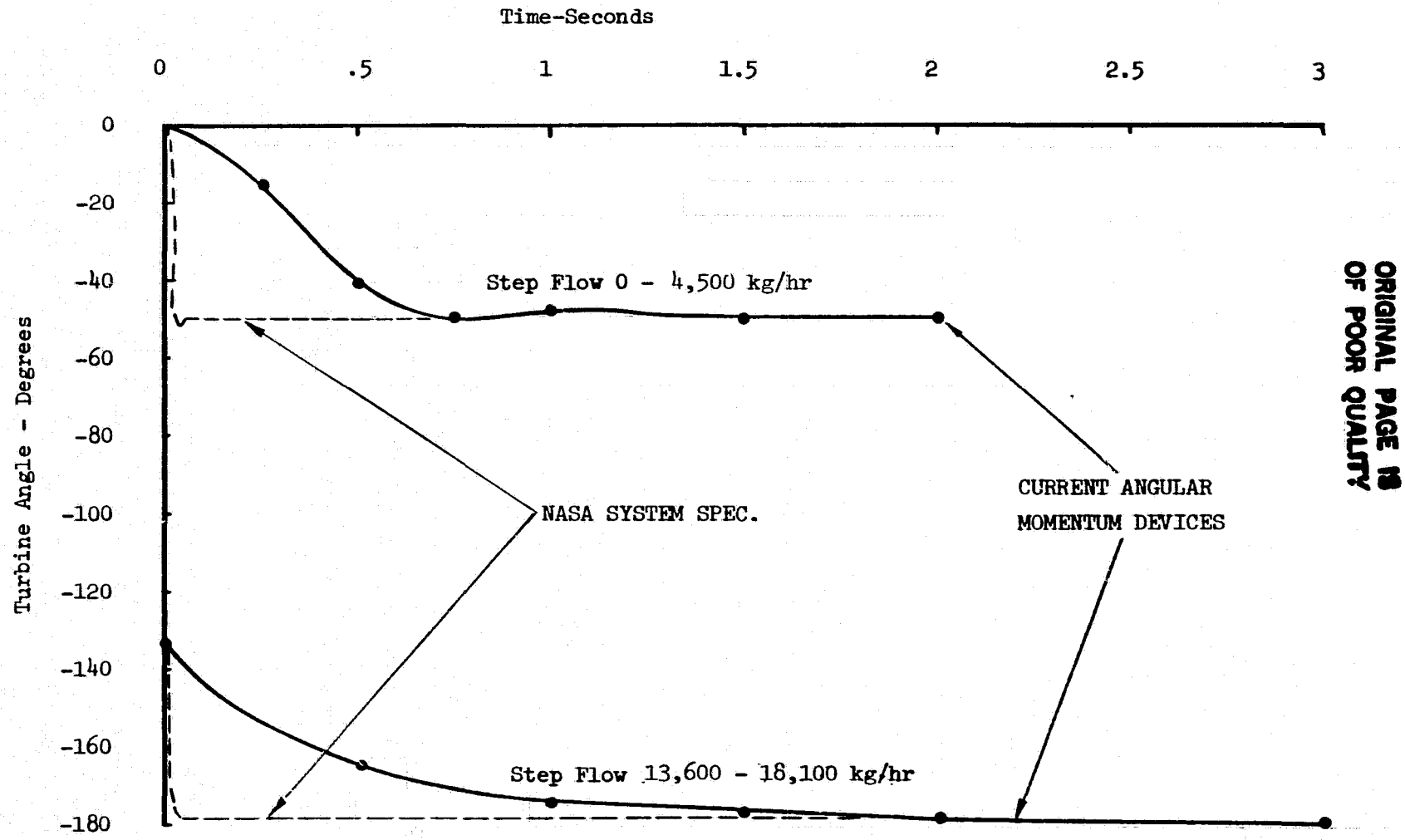

Figure 9 Typical Response Time of Angular Momentum Flowmeter

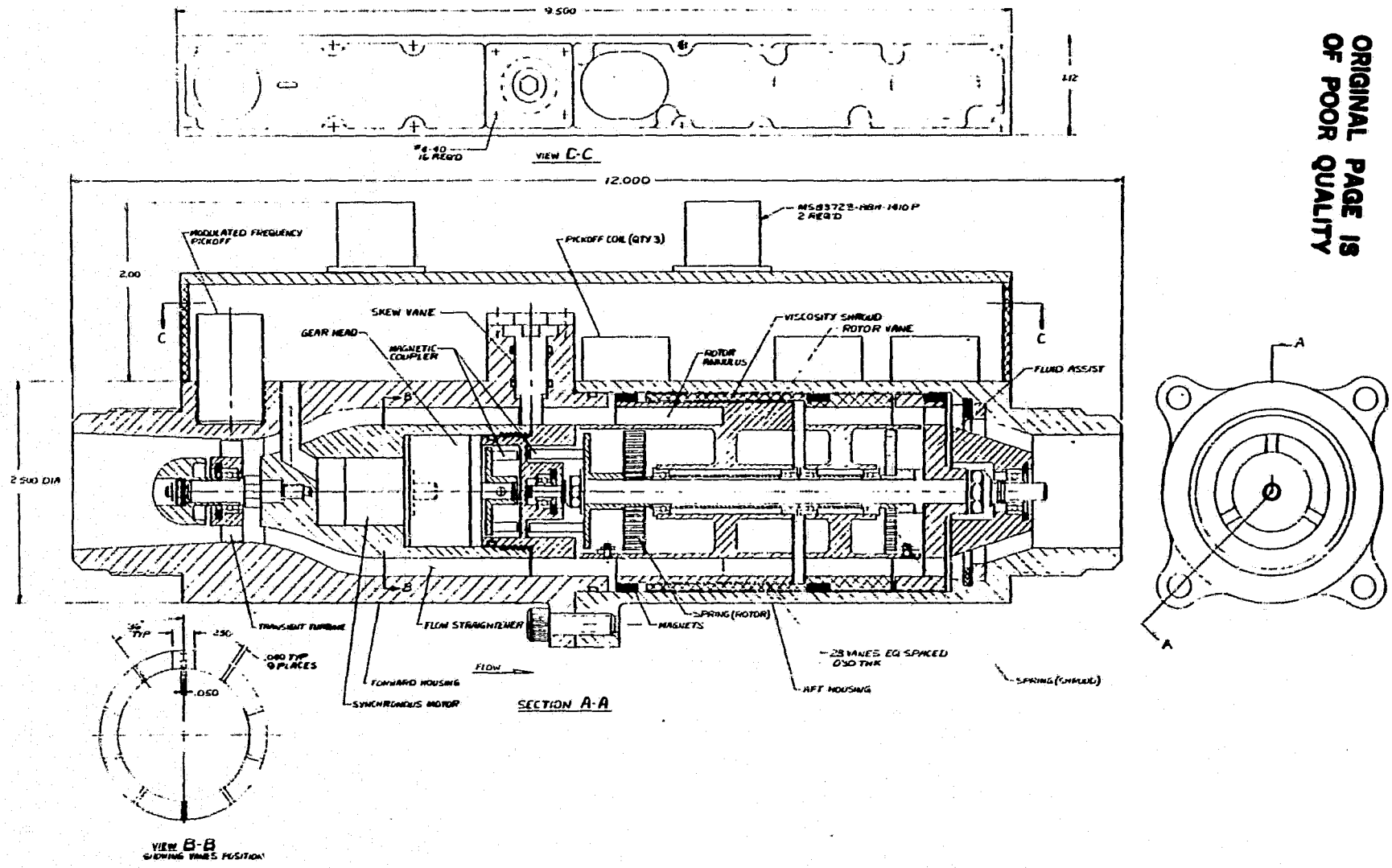

Figure 10 Layout of Angular Momentum Flowmeter

4.2.1 Transient Turbine - A transient turbine consisting of multiple fixed-angle blades on a rotating hub has been added whose frequency of rotation is directly proportional to the volumetric fuel flow rate as given by:

$$Q = K_T \omega_T \tag{4-13}$$

where Q = volumetric flow rate

K_T = transient turbine proportional constant

ω_T = angular speed of transient turbine

The main task of this transient turbine is to provide the fast response for the whole system since the typical angular momentum rotor has a very poor response time. The response time of the transient turbine is governed by the following equation:

$$a_T = \frac{J_T}{\rho Q \bar{r}_T^2} \tag{4-14}$$

where a_T = response time constant of transient turbine

ρ = fluid density

$\bar{r}_T$ = average radius of gyration of transient turbine

J_T = mass moment of inertia of transient turbine.

4.2.2 Constant Speed Motor - As fuel enters the flowmeter, angular momentum is generated by the synchronous motor. This synchronous motor is designed to operate from a 26 volt, 400 Hz square wave power supply. This motor maintains constant angular speed, thus eliminating any error or flow instability due to change in speed. Its high angular speed is reduced to the desired level of 2.5 RPS by a compact reduction gearhead. The motor and gearhead are installed in the forward housing cavity and is isolated from the fuel by a magnetic coupler. The torque transmitted by the magnetic coupler, provides the required torque to maintain a constant speed of the rotating elements.

4.2.3 Flow Straightener - The forward housing in the current design has a relatively long inlet section for flow stablization purpose. As fuel enters a channel, the shear effects will grow outward from the wall as the streamwise distance is increased. An ever increasing portion of the flow will be sheared until the entire channel is under the influence of stress effects. Downstream of the location at which the shear effects has propagated to the center of the flow, the stresses come into equilibrium condition such that the mean velocity is invariant with respect to streamwise position; that is the flow is fully developed at this position. The fully developed length is different for laminar or turbulence flow but is roughly equal to 50 times the hydraulic diameter of the channel, that is

$$\frac{L}{D_h} \simeq 50 \qquad (4\text{-}15)$$

where L = entrance length

D_h = hydraulic diameter of channel

The hydraulic diameter is defined as twice the flow area divided by the wetted perimiter. Most conventional flowmeters, due to size restrictions, have a L/D_h ratio of about 10. The current design will have a ratio of about 20 which should greatly enhance stability and reduce flow fluctuation exiting the transient turbine.

4.2.4 External Skew Adjustment - The proper operation of angular momentum type fuel flowmeters requires that fuel leaves each vane parallel to the central axis. A rotor or inlet flow straightener are examples of such vanes. If the fuel leaves a vane other than parallel to the axis, the calibration curve of the flowmeter will "skew" up or down at the high flow rates. The skew error is proportional to the flow rate squared. Although every element is pre-skewed to zero value before being assembled, fine adjustments are still needed during calibration which often involves tedious disassembling and re-assembling of flowmeter. In order to calibrate a flowmeter for high accuracy, it will certainly be desirable and perhaps absolutely necessary, that fine adjustments can be made with fuel flowing through the flowmeter. The current design has an external skew adjustment port which accesses a skew vane which contacts the fuel, and will ease some of the difficulties involved in calibration for high accuracy.

4.2.5 Rotor Design - The rotor is a cylindrical element, with multiple axial flow passages. Prior experience with this kind of rotating element has demonstrated that the surface finish and edge conditions of the vanes in flow passages greatly influence the accuracy, linearity and repeatability of calibration, especially at adverse temperature environment. The rotor, therefore, is a fabricated structure with surface conditions superior to those acheivable in a cast structure.

The sizing of the rotor is restricted by the physical dimensions of the flowmeter. The trade-off is to maximize the flow area (minimize the flow velocity) in the channel without increasing the average radius of gyration of the channel which would require higher motor torque.

The rotor has an annulus area at the inlet which allows mixing of any wakes coming from the trailing edges of the inlet straightener before flow enters any axial passage.

The spiral spring which measures the torque on the rotor is held rigidly to the rotating shaft and inner hub of the rotor. The total angle of deflection is about 140° due to the 25% overrange requirement and restriction imposed by the dual magnet concept. The angle of spring deflection, which is a direct measure of the mass flow rate, is converted into time base signal as discussed in Section 4.1.3.

Signal generation is achieved by placing two sets of magnets in grooves on the periphery 180° degrees apart. The dual magnet concept is selected over the single magnet concept because it practically eliminates timing errors resulting from cyclic speed variations of the rotor that are caused by alternate acceleration and deceleration torques of an imbalanced rotor in a steady g field (such as encountered in aircraft maneuvers). The dual magnet concept produces a pair of time intervals, the average of which provides true indication of spring deflection angle.

4.2.6 Viscosity Shroud - The operating principle of the viscosity shroud has been discussed in detail in Section 4.1.2. The viscosity proportional constant as given in equation 4-5 is a function of the shroud geometry, i.e.,

$$K_\mu = \frac{4\pi r_i^2 r_o^2 L_s}{r_i^2 - r_o^2} \qquad (4\text{-}16)$$

where r_i = radius of inner wall of housing

r_o = radius of outer surface of shroud

L_s = length of shroud

and equation (4-16) can be approximated (assuming $r_i = r_o$) by the following

$$K_\mu = \frac{2\pi r_i^3 L_s}{r_i - r_o} \qquad (4\text{-}17)$$

The viscosity measurement is particularly important to the high accuracy requirement. In most conventional flowmeter design, there is no compensation for the changes in viscosity at adverse temperature condition. As a result of the varying velocity profile at different viscosities expanded error limits are necessary at high (130°C) and low (-55°C) temperatures. The current viscosity shroud design measures the viscous drag directly and this viscous torque is converted to spring torque by means of the spiral spring. The spring deflection which is a direct measure of the viscosity is converted into time base signal as discussed in Section 4.1.3. This time base viscosity signal, when combined with the mass flow rate, will provide Reynolds Number information. Thus, the microcomputer and related electronics can perform compensation for changes in Reynolds Number.

The viscosity shroud has dual magnets like the rotor.

4.2.7 Fluid-Assist - The fluid assist is a structure similar to the transient turbine, and is held rigidly to the rotating shaft of the motor. The primary function of the fluid-assist is to provide a zero reference point for the time base signals. Also, the vanes on the fluid-assist are pitched to generate torque at high flow rates which helps reduce motor size and power input.

4.2.8 Pickoff Design - The accurate measurement of mass flow rate requires a modulated frequency pickoff for the transient turbine and three magnetic pickoff coils for rotor, viscosity shroud and fluid assist.

The modulated frequency pickoff is a coil which operates at about 45 KHz. The passage of a transient turbine blade through the field of the coil changes its impedance. This results in amplitude modulation of the carrier at the blade passing frequency. This frequency is directly proportional to the rotational speed of the transient turbine.

The pickoff coil is a simple structure that has insulated conductive wire wrapped around a core and is mounted on the housing and located along the path of the moving magnets. When the magnets on the rotating element pass by the pole piece of the coil, the changing flux level in the core generates a signal pulse.

4.2.9 System Block Diagram - The flowmeter output consists of three signals, namely the frequency of rotation of the transient turbine and the time periods of the rotor and viscosity shroud. The system block diagram is shown in Figure 11.

4.2.10 Transient Response Algorithm - At flow rates above 409 kg/hr (900 pph) the transient turbine responds to step changes in flow within 25 ms, but with limited accuracy while the rotor responds in one to two seconds with the required accuracy. The rotor signal has a further restriction since the pulse sample rate is 5 Hz (2 pulses per revolution, 2.5 revolutions per second). Combining the two signals with proper attention to the 5 Hz sample rate of the rotor can be accomplished by digital filtering techniques. However, for purposes of explanation, the following R-C network filter has been devised and is shown in Figure 12. In the circuit, the fast responding turbine signal passes through a hi-pass filter with a time constant of two seconds, while the angular momentum signal passes through a low-pass filter having the same time constant. These filtered outputs are summed to create the fast responding output signal. The figure shows the contributions each sensor makes as time progresses. Although the turbine response lacks accuracy that results in momentary errors which exceed the requirement of .25% of rate, the error is far less than if the turbine were not included. In addition to filtering, the computer algorithm will continually calibrate the turbine to the angular momentum readings.

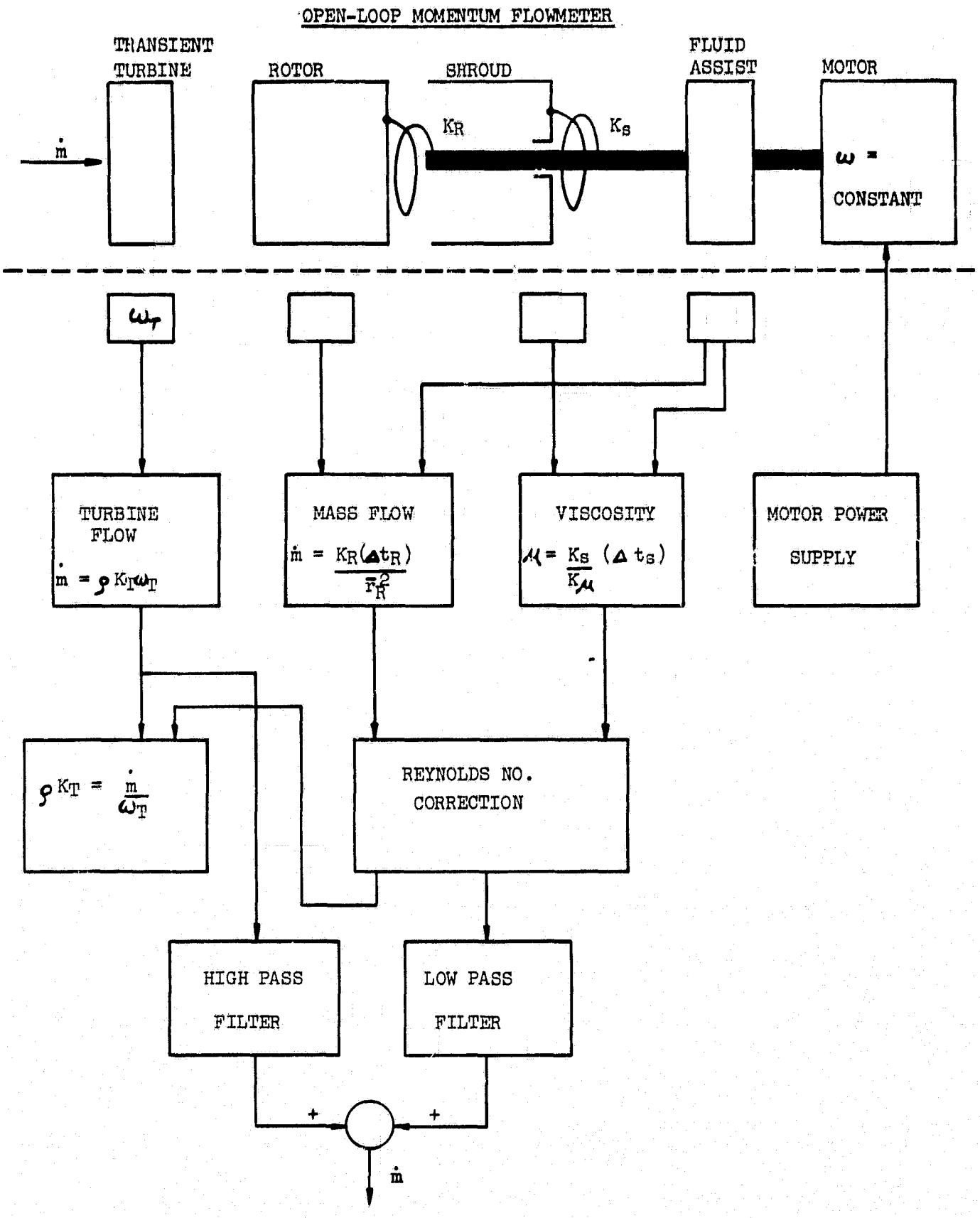

Figure 11 System Block Diagram of Angular Momentum Flowmeter

ANGULAR MOMENTUM FLOWMETER

TRANSIENT AND MOMENTUM SIGNAL COMBINATION

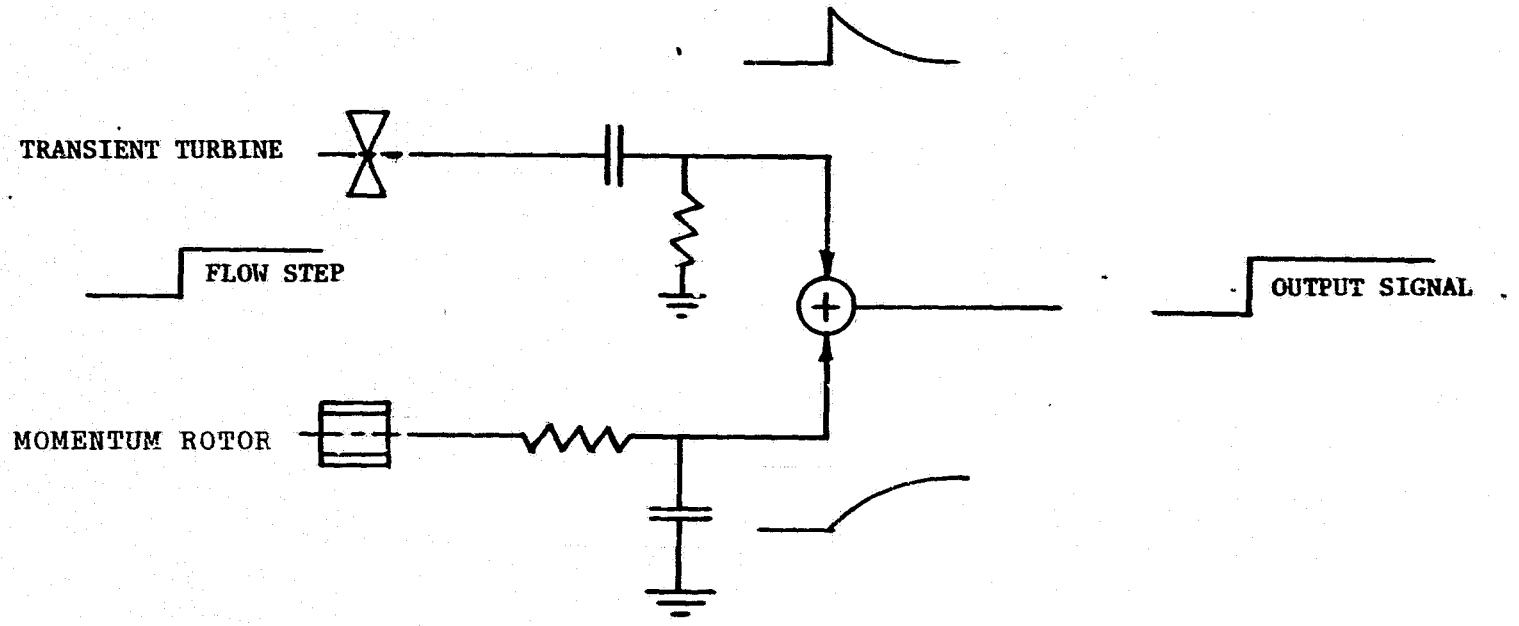

DIGITAL FILTERS WITH EQUAL TIME CONSTANTS

FIGURE 12

4.3 Accuracy Analysis -

The preliminary design of the NASA high accuracy flowmeter has incorporated many new features that have never been used in conventional flowmeters. As a result, the overall system accuracy is expected to improve but there are inherent problem areas where error contributions can not be eliminated. This section describes the major error sources, the nature of the problem and potential methods to minimize these errors. An estimate of the root sum square of random errors for the proposed flowmeter is summarized in Table 4.

Table 4 Sources And Magnitude Of Error Of NASA Flowmeter

Error Source	Error Magnitude (% of Flow Rate)
Spring - Thermoelastic Coefficient	0.1
- Hysteresis	0.025
Electrical Noise	0.05
Viscosity and Related Skew	0.1
Transient Turbine Interaction	0.1
Bearing Friction	0.1 (2,270 kg/hr and above)
Signal Processing	0.1
Orientation	Negligible
Total Error (RSS)	0.23 (2,270 kg/hr and above)

4.3.1 Spring - Most metals and alloys have a negative temperature coefficient of modulus of elasticity, that is to say they lose stiffness when heated. They also have a positive coefficient of thermal expansion, increasing in length when heated. These two effects are due to increase in energy of the atoms with increase in temperature and render most material unsuitable for high accuracy spring application. Some ferromagnetic materials, however, exhibit markedly different behavior, which can be utilized to design constant modulus alloys. The rate of change of the modulus of elasticity with change in temperature of an alloy is known as the thermoelastic coefficient (TEC). It is usually expressed as parts per million per degree C (e.g., 5×10^{-6}/C).

Another limitation of obtaining an ideal spring is mechanical hysteresis. When a spring is loaded and then unloaded, the load deflection curves do not coincide, even though the elastic limit of the material is not exceeded. This departure from linear elastic behavior, termed mechanical hysteresis, is expressed quantitatively by the expression

$$\% \text{ Hysteresis} = \frac{(100) \times \text{Maximum Width of Hysteresis Loop}}{\text{Maximum Deflection}}$$

The most widely used spring material in flowmeters is a nickel-iron-chromium-titanium alloy strip. The usual range of TEC for this alloy is $\pm$ 20 X 10^{-6}/°C. Both the TEC and % hysteresis depends on the heat treatment temperature and the percentage of cold works of the alloy. By controlling the amount of cold work and optimizing the heat treatment temperature, the percentage error could be reduced to 0.025% and 0.1% of flow rate for hysteresis and TEC respectively.

4.3.2 Electrical Noise - An electrical noise voltage or current is any unwanted component that tends to interfere with the transmission or reception of information or signals. Some sources of electrical noise are inherent in the apparatus, other noise voltages arise due to surrounding elements.

The proposed design has a 45 kHz high frequency pickoff, a 400 Hz synchronous motor, and three low frequency pickoff coils. The frequency of the motor is in a range which is sufficiently smaller than the 45 kHz pickoff that the interference between them can be eliminated by filtering. The low frequency pickoff on the other hand, is quite close to the motor frequency which makes the induced noise between them hard to be separated. The potential remedy is to shield both motor and pickoff coils with Mu metal and use separate electrical receptacles for each element. The best estimate of error due to electrical noise is about 0.05% of flow rate.

4.3.3 Viscosity And Related Skew - Fuel viscosity is an inverse logarithmic function of temperature and the velocity profile changes drastically when viscosity changes. The skew effect of rotating parts depends on the velocity profile and the boundry layer thickness. Small surface and edge defects cause skew, but the magnitude of the skew depends on how much of the defect is "buried" in the low velocity boundary layer. Flowmeter elements are usually bought to the zero skew condition by honing or bending the exit ends of flow passages. Thus mechanical defects are balanced at one viscosity to obtain a zero skew value. This balance is not exactly maintained for all viscosity values. Therefore, even though every flowmeter element is pre-skewed to zero before assembly, the temperature effect on the skew cannot be totally eliminated. The hydraulic design of the viscosity shroud described in Section 4.2.6 helps to compensate the viscous effect and fabricated structures allow better surface finish, which also mininze surface defect skew effects more than castings allow. The viscosity signal, when combined with mass flow rate, provides Reynolds Number information which compensates and improves the overall accuracy of the flowmeter. The effect on accuracy due to these viscosity related phenomenon is about 0.1%.

4.3.4 Transient Turbine Interaction - As flow leaves the transient turbine, a wake may be formed. This wake, which is separated from the main flow, is highly vortical and would affect the accuracy of the flowmeter if it propagated into the rotor channel. This design has a much longer flow straightener than any conventional flowmeter. This long entrance length allows sufficient viscous dissipation such that the separated flow or wake can be reduced before it enters the rotor and this source of error should be no more than 0.1% of the flow rate.

4.3.5 Bearings - Of the three sets of ball bearings (shaft support, rotor support, and viscosity shroud support), only those supporting the rotor can significantly affect accuracy. Drag in these bearings will lessen the spring torque required to drive the rotor, thereby lessening the indicated flowrate. Since the shaft speed is constant, the bearing drag torque is nearly constant (varying slightly with flow induced axial loading, and fuel lubricity). The percentage contribution of the bearing torque then decreases as the fluid torque (proportional to flow) increases. It is conservatively estimated that above 2270 kg/hr (5000 PPH) this error is less than 0.1% of flowrate.

Viscosity shroud bearing torques will similarly alter the viscosity measurement. Since viscosity is used in a second order correction, insignificant flow error is induced. High quality instrument bearings are used to minimize the bearing torque.

4.3.6 Signal Processing - This flowmeter utilizes three zero-crossing detectors, one 45 KHz detector and related electronics to provide mass flow rate, aboslute viscosity and volumetric flow rate information. The primary concern is to measure accurate mass flow rate which depends on the performance of the zero-crossing detector.

Accuracy of zero-crossing detection is achieved by using an input amplifier with low offset voltage, and low offset voltage drift with temperature. The accurate detection of zero-crossing is critical because any error in detecting zero-crossing causes an error in measurement of the time interval between start and reference pulses. The amount of error introduced also depends on the slope of the zero-crossing pulse. The sharper the pulse, the less will be the introduced error. Also, identical fabricated coils will eliminate any error due to different pulse shapes. This error is estimated to be 0.1% of flow rate.

4.3.7 Orientation - The imbalance of rotating parts, rotor and viscosity shroud, is a potentially significant error contributor and is addressed in the design. The imbalance effect tends to speed up or slow down the rotational speed when the flowmeter is operating at different orientation or in acceleration fields. This varying rotational speed causes inconsistent time interval between start and reference pulses, resulting in flow measurement error. The present high accuracy flowmeter uses two sets of magnets for each rotating part and are placed at 180° apart. This pickoff arrangement will eliminate error caused by material imbalance in the rotating parts, when two successive signal pulses (time differences) are averaged .

4.4 Specification Requirements And Conformance -

The following is a summary of how the angular momentum approach conforms to the design guidelines and specifications of this program.

4.4.1 Repeatability - One of the major concerns for the high accuracy flowmeter is its repeatability which is restricted by the hysteresis of spiral springs and bearing friction. The root-sum-square of these error source estimates made above is 0.10% for flowrates equal or greater than 2,270kg/hr. (5,000 PPH).

4.4.2 Accuracy - The analysis of 4.3 resulted in an overall RSS accuracy of 0.23% for flowrates equal or greater than 2,270 kg/hr (5,000PPH) which is slightly better than the requirement of 0.25%.

4.4.3 Response Time - The flowmeter has a response time of 25 msec. for any flow rate above 910 Kg/hr. (2000 PPH) or 10% of maximum flow rate. At the minimum flow, due to the physical dimension constraint, the flowmeter has a response time of about 80 msec.

4.4.4 Vibration - The specified vibration inputs are characteristic of those in many specifications for engine mounted flowmeters. The structure and the component parts of the present design will meet vibration requirements without structural degradation. However, vibration can affect the high accuracy and stability; these have to be further evaluated in Phase II.

4.4.5 Pressure Drop - The NASA flowmeter design includes sound hydraulic design practice in order to minimize the pressure drop across the flowmeter. The flow passages have been contoured such that there are no abrupt changes in flow area. The biggest pressure drop comes from the transient turbine. Other contributing factors are due to rotor channels and contraction and expansion of flow areas.

The overall pressure drop of the flowmeter should be less than 68 kPa (10 psi) and a conservative estimate is about 65 kPa (9.5 psi) at maximum flow rate of 9100 kg/hr. (20,000 PPH).

4.4.6 Pressure Pulsation - A pressure pulsation requirement is specified in most mass flowmeters.

This flowmeter design incorporates measurement techniques which are independent of pressure. Also, the mechanical dimensions of the flowmeter housing will remain stable when subjected to pulsations as required by the design guidelines and specifications.

4.4.7 10g Acceleration - A design similar to the current NASA flowmeter has demonstrated satisfactory performance under the dynamic load of 10g. In addition, the current design has dual pickoffs to eliminate the imbalance effect of rotating parts.

Table 6 Specification And Deviation Of Flowmeter Dimensions

	Specification	Deviation
Tube Diameter (D)	MS 33656-24 Tube 3.81 cm (1.5 inches)	-
Length (8D)	30.48 cm (12 inches)	-
Body Diameter	Across Corner of MS33656-24 Tube Fitting Approx. 6.23cm (2.454 inches)	6.35cm (2.5 inches) flowmeter body and four mounting ears D=8.89cm (3.5 inches)
Protrusions (3D x 2D x 3/4D)	11.43cm x 7.62cm x 2.86cm (4 1/2" x 3" x 1 1/8")	24.13cm x 5.08cm x 2.86cm (9 1/2" x 2" x 1 1/8")

4.4.8 Size and Weight - The end fitting of the flowmeter is 3.81cm (1 1/2 inches) nominal per MS 33656. The maximum dimension of the flowmeter is the envelope of the across corner of this end fitting. The current design has certain dimension deviations from the specifications and are briefly described in Table 6.

4.4.9 Down Sizing To 1400 kg/hr (3000 lb./hr.) - One of the specification requirements is to down size the flowmeter to 1400 kg/hr. The flowmeter size cannot be downsized linearly with the decrease of flow rate from 9100 kg/hr to 1400 kg/hr. Every flowmeter component has size limitation from the manufacturing point of view and it is impossible to reduce most of the components by a factor of 6.7. Another limitation is the availability of a suitable motor size for the downsized flowmeter. Also, the 0.25% accuracy would not be met at the low flow range due to bearing friction.

4.5 Further Development Work -

It was identified in the accuracy analysis of Section 4.3 that further development work is necessary to circumvent or eliminate some of the error contributing factors. The following is a brief summary of the development work required for the angular momentum flowmeter:

a) The dependence of hysteresis and thermoelastic coefficient on spring geometry, chemical composition and heat treatment temperature must be investigated.

b) From past experience, the surface roughness and trailing edge condition affect the skew stability. Also, the skew is quite unstable over the operating temperature range. These effects have to be further examined.

c) The velocity profile for different operating ranges needs to be analyzed using computer techniques.

d) The pickoff magnetics and coil characteristics should be optimized for signal processing.

e) The transient turbine response time and flow channel geometry needs to be evaluated in a prototype unit, along with the computer algorithm to recover fast response.

f) The Reynolds Number compensation algorithm needs to be developed.

4.6 Nomenclature

a_T	Response time constant of transient turbine
D_h	Hydraulic diameter of channel
J_T	Mass moment of inertia of transient turbine
K_R	Spring constant of rotor spring
K_S	Spring constant of shroud spring
K_T	Transient turbine proportional constant
K_μ	Viscosity proportionality constant
L	Entrance length
L_S	Length of shroud
$\dot{m}$	Mass flowrate
Q	Volumetric flowrate
r_i	Radius of inner wall of housing
r_o	Radius of outer surface of shroud
r_{ID}	Inner radius of rotor flow passage
r_{OD}	Outer radius of rotor flow passage
$\bar{r}_R$	Average radius of gyration of rotor flow area
$\bar{r}_T$	Average radius of gyration of transient turbine flow area
Δt_R	Time signal from rotor
Δt_S	Time signal from shroud
Θ_R	Angle of deflection of rotor spring
Θ_S	Angle of deflection of shroud spring
μ	Absolute viscosity
ρ	Fluid density
τ_f	Fluid torque
τ_{SR}	Torque of rotor spring
τ_{SS}	Torque of shroud spring
τ_μ	Torque due to viscous drag
V_{op}	Signal voltage amplitude
ω	Angular speed
ω_T	Angular speed of transient turbine

5.0 TURBINE

5.1 Introduction -

The Turbine Flowmeter is a widely accepted flowmeter with proven precision and accuracy. It was therefore considered an excellent candidate for a high accuracy mass flowmeter. Before describing the proposed G.E. concept, a brief review of the theory of operation will be undertaken in order to better understand the functioning and interaction of the operational parameters later discussed.

5.1.1 Review Theory of Operation - The central operating element of a turbine flowmeter is a propeller type rotor whose rotational speed is a function of the velocity of the fluid stream. A perfect turbine flowmeter would have an angular velocity exactly proportional to volumetric flowrate, and the output would be (refer to Section 5.8 for a complete nomenclature listing):

$$\frac{\omega}{Q} = \frac{\tan \alpha}{A \bar{r}} \qquad (5\text{-}1)$$

where:
- ω = Rotor angular velocity
- Q = Volumetric flowrate
- $\bar{r}$ = Mean blade radius
- α = Angle of blade to direction of fluid flow
- A = Area of flow stream

For an accurate flowmeter, meter registration ω/Q must be predictable and repeatable. Several effects can affect the above expression:

Swirl: Changes angle of fluid flow with respect to turbine blade and is unpredictable.

Leakage: Affects the proportion of the fluid stream which passes through the turbine measuring element. Leakage is a function of Reynolds number (R_e).

Velocity Profile: Modifies the effective mean blade radius - is also a function of R_e (Ref. 3).

These effects apply to a perfect flowmeter. In actual practice, some torque is required to drive the turbine. This torque is proportional to the product of mass flowrate and change in fluid velocity ΔV (Ref. 1 and 2):

$$\tau_D = \rho Q \bar{r} \Delta V \qquad (5\text{-}2)$$

$$\tau_D = \rho Q \bar{r}^2 \Delta \omega \qquad (5\text{-}3)$$

Where:
- τ_D = Driving torque
- ρ = Mass density
- $\Delta\omega$ = Change in turbine speed (from ideal)

At steady state, the driving torque equals the total restraining torque τ_R so:

$$\tau_R = \rho Q \bar{r}^2 \Delta\omega . \qquad (5\text{-}4)$$

Rearrange and divide by Q:

$$\frac{\Delta\omega}{Q} = \frac{\tau_R}{\rho Q^2 \bar{r}^2} . \qquad (5\text{-}5)$$

The expression for the actual flowmeter ω/Q can thus be written in terms of a theoretical term for a perfect flowmeter less a slip term:

$$\frac{\omega}{Q} = \frac{\tan\alpha}{A\bar{r}} - \frac{\Delta\omega}{Q} = \frac{\tan\alpha}{A\bar{r}} - \frac{\tau_R}{\rho Q^2 \bar{r}^2} . \qquad (5\text{-}6)$$

Restraining torques come from several sources:

Bearing Friction: A function of bearing design and load. Bearing friction stays fairly constant and is influential primarily at low speed.

Pick-off Torque: Negligible with careful design

Fluid drag torques: Some fluid drag torques are proportional to Q^2. For these, the expression $\tau_R/\rho Q^2 \bar{r}^2$ remains constant for all flowrates and does not affect the meter registration as flow changes.

Other fluid drag forces are a function (generally not a linear function) of Reynolds number (R_e), and the restraining torque can be expressed as

$$\tau_R = C_D \rho V^2 A_B \bar{r} , \qquad (5\text{-}7)$$

Where: C_D is a dimensionless constant and a function of R_e.
V is the average fluid velocity.
A_B is the wetted area of the turbine.

In summary, except for swirl effects, the meter calibration can be expressed in terms of constants and variables which can be related to R_e. The most significant restraining torques come from:

1. Bearing friction (at low fluid flow)
2. Skin friction

5.1.2 Typical Performance Curve

Because turbine meter variables depend primarily on Reynolds number, the turbine meter calibration is commonly shown as a function of Reynolds number as in Figure 13. The ordinate is the actual flowmeter output divided by the output from a perfect turbine meter. The abscissa is a particular Reynolds number R_{ch} which is calculated using the chord of the propeller blade (the slant distance along the blade) as the length parameter.

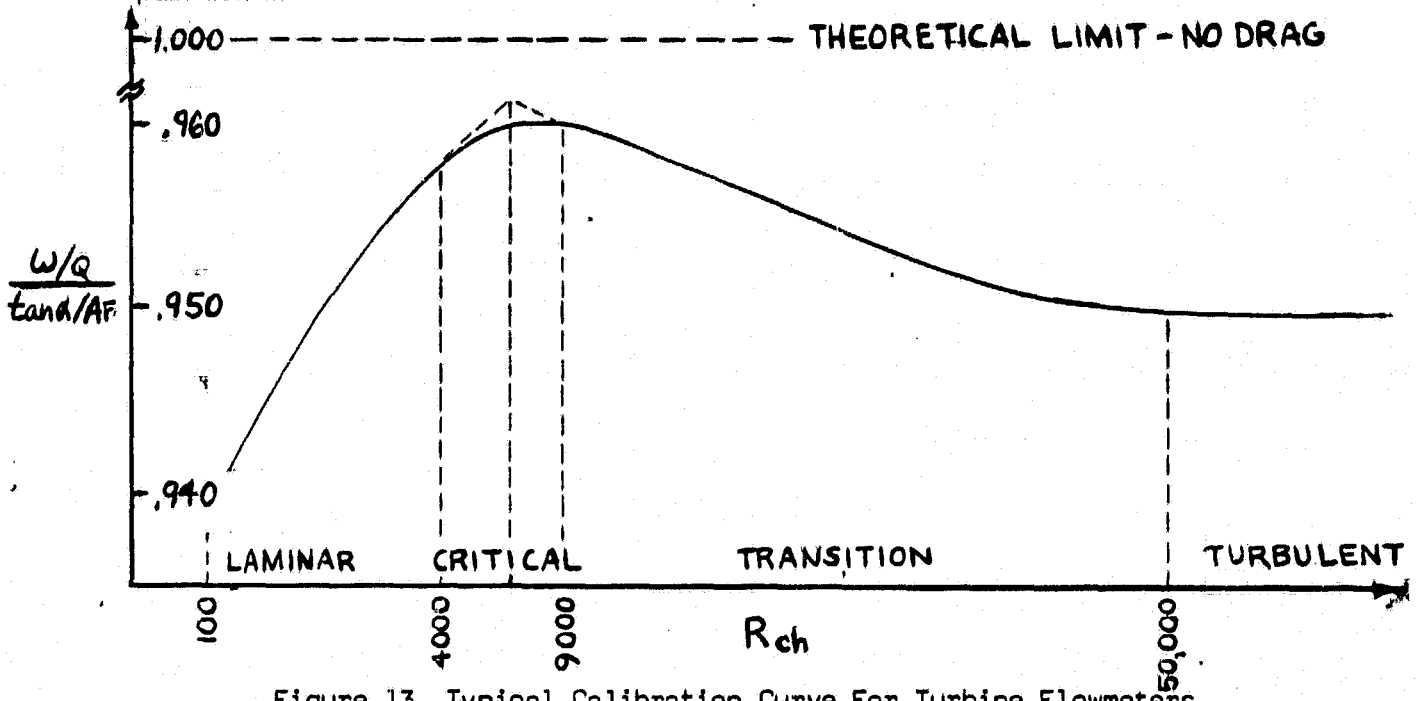

Figure 13 Typical Calibration Curve For Turbine Flowmeters

At low Reynolds number, the boundary layer on the turbine blade is fully laminar and the skin drag coefficient can be expressed as:

$$\text{Laminar, } C_D = \frac{B_L}{\sqrt{R_{ch}}} \qquad (5\text{-}8)$$

where B_L is a numerical constant derived empirically. The upper limit of laminar flow is about $R_{ch} = 4000$.

At sufficiently high Reynolds number, the flow is fully turbulent, and skin drag becomes proportional to the square of velocity and independent of R_{Ch}, so the drag coefficient in equation 5-7 is a constant.

$$\text{Turbulent, } C_D = B_T \qquad (5\text{-}9)$$

B_T is the turbulent drag constant

In the transitional region C_D can be expressed by:

$$\text{Transition, } C_D = B_T - \frac{B_{TR}}{\sqrt{R_{ch}}}$$

B_{TR} is the transition drag constant (5-10)

Under actual conditions, the shift from laminar to turbulent flow does not occur simultaneously for all blades, but occurs over a small range defined as the critical zone and the calibration follows a rounded curve rather than the peak derived from the laminar and transition expression. In this area, repeatability is not as good as in other areas.

5.1.3 Advantages/Disadvantages - The principal advantages of the turbine flowmeter are:

a) Proven Reliability
b) Excellent Repeatability - 0.1% over useful life.
c) Good Accuracy ± 0.5% (when viscosity is known).
d) Pulsed Output - readily digitized
e) Fast Response - 10 ms obtainable

Its disadvantages are:

a) Volumetric Type
b) Susceptible to Swirl
c) Affected by Velocity Profile Variation
d) Susceptible to Viscosity Changes
e) Affected by Bearing Friction

The proposed G.E. concept either eliminates or significantly reduces the disadvantages listed for the standard type turbine flowmeter.

5.2 High Accuracy Concept

The High Accuracy Turbine Mass Flowmeter is conceptually shown in Figure 14. Its unique features are the addition of a torsionally vibrating density/viscosity sensor; a second, reduced speed, counter-rotating sensor turbine, and a friction reducing dither shaft.

5.2.1 Counter - Rotating Turbines (Ref. 4) - The main function of the sensor turbine is to measure swirl. Fluid swirl entering the flowmeter introduces a non-axial velocity vector resulting in a change of speed of the main turbine and, therefore, in a fluid velocity measurement error. However, this change in velocity vector angle is sensed by the second rotor. Since its direction of rotation is opposite to that of the main turbine, a vector change causing a reduction in main turbine speed would produce an increase in sensor turbine speed. The net change of the summation of main turbine and sensor turbine speeds would be zero, and swirl effects therefore eliminated.

FIGURE 14 - HIGH ACCURACY TURBINE MASS FLOWMETER

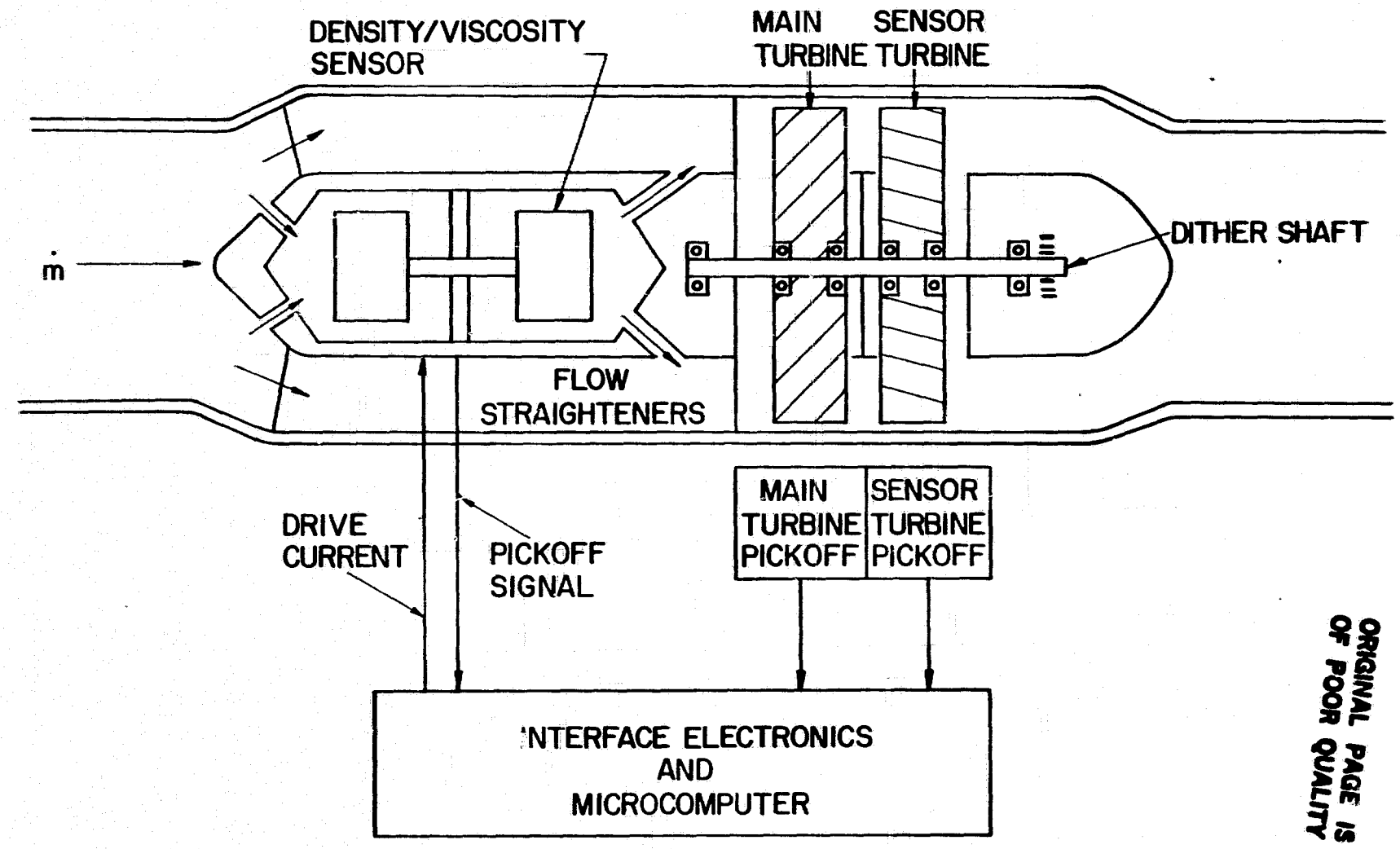

The sensor turbine also senses the change in velocity vector exiting from the main turbine caused by "slip". Because of its counter rotation, slip produces an increase of driving torque of the sensor turbine and an increase of its speed. The net result is that the main turbine slip term is eliminated from the calibration expression and replaced by a sensor turbine slip term which is significantly smaller since the sensor turbine rotates at approximately 20% of the main turbine speed. This results in improved linearity of the performance curve and reduces the need to measure viscosity accurately.

Counter rotation of the sensor turbine also provides another important function. The sensor turbine, to reduce its own slip, operates at a much lower speed than the main turbine. However, this results in less torque available at low flows to overcome bearing and skin friction. Counter-rotation provides, with increased main turbine slip at its start, more torque to get the sensor rotating, thus widening the dynamic range of the flowmeter.

5.2.2 Microcomputer - The microcomputer associated with the turbine flowmeter provides two functions. First it derives mass flow information ($\dot{m}$) by multiplying volumetric flow rate (Q) (obtained from the main and sensor turbine rotational speeds) with density (ρ) information (obtained from the densitometer mounted within the flowmeter).

Secondly, using (Q) and viscosity (ν) (derived from the densitometer damping factor) it calculates the chord Reynolds number (R_{Ch}) and uses "look up" curves stored in the digitial computer memory to modify the flowmeter calibration as a function of Reynolds number.

5.2.3 Densitometer - The torsionally vibrated, mass loaded densitometer used to provide density information is a General Electric, highly accurate, already proven design. Since temperature has an affect on densitometer accuracy, a temperature sensor has also been provided in the flowmeter to further upgrade the densitometer's accuracy. Densitometer operation and accuracy is more fully described in Section 7.0.

5.2.4 Dither Shaft - A dither shaft mechanism has been added to reduce bearing friction and thus increase the dynamic range. Dynamic bearing friction is usually one-half the value of static friction. The dither mechanism consists of an unbalance weight and torsional spring. Normal fluid flow and aircraft acceleration forces keep the dither mechanism in a state of oscillatory motion and thus reduce bearing friction to half its static value.

5.3 Analysis Of Components -

5.3.1 Operating Conditions - The following operating conditions were applied in deriving the detailed flowmeter design discussed in this report

Max. Conditions:
$\dot{m}$ = 2.52 kg/sec (20,000PPH)
T_F = 403°K (130°C)
ρ = 649 kg/m^3 (40.5 lb/ft^3)
ν = 2.5 x 10^{-7} m^2/sec (0.25 cstks)
Q = 3.88 x 10^{-3} m^3/sec (1.372 ft^3/sec)

Min. Conditions:
$\dot{m}$ = 0.05 kg/sec (400 PPH)
T_F = 318°K (-55°C)
ρ = 849 kg/m^3 (53 lb/ft^3)
ν = 2.0 x 10^{-5} m^2/sec (20 cstks)
Q = 5.66 x 10^{-5} m^3/sec (0.002 Ft^3/Sec)

These operating conditions result in a volumetric dynamic range of 65/1.

5.3.2 Flowmeter Sizing - A volumetric dynamic range of 65/1 is greater than that typically found for a turbine type flowmeter. To achieve this, it is desirable to keep turbine "slip" small relative to the theoretical driving torque. By using V = QA, equation 5-6 can be rewritten as:

$$\frac{\omega}{Q} = \frac{1}{FA}\left(\tan\alpha - \frac{2\tau_R}{\bar{r}\rho QV}\right) \qquad (5\text{-}11)$$

It can be seen that the slip term can be reduced by increasing (r) and (V) as greatly as possible within the confines dictated by the specified pressure drop.

To achieve a large V, the flowmeter was designed around the 2.54 x 10^{-2}m (1 in) tube configuration with an entrance diameter of 2.14 x 10^{-2} m (0.844 in) or an area of 3.6 x 10^{-4} m^2 (0.56 in^2).

While desiring a large (r), the retarding torque is dependent on rotor blade area and therefore keeping the annulus as thin as possible. By starting with the standard densitometer configuration and allowing sufficient spacing between it and the surrounding wall, an inner hub diameter was derived which in turn gave as a starting point, a hub radius of the turbine of 1.52 x 10^{-2} m (0.6 in.). Keeping the cross sectional area of the turbine slightly less than the entrance area resulted in a turbine tip radius of 1.78 x 10^{-2} m (0.7 in.) and an area of the turbine (A) of 2.6 x 10^{-4} m^2 (0.41 in^2). The ratio of turbine area to entrance area is 0.73.

5.3.3 Main Turbine Design - In addition to using a thin annulus as previously discussed to achieve maximum torque and minimum slip, proper turbine design requires full guidance of all fluid particles passing through the turbine. To insure full guidance, two flow models were examined.

First: The airfoil approach shows that a turbine with a small number of blades should have a solidity factor which has been empirically found to be 2.53 where:

$$\text{Solidity Factor} = \frac{NW}{D_T} = \frac{\text{No. Of Blades X Blade Width}}{\text{Blade Tip Diameter}} \qquad (5\text{-}12)$$

Second: As the number of blades increase, the momentum derivation is more relevant and, for full guidance the solidity ratio should be 1.00 where:

$$\text{Solidity Ratio} = \frac{C}{S} = \frac{\text{Blade Chord}}{\text{Blade Spacing At } D_T} \qquad (5\text{-}13)$$

For the turbine selected:

No. of blades (N) = 12
Blade width (W) = 7.6×10^{-3} m (0.3 in.)
Blade angle (α) = 0.785 rad (45°)
Tip diameter (D_T) = 3.6×10^{-2} m (1.4 in.)
Hub diameter (D_H) = 3.0×10^{-2}m (1.2 in.)
Blade chord (C) = 1.08×10^{-2} m (0.424 in.)

These result in a solidity factor of 2.57 and a solidity ratio of 1.16, both of which satisfy the above criteria.

5.3.4 Start-Up Torques - For good accuracy at low flow, the main turbine speed should be as high as feasible, preferably within 80% of the theoretical speed of a perfect flowmeter. Thus slip should not exceed 20%. Percent slip is calculated as follows:

At a flowrate of 0.05 kg/sec (400 PPH) the theoretical driving torque (equation 5-2) for a stalled turbine is:

$$\tau_D = 14.8 \times 10^{-5} \text{ N-m } (10.9 \times 10^{-5} \text{ ft-lb}) \qquad (5\text{-}14)$$

The restraining torque consists of bearing friction torque, (τ_B) plus skin friction drag (τ_F). Starting torque for miniature ball bearings is about 7.5×10^{-6} N-m. With the dither mechanism, rolling torque, which is about one-half of static torque, will apply. Therefore:

$$\tau_B = \frac{7.5 \times 10^{-6} \text{ N-m} \times 2 \text{ bearings}}{2} = 7.5 \times 10^{-6} \text{ N-m} \qquad (5\text{-}15)$$

Skin drag: Drag torque = $\tau_F = N \bar{r} D_f \sin\alpha$ (5-16) (Ref 5)

where

$$D_f = C_D \rho \left(\frac{V^2}{\cos^2\alpha}\right) C \left(\frac{D_T - D_H}{2}\right), \quad \text{(Ref 5)}$$

Substituting:

$$\tau_f = N \bar{r} \rho C V^2 C_D \left(\frac{D_T - D_H}{2}\right) \frac{\sin\alpha}{\cos^2\alpha} \quad \text{or}$$

$$\tau_f = 1.98 \times 10^5 \text{ N-m}, \quad (5\text{-}16.1)$$

% Slip = $\frac{\text{Restraining Torque}}{\text{Driving Torque}} \times 100$

$$= \frac{\tau_B + \tau_F}{\tau_D} * 100 = \frac{7.5 + 19.8}{148} * 100 = 18\%,$$

Turbine speed is (100-18) = 82% of maximum possible speed.

5.3.5 Speed Range - The theoretical main turbine speed without slip is

$$\omega = \frac{V \tan\alpha}{\bar{r}}. \quad (5\text{-}18)$$

At the minimum flow of 0.05 kg/sec and at cold temperature (318°K), V = 0.177 m/sec.

$$\omega = \frac{0.177 \tan 45^\circ}{0.0166} = 10.7 \text{ rad/sec.} \quad (5\text{-}19)$$

The output frequency for a 12 blade design is:

$$\text{Frequency} = \frac{10.7}{2\pi} * 12 = 20.4 \text{ Hz.} \quad (5\text{-}20)$$

At the maximum flow of 2.52 kg/sec and at hot temperature (403°K), V = 11.51 m/sec.

$$\omega = \frac{11.51 \tan 45^\circ}{0.166} = 695.5 \text{ rad/sec.} \quad (5\text{-}21)$$

Frequency = 1328 Hz

5.3.6 Sensor Turbine Design - As discussed previously, the flowmeter utilizes a slow speed, counter-rotating second turbine to sense the "slip" in the main turbine. The equation for its operation is:

$$\frac{\omega_S}{Q} = \frac{\tan\alpha_S}{A\bar{r}} - \frac{\tau_{RS}}{\bar{r}^2 e Q^2} + \frac{\tau_{RT}}{\bar{r}^2 e Q^2}, \quad (5\text{-}22)$$

Where: ω_S = Sensor turbine speed
α_S = Sensor turbine blade angle
τ_{RS} = Restraining torque on sensor
τ_{RT} = Restraining torque on main turbine

Which is similar to that of the main turbine, except the slip term of the main turbine has been added. The summation of the main turbine and sensor turbine registrations becomes:

$$\frac{\omega_S + \omega_T}{Q} = \frac{\tan\alpha_T + \tan\alpha_S}{\bar{r}A} - \frac{\tau_{RS}}{\bar{r}^2 \rho Q^2} \quad (5\text{-}23)$$

Subscript T refers to the main turbine.

In essence, restraining torques which reduce the speed of the main turbine act to add angular velocity to the fluid leaving the main turbine. Because the sensor turbine rotates in the opposite direction from the main turbine, the added angular velocity appears as in increased angle of attack to the sensor turbine and acts to increase the speed of the sensor turbine. Thus the slip of the main turbine is eliminated in the combined speed equation (5-23) and only the slip term of the sensor turbine remains.

The sensor turbine slip is determined by restraining torques on the sensor turbine, some of which (bearing torque for instance) are not related to turbine rotation speed and some of which (such as tip clearance drag) increase with increasing turbine speed. Thus to reduce the error, the slip term of the sensor turbine should be kept low, and a low sensor turbine speed will help. Therefore, the sensor turbine speed is designed to be much lower than the main turbine speed.

As a starting point, the sensor was designed to rotate at approximately 20% of the speed of the main turbine. The analysis then showed that at this speed, sufficient start up torque was provided while the drag term was reduced by 80%.

For the actual design:

No. of Blades (N) = 24
Blade Angle (α_S) = 0.17 rad (10°)
Tip Diameter (D_T) = 3.6×10^{-2} m (1.4 in)
Hub Diameter (D_H) = 3.0×10^{-2} m (1.2 in)
Blade Chord (C) = 5.2×10^{-3} m (0.203 in)

This results in a start up torque (with the addition of main turbine slip) of:

$$\tau_D = \underset{\text{(Theoretical)}}{2.51 \times 10^{-5}} + \underset{\text{(Turbine Slip)}}{2.66 \times 10^{-5}} = 5.17 \times 10^{-5} \text{ N-m} \quad (5\text{-}24)$$

The retarding torque is:

$$\tau_R = \underset{\substack{\text{(Bearing} \\ \text{Friction)}}}{.68 \times 10^{-5}} + \underset{\text{(Drag)}}{.34 \times 10^{-5}} = 1.02 \times 10^{-5} \text{ N-m} \quad (.007 \text{ g-cm}) \quad (5\text{-}25)$$

$$\% \text{ Slip} = \frac{1.02}{5.17} = 20\%$$

At a minimum flow of 400 pph, theoretical sensor speed is approximately 1.88 rad/sec or 7.2 Hz. At maximum flow it becomes 123 rad/sec or 469 Hz.

5.3.7 Predicted Performance - An expression for flowmeter registration can now be derived and a performance curve generated if the following assumptions are made.

1. Bearing friction is negligible at high flow rate.
2. Of all drag terms which affect calibration, skin drag predominates.

The general calibration equation can then be written in terms of drag coefficient C_D:

$$\frac{\omega}{Q} = \frac{\tan\alpha}{\bar{r}A} - C_D \frac{\sin\alpha\, C N (D_T - D_H)}{2\cos^2\alpha\, \bar{r} A^2} \qquad (26)$$

For the main turbine:

$\bar{r} = 1.65 \times 10^{-2}$ m
$A = 2.6 \times 10^{-4}$ m^2
$\alpha = 0.785$ rad (45°)
Axial length = $W = 7.62 \times 10^{-3}$ m
$C = W/\cos\alpha = 0.0108$ m
$(D_T - D_H)/2 = 0.00254$ m (0.1 in)
$N = 12$ blades

$$\frac{\omega_T}{Q} = 2.33 \times 10^5 - 4.18 \times 10^5 C_{DT} \text{ rad/m}^3 \qquad (5\text{-}27)$$

For the sensor turbine:

$\bar{r} = 1.65 \times 10^{-2}$ m
$A = 2.6 \times 10^{-4}$ m^2
$\alpha = 0.174$ rad (10°)
$W = 5.08 \times 10^{-3}$ m
$C = W/\cos\alpha = 0.00516$ m
$(D_T - D_H)/2 = 0.00254$ m (0.1 in)
$N = 24$ blades

$$\frac{\omega_S}{Q} = 4.11 \times 10^4 - 4.99 \times 10^4 C_{DS} + 4.18 \times 10^5 C_{DT} \text{ rad/m}^3 \qquad (5\text{-}28)$$

Combined main turbine and sensor turbine:

$$\frac{\omega_T + \omega_S}{Q} = 2.74 \times 10^5 - 4.99 \times 10^4 C_{DS} \text{ rad/m}^3 \qquad (5\text{-}29)$$

Empirical data is available on values of drag coefficients for turbine flowmeters, (Ref. 5). In terms of Reynolds number through the rotor chord (R_{Ch}) they are:

Laminar Flow $$C_{DS} = \frac{B_L}{\sqrt{R_{ch}}} = \frac{0.956}{\sqrt{R_{ch}}} \qquad (5\text{-}30)$$

Turbulent Flow $$C_{DS} = B_T = 0.021 \qquad (5\text{-}31)$$

Transitional Flow $$C_{DS} = B_T + \frac{B_{TR}}{\sqrt{R_{ch}}} \qquad (5\text{-}32)$$

$(B_{TR} = 37.4)$

Rewriting equation (5-29) as a change from theoretical where K is the calibration constant:

$$K = \frac{2.74 \times 10^5 - 4.99 \times 10^4 \, C_{DS}}{2.74 \times 10^5} = 1 - 0.182 \, C_{DS} \qquad (5\text{-}33)$$

then for Laminar Flow:

$$K_L = 1 - \frac{0.182 \times 0.956}{\sqrt{R_{ch}}} = 1 - \frac{0.174}{\sqrt{R_{ch}}} , \qquad (5\text{-}34)$$

for Turbulent Flow:

$$K_T = 1 - 0.182 \times 0.021 = 0.996 , \qquad (5\text{-}35)$$

for Transitional Flow:

$$K_{TR} = 1 - 0.182\ (0.021 - \frac{37.4}{\sqrt{R_{ch}}}) = 0.996 + \frac{6.81}{\sqrt{R_{ch}}} \quad (5\text{-}36)$$

The resulting performance curve of Calibration Factor (K) versus Reynolds number is shown in Figure 15. It is seen to be linear within 0.1% for an R_{ch} from 1000 to 100,000.

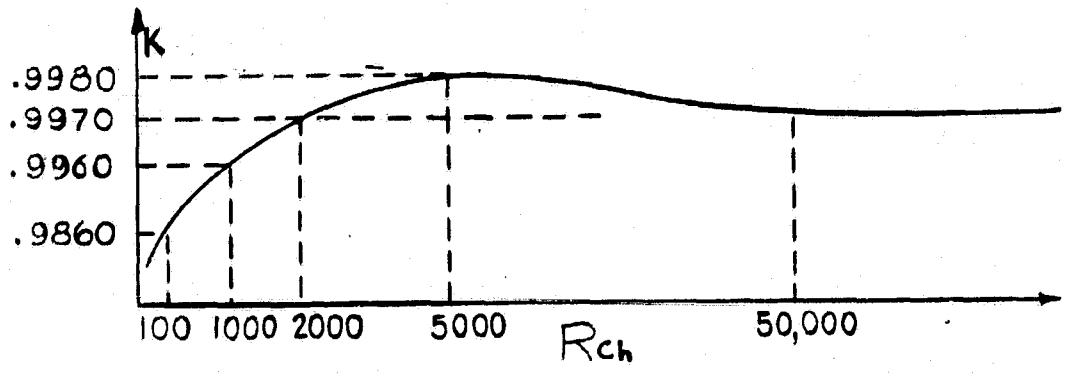

Figure 15 - Calculated Performance Curve

5.3.8 Viscosity Effects - The improved linearity of the performance curve due to the addition of the second rotor is significant in that it reduces the requirement to accurately measure viscosity. Figure 16 is a graph of allowable viscosity error versus viscosity. It shows curves for volumetric error 0.05% and 0.1%. These curves were generated by modifying the calibration constant (K) by these percentages and then determining the resulting change in Reynolds number and the equivalent viscosity. For fluids with viscosity less than 1 centistoke, viscosity need only be measured to 30% accuracy for a .05% change in calibration.

5.3.9 Response Time - Response time, neglecting losses, for a first order system is:

$$\text{Response time} = \frac{\text{Inertia}}{\text{Torque}} = t \quad (5\text{-}37)$$

$$t = \frac{\rho_T V_T r^2}{\rho_F Q \bar{r}^2} \quad (5\text{-}38)$$

Where:
- ρ_T Density Of Turbine Material
- ρ_F Density Of Fluid
- r Radius of Gyration Of Turbine
- $\bar{r}$ Average Radius Of Flow Passage
- V_T Volume of Turbine

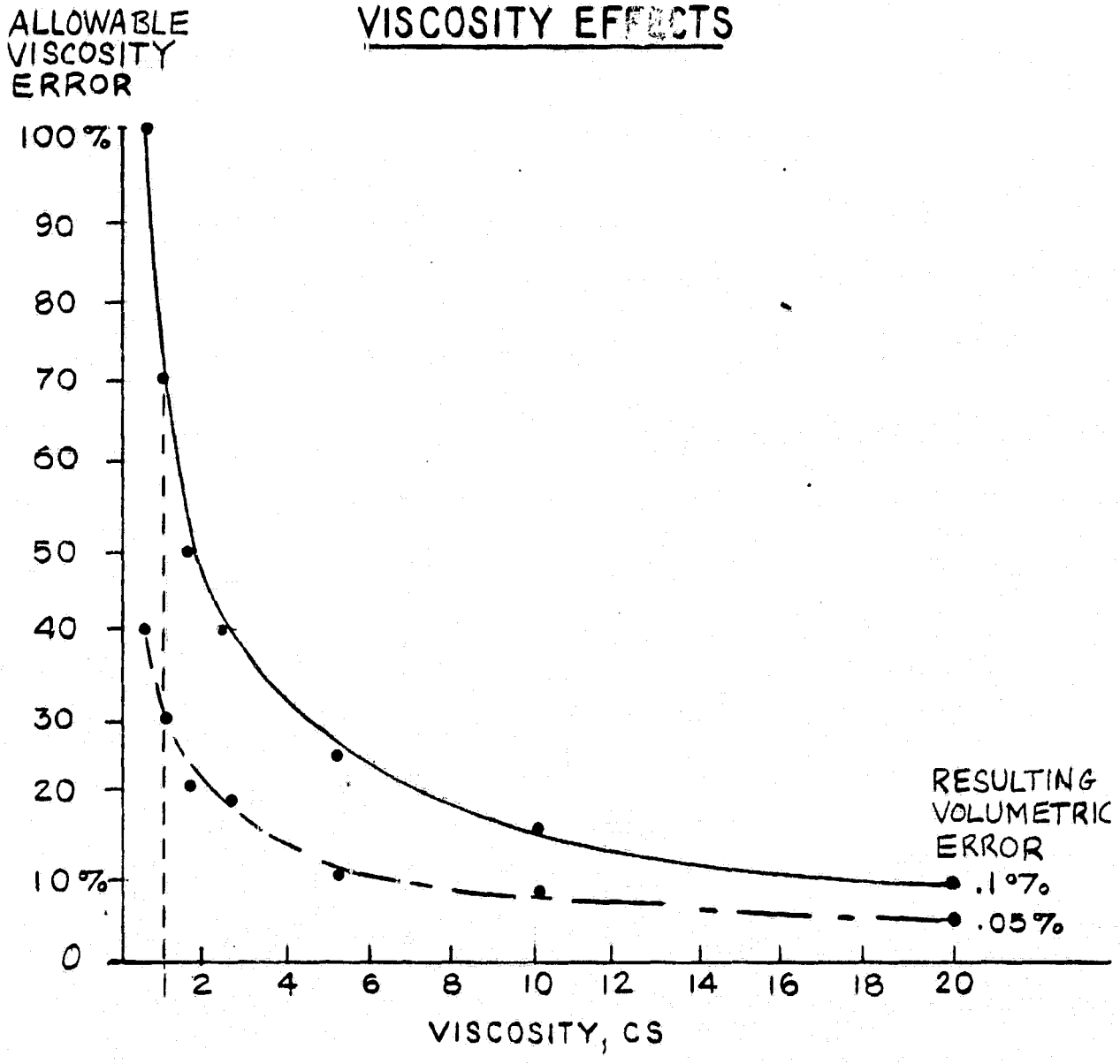

FIGURE 16 Allowable Viscosity Error Versus Actual Viscosity When .05% Error In Total Flowmeter Is Allowed From This Source.

In addition to the inertial time constant is that associated with the discrete, rather than continuous, nature of the turbine speed signal. At least one full blade passing cycle must occur for the turbines speed change to be recognized by the electronics. The longest time constnat occurs at the low flow, high viscosity (cold) conditon of 400 pph and 20 ctks. Here a sensor turbine inertial time constant of 32 msec and blade passing frequency of 7.2 Hz combine for a net time constant of 170 msec. Since both components of the time constant are inversely proportional to flow rate, the flowmeter's response rate will be within the 25 msec specification at flows over about 2700 pph.

The proposed two turbine flowmeter design was based on attaining maximum accuracy over the specified flow and temperature range. In many cases accuracy will be of greatest importance and fast response will not be needed, so the design as presented will be suitable. In applications where fast response is essential, some auxilliary means, such as a strain gauge flow sensor, could be used for transient conditions while the two turbine flowmeter would be used for steady state flowrate.

5.3.10 Down Sizing (3 KPPH Flowmeter) - Downsizing the flowmeter for a 3000 PPH (1364 kg/hr) maximum flow device presents two problems. They are reducing the densitometer size and providing sufficient torque at startup.

Reviewing the parameters governing the densitometer design, a reduction in densitometer diameter can be achieved by reducing the inner core of the vaned fluid rotator and reducing the wall thickness of the torsion spring. Output frequency and sensitivity would then not be materially changed. The piezoelectric crystal presently being used could also be retained.

Achieving the specified accuracy over a volumetric dynamic range of 65/1 however, would be much more difficult. To achieve the same theoretical drive torque to offset bearing friction the velocity must be increased by the same ratio that the flow is decreased. The maximum available drive torque is proportional to the mean turbine radius, mass flowrate, and fluid velocity, the first two of which will decrease for a flowmeter which is designed for a lower flow range. Maximum torque is developed at start just before the turbine starts to turn, and the load to be overcome is almost entirely due to bearing torque which will not be much less than for the 20,000 pph design which uses high quality low torque miniature ball bearings. Even though the fluid velocity is increased as much as possible above that of the 20,000 pph design, the turbine of the 3000 pph design will not start at as small a percent of full flow as the 20,000 pph design. Thus, the volumetric flow range of the 3000 pph design will be less than for the 20,000 pph design, and will probably not equal 65:1.

5.3.11 Flow Division Through Densitometer - The flow past the densitometer should be of a rate to get a reasonable update of density information due to fluid temperature changes while not affecting densitometer performance.

Several considerations must be examined before a flow division is selected. The relationship of flow versus densitometer accuracy must still be determined since previous applications were in static (0 flow) conditions. However, since the densitometer's performance has not been affected by a vibrating, fuel sloshing, environment, it is believed that the effect of a controlled flow will be negligible.

In addition, since a flow divider is used to introduce fuel into the densitometer chamber, the time interval for a single change over will vary with flow rate. For example, with an 2.8×10^{-5} m^3 chamber volume for the proposed design, a 1% flow divider will refill the densitometer container from less than one second to approximately 50 seconds over the dynamic operating range.

Ideally, once the relationship between flow rate and densitometer performance is established, the filter/orifice size controlling the flow to the densitometer can be determined and a temperature response time versus flow rate derived.

5.4 Conceptual Design -

Figure 17 is the conceptual design layout for the turbine flowmeter. The inlet and outlet parts have been designed in accordance with MS33658-16 (1" TUBING) FITTINGS and meets the overall size objectives with the exception of the protrusion width. This was widened to 1.5 in. to permit the use of a single connector.

As a guide in reviewing the proposed construction, a list of parts' material and description has been generated and is presented in Table 7.

5.5 Accuracy Analysis -

For the accuracy analysis, errors from repeatability, curve fit, viscosity measurement, density measurement and signal processing were combined by RSS to obtain the total error. The analysis was further divided into flow categories because of their relationship to Reynolds number, as listed in Table 8.

5.5.1 Error Contributors -

5.5.1.1 Repeatability - Typical repeatability error for a turbine flowmeter is 0.1%. By linearizing the performance curve through the use of a sensor turbine, it is estimated that the repeatability error can be halved through most of the flow range except in the area of uncertainty between laminar and transitional flow and at cold start, due to bearing friction.

5.5.1.2 Curve Fit - It is expected that small anomalies in the calibration curve due to mechanical variances in the detailed parts will make an exact curve fit unlikely without significant added complexity in the signal processor.

5.5.1.3 Viscosity Measurement - Analysis of the densitometer and associated electronics (see Section 7.3) indicate that viscosity can be measured within the figured accuracy to achieve the value listed in Table 7.

FIGURE 17 - TURBINE MASS FLOWMETER

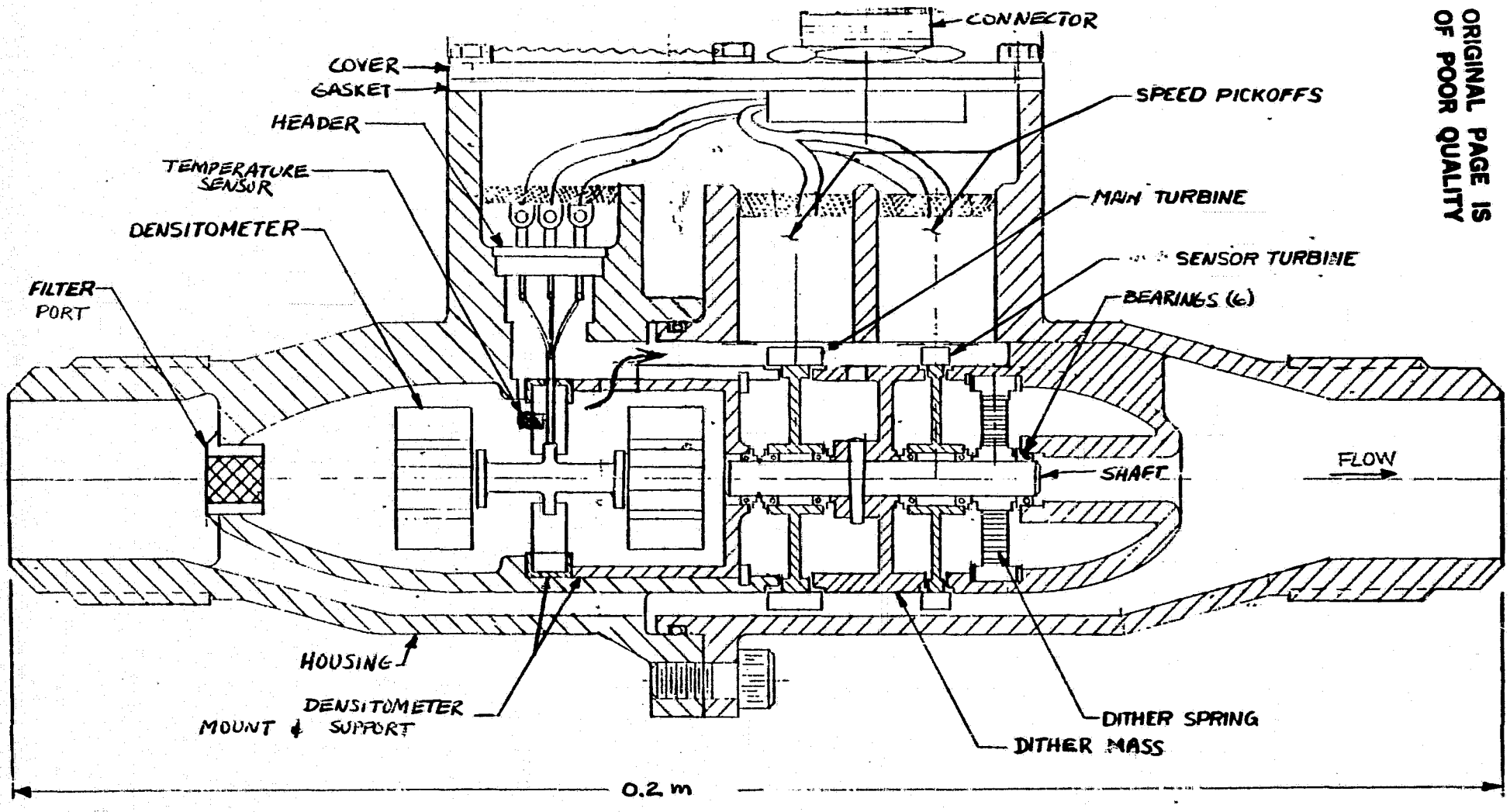

Part	Description	Material
Housing	Two piece casting. Flow straightener and densitometer housing integral part of housing.	Investment Casting 356-T6 Aluminum
Densitometer	Described in Section 7.0	
Dens. Support	Molded plastic part. Serves as insulator and vibration isolator.	Polyester (Valox 420)
Dens. Mount.	Machined part. Serves as both front bearing support and densitometer clamp. Held in position by bowed retaining ring.	6061-T6 Aluminum
Main Turbine	Cast 12 bladed, 45° helix, thin annulus, narrow hub, low inertia design.	Investment/Casting 356-T6 Aluminum
Sensor Turbine	Cast 24 bladed, 10° helix - opposite rotation from main turbine.	Investment/Casting 356-T6 Aluminum
Pick-Offs	Encapsulated RF (40,000 Hz) Coil	
Bearings	Miniature stainless ball bearings with lubricant impregnated retainer	Barden Bartemp SFR156 or equiv.
Dither Mass	Combined separator and dither mass. Pinned to oscillating center shaft. Torsionally unbalanced.	6061-T6 Aluminum alloy
Shaft	Precision, centerless ground, no step construction	Type 303 Stainless Steel
Dither Spring	Torsion wound clock spring welded to inner and other rings. Inner ring pressed on. Other ring held by retaining ring.	Type 316 Stainless Steel
Connector	Miniature MIL-C-83723/81A. Provides 13 pins in No. 10 shell. Is available with EMI filter pins if required.	
Temperature Probe	Surface type - thin film platinum RTD - ceramic coated.	Omega W581 or equivalent
Header	Compression-glass sealed - multi pin type MIL-H-28719 for bringing out densitometer leads.	Hermetic Seal 2709-4
Cover	Metal stamping	2024 T4 Alum. alloy
Gasket	Die cut flat gasket	Synthetic Rubber
Inlet/Filter	Combined flow controller/filter for densitometer. Pressed into housing.	Sintered Porous Metal Filter

Table 7 ERROR ANALYSIS OF TURBINE METER
(All Numbers Percent of Point)

FLOW REGIME, R_{Ch}	START/COLD 50 - 500	LAMINAR 500 - 4000	CRITICAL 4K - 9K	TRANS. 9K - 50K	TURB. 50K+
REPEATABILITY	0.20	0.05	0.10	0.05	0.05
CURVE FIT	0.10	0.05	0.05	0.05	0.05
VISCOSITY	0.05	0.05	0.05	0.05	0.05
DENSITY	0.12	0.12	0.12	0.12	0.12
SIGNAL PROC.	0.10	0.10	0.10	0.10	0.10
TOTAL (RSS)	0.277	0.179	0.198	0.179	0.179

5.5.1.4 Densitometer Error - The derivation of the densitometer error can be found in Section 7.4.

5.5.1.5 Signal Processor - The deduction of the error associated with the signal processing can be found in Section 8.3.

5.5.2 Risk Areas - There are a number of areas of uncertainty which could affect the overall flowmeter accuracy. These areas will be investigated in the next phase. They are:

1. Level and repeatability of bearing friction.
2. Repeatability of calibration in the critical flow range.
3. Velocity profile symmetry and change as related to Reynolds number.
4. Leakage dependence on viscosity.
5. Attainable accuracy of viscosity measurements.

5.6 Conformance To Specification Summary -

The following is a summary of the specifications achieved by the proposed turbine flowmeter design with comments on deviations to the original objectives.

REQUIREMENT	SPEC.	COMMENT
Max. Flow	2.52 kg/sec	As Designed
Dynamic Range	50/1	Designed for 65/1 volumetric flow range.
Burst Pressure	2.07×10^7 N/m^2	Housing as designed - possible problem with electrical header and its attachment to housing need further investigation.
Pressure Drop	6.9×10^4 N/m^2	Within at room temperature - estimated from empirical turbine flowmeter data to be 1.38×10^5 N/m^2 at 20 CS. Can only be reduced by increasing flow area, at the expense of starting torque.
Size		Within, except for 1.5 width required for single connector. Might use multiple connector if electrical coupling becomes a problem.
Weight	5 kg	Less than 1 KG by weight analysis
Response	25 m sec	171 ms
Power	28 V	As designed, wattage minimal
Pressure Pulsation	$\pm$ 2%	Might have some effect on accuracy. Must be further investigated.
Accuracy	$\pm$0.25% of Reading	Within, except start up at cold temperature.
Resolution	$\pm$0.125% of Reading	As designed.

5.7 Further Development Work -

Those areas listed in Section 5.5.2 relating to the attainment of the specified accuracy need to be investigated and clarified. This may be accomplished in the following phases.

5.7.1 Bearing Friction And Skin Drag - Determine bearing friction and drag forces under flow loading and viscosity conditions by fabricating and separately testing a main turbine and sensor turbine.

5.7.2 Rotor Blade Geometry - Once the level of restraining torques has been ascertained, the main turbine and sensor turbine blade geometry will be optimized to minimize both rotor slip and size. A model will be fabricated containing the optimized rotors.

5.7.3 Calibration Fit - The actual calibration curve will be derived and variations from predicated values investigated. Measurements will be made over the temperature range and by introducing swirl effects.

5.7.4 Repeatability - Repeatability measurements will be made and, more specifically, closely examined in the critical and starting flow ranges. Any large variances will be further investigated and isolated as to cause.

5.7.4 Dither Mechanism - Results of the bearing friction testing will dictate the need of a further friction reducing mechanism. If required, a mechanism will be fabricated and tested for effectiveness of operation under actual flow conditions.

5.8 Nomenclature

A	Cross-section area of flow stream
A_B	Wetted area of turbine
B_L	Laminar flow drag constant
B_T	Turbulent flow drag constant
B_{TR}	Transition region drag constant
C	Blade chord
C_D	Drag coefficient
C_{DS}	Drag coefficient for sensor turbine
C_{DT}	Drag coefficient for main turbine
D_H	Diameter at hub
D_T	Diameter at blade tips
K	Calibration factor
L	Radial height of blades
m	Mass Fowrate
N	Number of turbine blades
Q	Volumetric flowrate
r	Radius of gyration
r	Mean (average) blade radius
R_c	Reynolds number for critical flow
R_{ch}	Reynolds number for chord of blade
R_e	Reynolds number
S	Blade spacing at tips
t	Response time
T_F	Temperature of fluid
V	Velocity of fluid stream
W	Axial length of turbine blade
α	Angle of rotor vanes
ρ	Mass density
τ_D	Driving torque
τ_B	Bearing torque
τ_F	Restraining torque due to skin friction
τ_R	Restraining torque
ω	Angular velocity
ω_S	Angular velocity of sensor turbine
ω_T	Angular velocity of main turbine
$\Delta\omega$	Change in angular velocity
V_T	Turbine volume

6.0 VORTEX PRECESSION

6.1 Introduction -

This section explores the attributes of a high-accuracy mass-flowmeter that employs the vortex precession technique to obtain volumetric flowrate, a densitometer to obtain fuel density and a microcomputer to multiply the two quantities and thereby derive true mass-flowrate. This section starts off with a review of literature that covers important experimental work, patents and recent improvements on vortex precession flowmeters. Then, the section covers the high accuracy concept with a description of important parts and operation. This is followed by analysis of expected performance, discussion of the conceptual design layout, analysis of accuracy and summation of conformance to specification. Lastly, there is a summary of problems which limit the concept from meeting the specification and the related development efforts for Phase II which are needed to rectify the problems.

6.1.1 Vonnegut's Whistle - In 1953, B. Vonnegut, then working for General Electric, discovered that forcing air or water through a tube via a tangential inlet, thereby producing strong rotation at the axial outlet, generated a tone that increased in pitch with increasing flowrate (Refs. 6, 7) (Figure 18). With water, the device produced frequencies in range of 120 to 550 Hz, and Vonnegut found that the output frequency was almost directly proportional to volumetric flow rate - independent of density of the fluid. He observed bubbles precessing about the axis at the exit and surmised that this produced the audible tones. Experiments on a similar whistle shown in Figure 19 produced similar results.

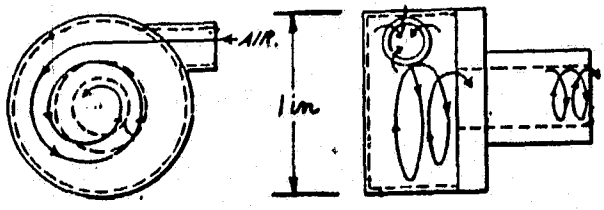

FIGURE 18 VONNEGUT'S FIRST WHISTLE

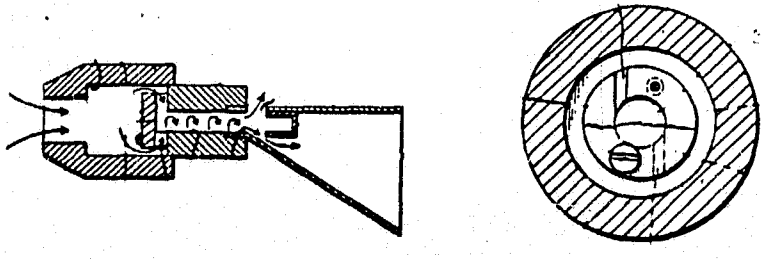

FIGURE 19 VONNEGUT'S SECOND WHISTLE

A few years later, I. Michelson offered a theory based on elementary physical considerations to show why the pitch of the vortex whistle depended on flow rate and was not strictly dependent on geometry as with more common whistles and organ pipes (Ref. 8).

6.1.2 Channaud's Work - Further work was not reported until 1963 when R. Channaud conducted an experimental investigation on the vortex whistle in both air and water (Ref. 9). He verified that the motion of fluid at the tube exit indeed generated sound pressure at the frequency of precession and that Reynolds number is a basis for dynamic similarity. He used a microphone, hot wire anemometer and wave analyser to investigate the sound output.

A year later, Channaud published two papers (Refs. 10, 11) detailing data from developmental models that layed the foundation for what has become a practical and accurate flowmetering device that performs much better than Vonnegut's whistle. However, he first attempted to explain how the precessing vortex was formed with the aid of photographs of dye injected upstream of the swirling flow. Figure 20 is an example of what Channand saw. From this, he postulated that flow reversal of the central core at the exit and extending 1.5 diameters upstream forced the vortex off axis and to then be swept around by the base swirling flow nearer the tube wall. He attributed the flow reversal to the sudden expansion at the exit, and elaborated further on the fluid mechanics of the phenomenon. Theoretical studies of Suzuki (Ref. 12) made some bold assumptions of velocity profile for an approximate analysis with several techniques. These analyses proved to be of limited use in designing flowmeters so instead of the analysis approach, gathering experimental data was used to learn how to improve the device and to determine how it performed.

6.1.3 Variables - Table 8 lists all of the relevant dimensionless quantities and parameters that make them up. The Reynolds number is taken in the smallest diameter, d, of the device, with the corresponding faster axial velocity, Va. The Rossby and Strouhal numbers are dimensionless and appear throughout Channaud's work without the factor of π shown in the list. I have added π to the formula and subscript (i.e.: Ro_{π}) to give true velocity ratios. For instance Ro_{π} = Va/Vt where Vt = π fo d. Be aware that Ro (without π) appears in the forthcoming graphs and is not representative of velocity ratio. Swirl ratio is the most useful term because of its direct physical meaning. The Strouhal number is equivalent to the calibration constant as it is based on the frequency of precession, fp. Both the Rossby and Strouhal numbers are on the order of unity. Frequency ratio is also a constant expressing the ratio of frequencies of precession to base swirling flow upstream of the precession, and is equivalent to $Ro_{\pi} \times S_{\pi}$.

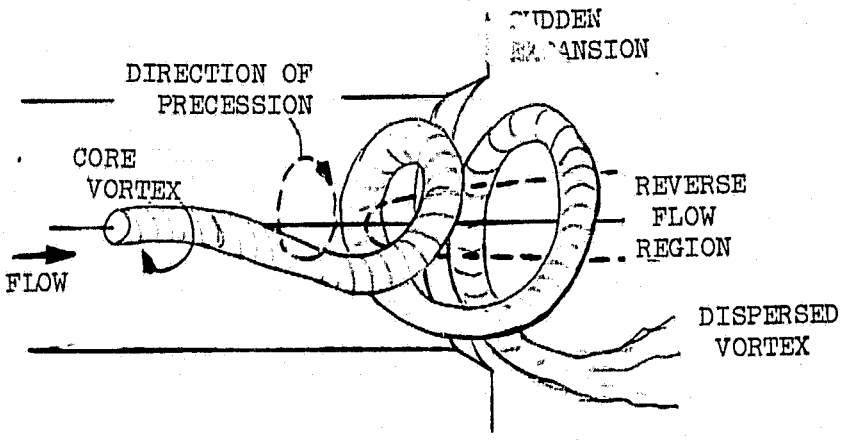

FIGURE 20 VISIBLE PRECESSING VORTEX CORE VIA DYE INJECTION

DIMENSIONLESS QUANTITIES

Table 8

$Re = Va\ d\ /\ \nu$	Reynolds Number
$Ro_\pi = Va\ /\pi\ fo\ d$	Rossby Number
$1\ /\ Ro_\pi$ or $Vt\ /\ Va$	Swirl Ratio
$S_\pi = \pi\ fp\ d\ /\ Va$	Strouhal Number
$fp\ /\ fo$	Frequency Ratio

fp = Frequency of vortex precession

fo = Frequency of base swirling flow upstream of precessing vortex.

d = Smaller inside diameter.

Va = Axial velocity through d.

Vt = Tangential Velocity = π fo d

ν = Kinematic viscosity

6.1.4 Experimental Results - Channaud conducted experiments on several laboratory models and prototypes suitable for field evaluation (Refs. 9, 10). The first lab model demonstrating a dramatic improvement in linearity over the vortex whistle had eight blades curved and exiting at 60° from the meter axis placed inside the inlet of a one inch diameter tube then exiting into a plenum of free fluid. When testing with air and water, he found the unit had linearity of ± 5% over a Reynolds number range of 500 to 7000, independent of density. Below Re of 500 the frequency of precession dropped off, and below Re of 250 precession did not occur. The Strouhal number (S_π) was 3.1; no Rossby number was reported.

Channaud tested another laboratory unit with 20 diameters of rotating tube upstream of a 3 to 5 diameter long section of fixed tube that finally exited into free standing fluid. Speed of rotation was controlled to produce various swirl ratios over a range of flows. With this device he demonstrated, first, a minimum Reynolds number of about 250 below which no vortex precession occurred and, second, a swirl ratio of 5 to 6 is needed to produce a strong and consistent precession with flows above the minimum Re. See Figure 21. The test also showed the frequency ratio (fp/fo) to be almost constant at .380. Transition from laminar to turbulent flow did not perturb linearity.

Channaud then built a prototype flowmeter with 7.62cm (3.0") diameter and fixed, curved blades at the inlet to produce swirl and with a slight venturi section, the diverging section of which generated the expansion and central flow reversal needed to create the vortex precession. A microphone was mounted at the inside diameter just upstream of the point where divergence started. With air and water he found the unit operated with a Strouhal number (S_π) of 5.20 ± .15 over a Reynolds number range of 25,000 to 150,000. Water produced frequencies from 20 to 52 Hz; air 120 to 500 Hz. The microphone produced r.m.s. pressure indications equalling two times velocity head of fluid entering the larger diameter. However, the single sensor proved to be very sensitive to longitudinal pressure waves from pumps and turbulence so Channand suggested differential type sensors to reduce this sensitivity, along with filtering. From this prototype, a 4" diameter meter was designed to operate in a natural-gas pipeline and performed as follows:

± 1.2% linearity over 20:1 range of Re.
± 12.0% linearity over 333:1 range of Re
22 to 1138 Hz precession frequency
Digital readout.

Channaud patented the flowmeter concept in 1966 (Ref. 13) with the following claims: (summary)

- fixed swirl blades
- downstream contraction and expansion
- precessing vortex
- sensors that detect the vortex
- deswirl blades downstream of sensor.

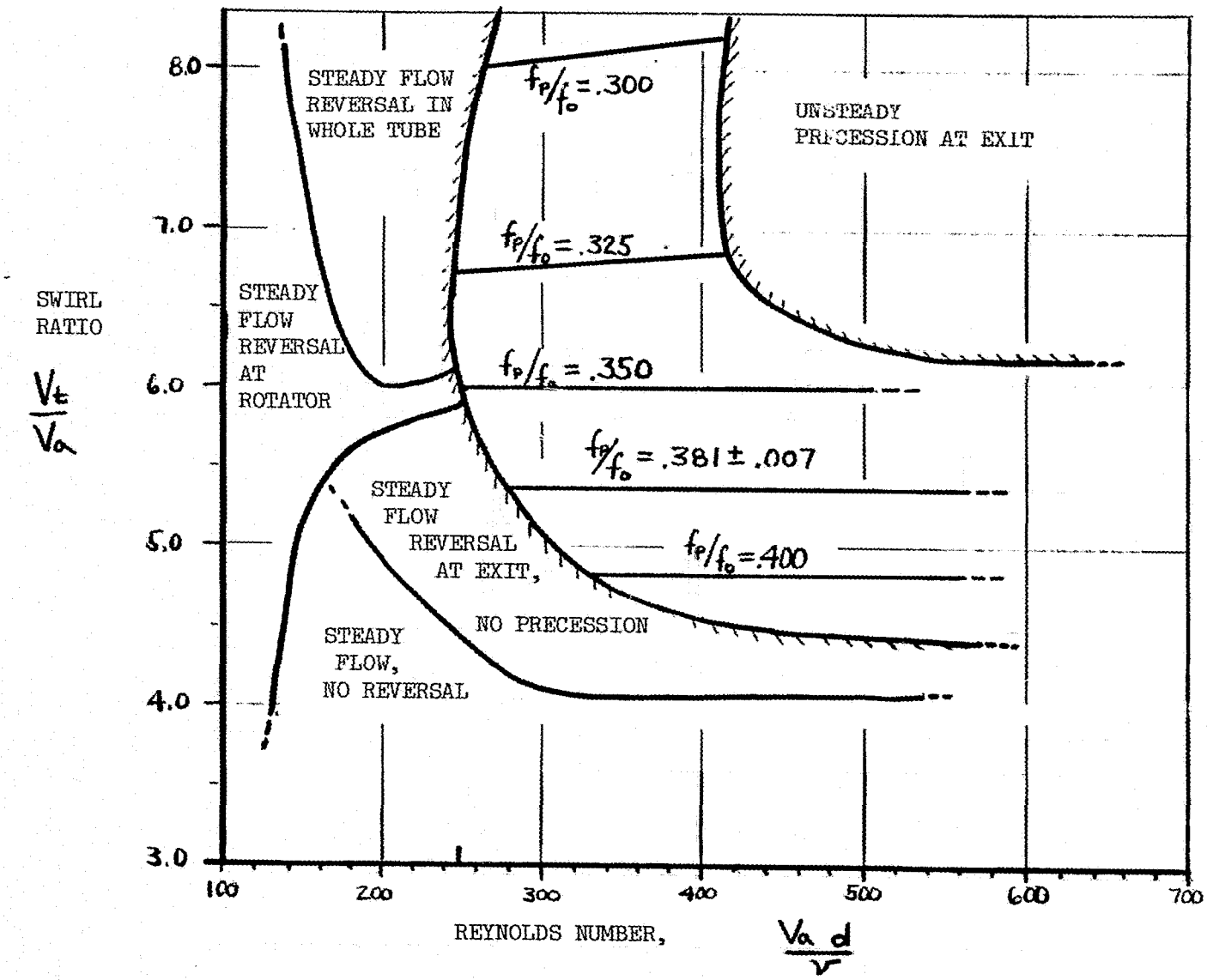

FIGURE 21 SWIRL RATIO VERSUS REYNOLDS NUMBER FOR THE LAB MODEL WITH 20D OF ROTATING TUBE UPSTREAM GENERATING SWIRL.

The preceding discussion leads from the discovery by Vonnegut to the patent and demonstration of a practical volumetric flowmeter by Channaud. This new type of flowmeter has no moving parts which is a distinct advantage over turbine and angular momentum types when considering reliability. Its dynamic range, linearity, independence of density, and signal output strength make it a candidate for a high accuracy flowmeter. Bailey (Ref. 14) makes a comparison of vortex precession and vortex shedding flowmeter's that may be of interest to the reader.

6.1.5 Improvements/Patents - As vortex precession flowmeters were put into use, attempts were accelerated to increase linearity, dynamic range, and signal to noise ratio and to even use signal amplitude for fluid density signals to make the device a mass-flowmeter. The following discussion lists the patents and summarizes the advancements made by each.

3,314,289 (A. Rodely, 1967)

Differential pressure sensors placed diametrically opposite so that the sum of the signals rejects static pressure variations and acoustic noise, and enhances the signal output. Piezoelectric crystals and other pressure sensitive transducers are covered.

3,434,344 (R. Brunner, 1969)

Three means of inducing flow reversal (instead of sudden expansion) are covered. One, a bullet shaped object is placed downstream of the swirl blades. Two and three: a flow inlet or outlet is placed in the tube center downstream of the swirl blades.

3,481,196 (A.. Rodely, 1969)

This patent presents data taken with a wedge-type hot-film anemometer placed at a matrix of points in the region where vortex precession occurs. The position for optimum signal-to-noise ratio is found to be 60% or more of the distance from the inner wall to meter center-line, axially placed at the point where rapid divergence starts. Signal amplitudes of 60 mv and signal-to-noise ratios of + 20 db are evident from graphs.

3,616,693 (T. H. Burgess, 1971)

This patent covers a unique approach to improving linearity from $\pm$ 5% to $\pm$ .5% over the same 100:1 range of Reynolds number. The technique involves preventing boundary layer separation on the backside of the highly curved blades, thereby maintaining constant swirl ratio. To do this, flow is gradually accelerated through the blades by tapering the inlet section and by progressively increasing blade thickness at the outer diameter in the downstream direction.

3,719,080 (T. H. Burgess, 1973)

A thermistor type vortex sensor is disclosed in this patent. The sensor assembly consists of a tube which traverses the flow passage at the start of rapid divergence. Inside the tube is a small thermistor bead fixed behind a flow focusing orifice. At both ends of the traverse tube are holes carefully oriented to produce internal flow oscillations via the precessing vortex. A claimed advantage to the design is protection of the fragile thermistor bead from the bulk of flow, and increased reliability and life.

4,010,645 (P. I. Herzl, 1977)

This covers a variation in the previously mentioned patent of the mass-flowmeter with vortex signal amplitude for density. In this case, the electronics are designed to determine if gas or liquid is flowing and to provide separate mass and volume information for each.

6.2 High Accuracy Design -

The General Electric concept for a vortex precession flowmeter meeting NASA's requirement for accuracy inherits the advantages of no moving parts, simple construction and frequency based output while it improves accuracy and density sensing with the addition of a microcomputer and General Electric's densitometer/viscometer, as shown in Figure 22.

6.2.1 Vortex Precession - Volumetric Meter - The vortex precession section consists of a fixed swirler to generate a swirl ratio of 5 to 6, a gradual 2:1 area reduction that is followed by a rapid expansion back to the inlet area, a differential vortex sensor like one of the previously mentioned types and a set of downstream straightening and pressure recovery vanes.

6.2.2 Densitometer/Viscometer - A densitometer is placed downstream of the vortex section along the meter axis. Density and viscosity information are obtained as described in Section 7.0. A temperature sensor is provided so that densitometer temperature sensitivity is compensated in the microcomputer.

6.2.3 Microcomputer - The capabilities of a microcomputer are employed to compensate the non-linearities of calibration versus Reynolds number, via the expression

$$\dot{m} = k\, fp\, \rho \quad \text{where} \qquad (6\text{-}1)$$

$$k = F\,(Re).$$

Interface electronics provide power and signal conditioning of the various sensor outputs and microcomputer inputs.

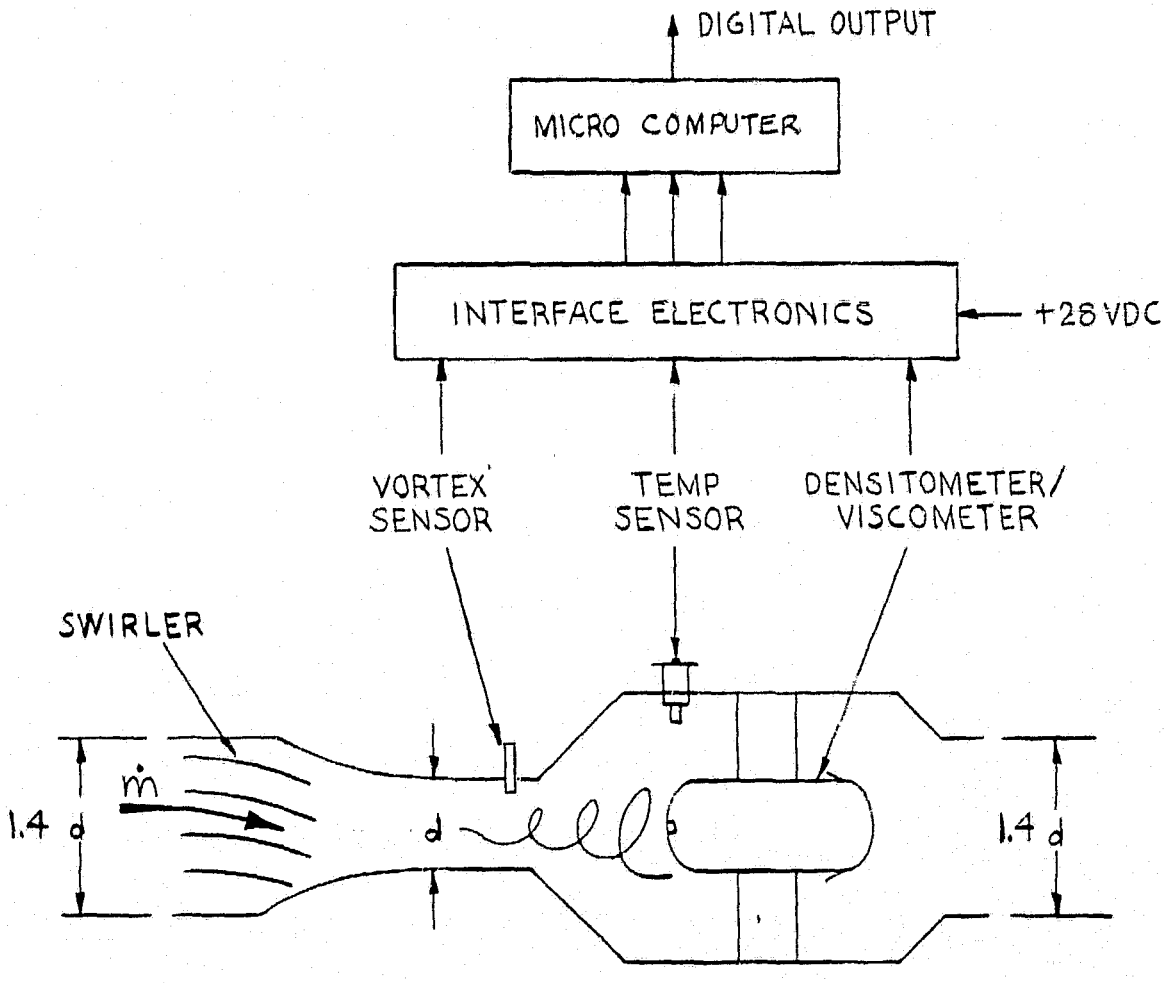

FIGURE 22 HIGH ACCURACY CONCEPT BASED ON VORTEX PRECESSION FLOWMETER.

6.3 Analysis of Performance -

The references cited in Section 6.1 provide the basis for designing and analyzing the vortex precession part of the conceptual model high accuracy flowmeter. In this section, we'll take closer looks at sizing, frequency range, time response, signal amplitude, and pressure drop and then look at certain tradeoffs and optimization. Swirler designs and sensor candidates will also be discussed.

6.3.1 Re Versus $\dot{m}$ and ν - Figure 23 is a plot of Reynolds number versus mass flow rate ($\dot{m}$) for viscosities ranging from .5 to 10 centistokes. The boxed region demonstrates the operational range of Reynolds numbers and is locked into the vertical position by the minimum Reynolds number of 300, occurring at minimum pph flow at 10 centistokes. This requirement also forces the meter diameter (d) to be no greater than 2.4cm (.93") at this flow condition (otherwise precession would not occur). A diameter less than this increases the Reynolds number at this flow condition and shifts the region upward. Specific gravity is assumed to be .90/for 10 Cs viscosity to simulated worst case cold conditions.

Shown in the right margin of Figure 23 are the operational ranges of previous units tested by Channand. Note that the new design must transcend all three: a fact that introduces some risk in the current undertaking.

6.3.2 f_p Versus $\dot{m}$ - Figure 24 is a plot of frequency of precession (fp) versus mass flowrate for various diameters. Again, shown in the right margin are the frequency ranges of units discussed in Section 6.1. Since this design closely resembles Channaud's 7.62cm (3.0") diameter fixed blade unit, the Strouhal number (S_π) used to obtain fp is the same as reported by him ($S_\pi = 5.0$). For the 2.4cm (0.93") diameter cubed. unit the frequency range is 10 to 500 Hz, with a calibration constant of 18kg/hr per hertz (40pph/hz).

6.3.3 f_p Versus d - Frequency of precession versus diameter is shown in Figure 25 to demonstrate the sensitivity of frequency range to diameter: ie, frequency of precession is inversely proportional to diameter.

6.3.4 Signal Amplitude Versus D - Experimental results on a Channaud's prototype meter (See 6.1.4) showed that static pressure variations generated by the precessing vortex is expressed by the equation,

$$\text{Psig (r m s)} \approx \rho V^2,$$

where V is the slower axial velocity through the inlet, upstream of any blades or taper. With a differential pair of sensors (to reduce noise) the effective signal is doubled. Figure 26 shows how the signal pressures at minimum and maximum flow rates rapidly increase as diameter decreases. In fact, signal pressure is inversely proportional to d^4. With maximum flow rates and diameters of 1.3cm (0.5") or less, static pressure can go below vapor pressure of fuel and cavitation ensue. This would be disastrous to accuracy and therefore must be addressed in future work, so that it can be avoided in the final design.

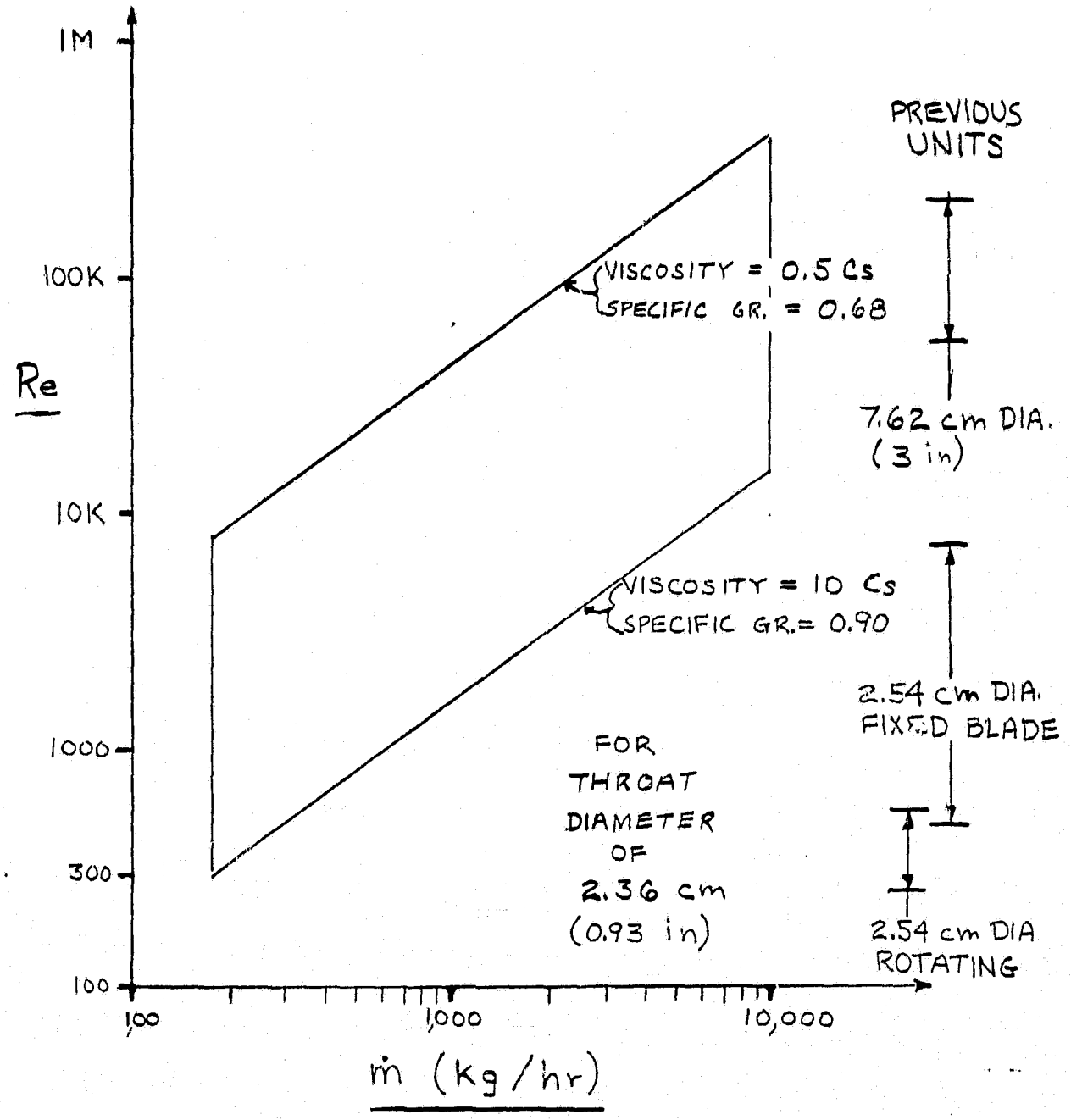

FIGURE 23 REYNOLDS NUMBER VERSUS MASS FLOW RATE AND VISCOSITY

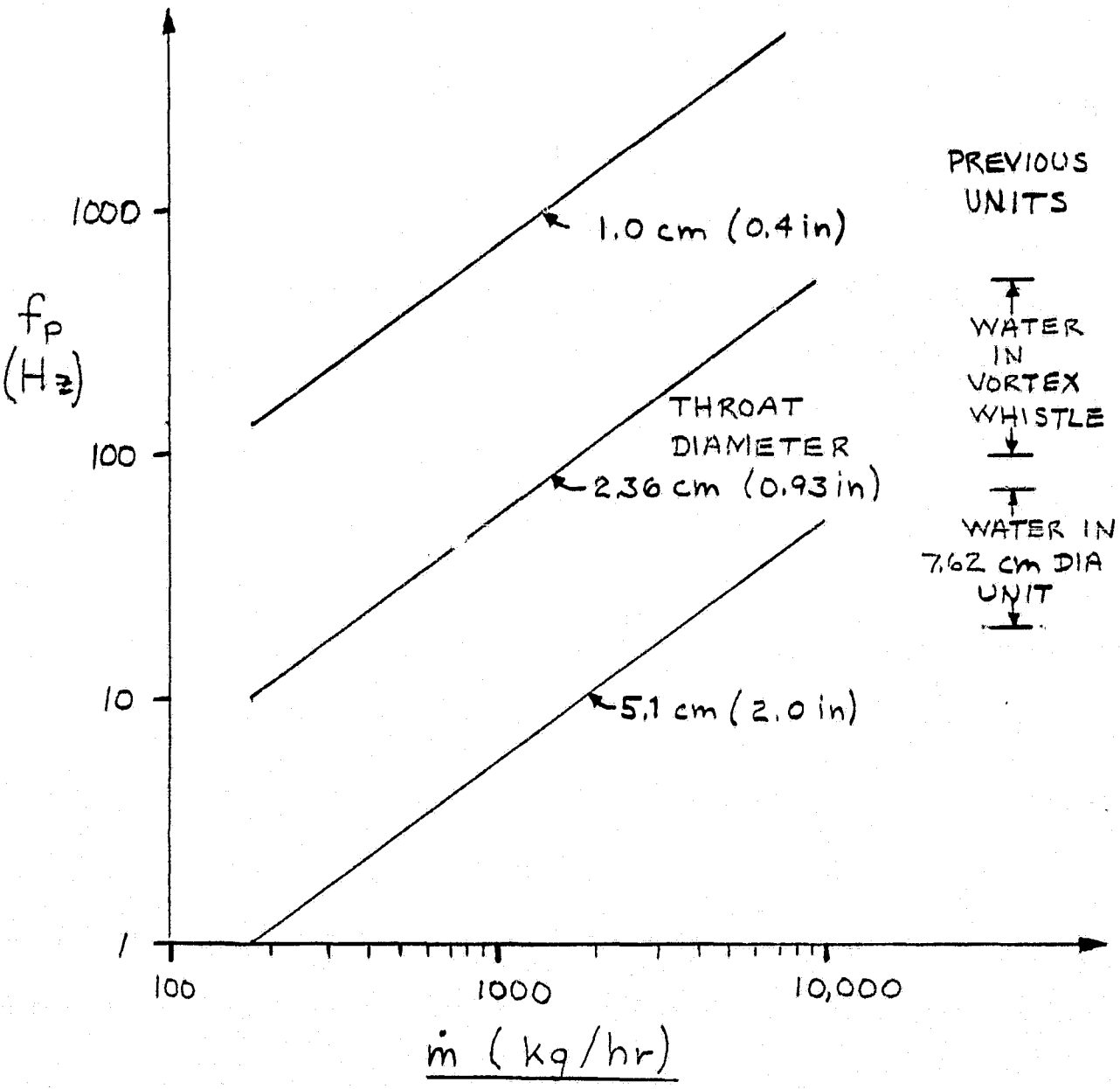

FIGURE 24 FREQUENCY OF PRECESSION VERSUS MASS FLOW RATE FOR VARIOUS DIAMETERS.

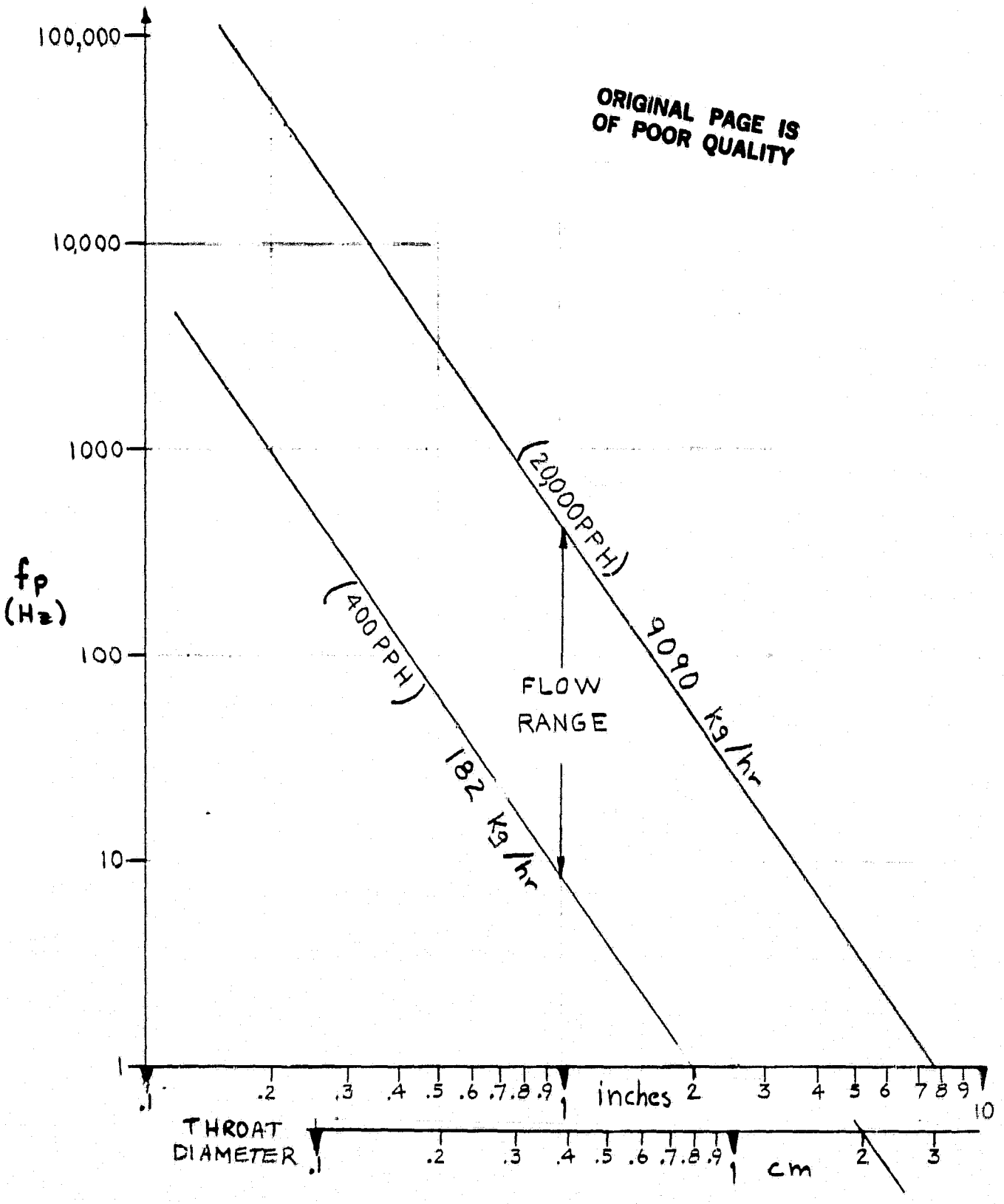

ORIGINAL PAGE IS OF POOR QUALITY

FIGURE 25 FREQUENCY OF PRECESSION VERSUS DIAMETER AND MASS FLOW RATE.

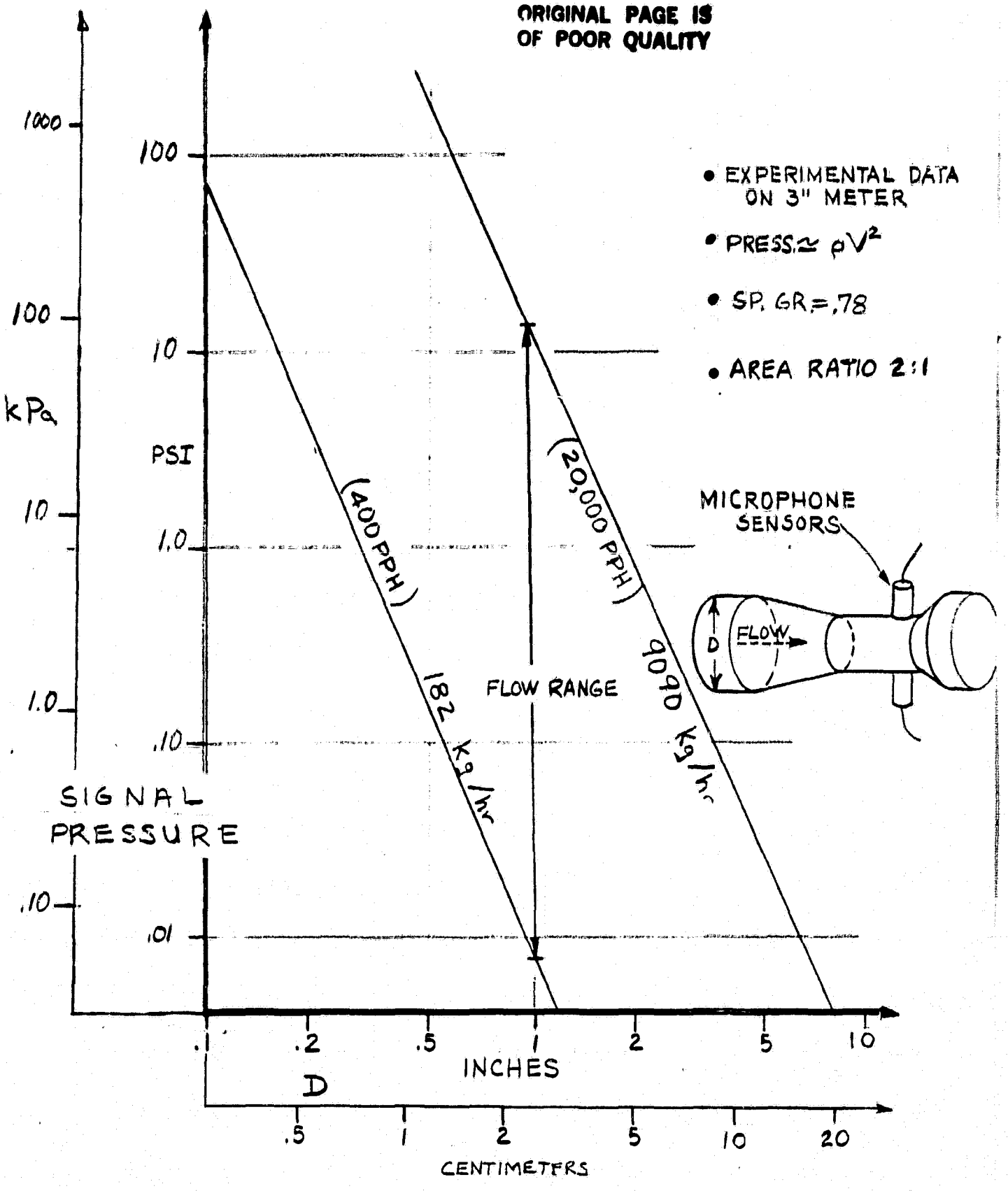

FIGURE 26 RMS SIGNAL PRESSURE VERSUS DIAMETER AND FLOW RANGE.

6.3.5 Response Time - When flow rate through the vortex generator undergoes a step change, the sensor output may appear as shown in Figures 27 a and b (a shows increasing step, b shows decreasing step). These responses are divided into four intervals where the following different lag mechanisms prevail: (1) transport lag; (2) vortex re-establishment; (3) pickoff of two new oscillation periods and(4) filtering. Of these four, transport and period sampling lags are readily analyzable whereas re-establishment and filtering lags can be ascertained only by conducting tests. However, filtering lag may be derived by assuming the frequency jitter of the new flow signal.

Transport lag has been derived for the contour shown in Figure 28. Simultaneous with the step change, axial velocity changes in regions 1,2 and 3 of the figure but tangential velocity remains constant and swirl ratio shifts, which in turn, perturbs the once steady vortex precession.

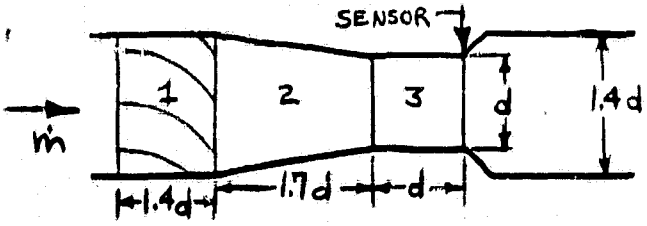

FIGURE 28- VORTEX PRECESSION METER CONTOUR FOR PURPOSES OF DERIVING TRANSPORT LAG.

The time it takes for a particle to travel from blade entrance to vortex sensor at the new flow rate is the transport lag time:

$$t(1) = \frac{1.4d}{V_1} + \frac{1.7d}{V_2} + \frac{d}{V_3}, \qquad (6\text{-}2)$$

where V_1, V_2 V_3 are the respective flow velocities in the regions numbered in the figure, and d is the throat diameter.

By the end of time t(1), a correct swirl ratio exits from the vortex generation region 3. The next interval, re-establishment, is unknown and t(2) is not evaluated here.

Once the vortex becomes strong and regular, it will require at most two periods to measure the new frequency of precession. This lag is expressed as:

$$t(3) = 2/\,fp, \qquad (6\text{-}3)$$

where fp is calculated assuming S_{tr} = 5.0; and fp = S_{tr} Va/πd

After t(1) + t(2) + t(3), the new flow has been measured but with an accuracy that depends on the regularity of precession and signal-to-noise ratio. Any jitter in the output frequency would constitute an instantaneous error when compared to a well filtered output. The filtering time t(4) needed to obtain an accurate reading depends on the amount of jitter, the signal frequency, and desired accuracy. Two approaches have been taken to evaluate filter time: statistical and digital filtering. The results are summarized below and the derivations appear in Appendix 10.2.

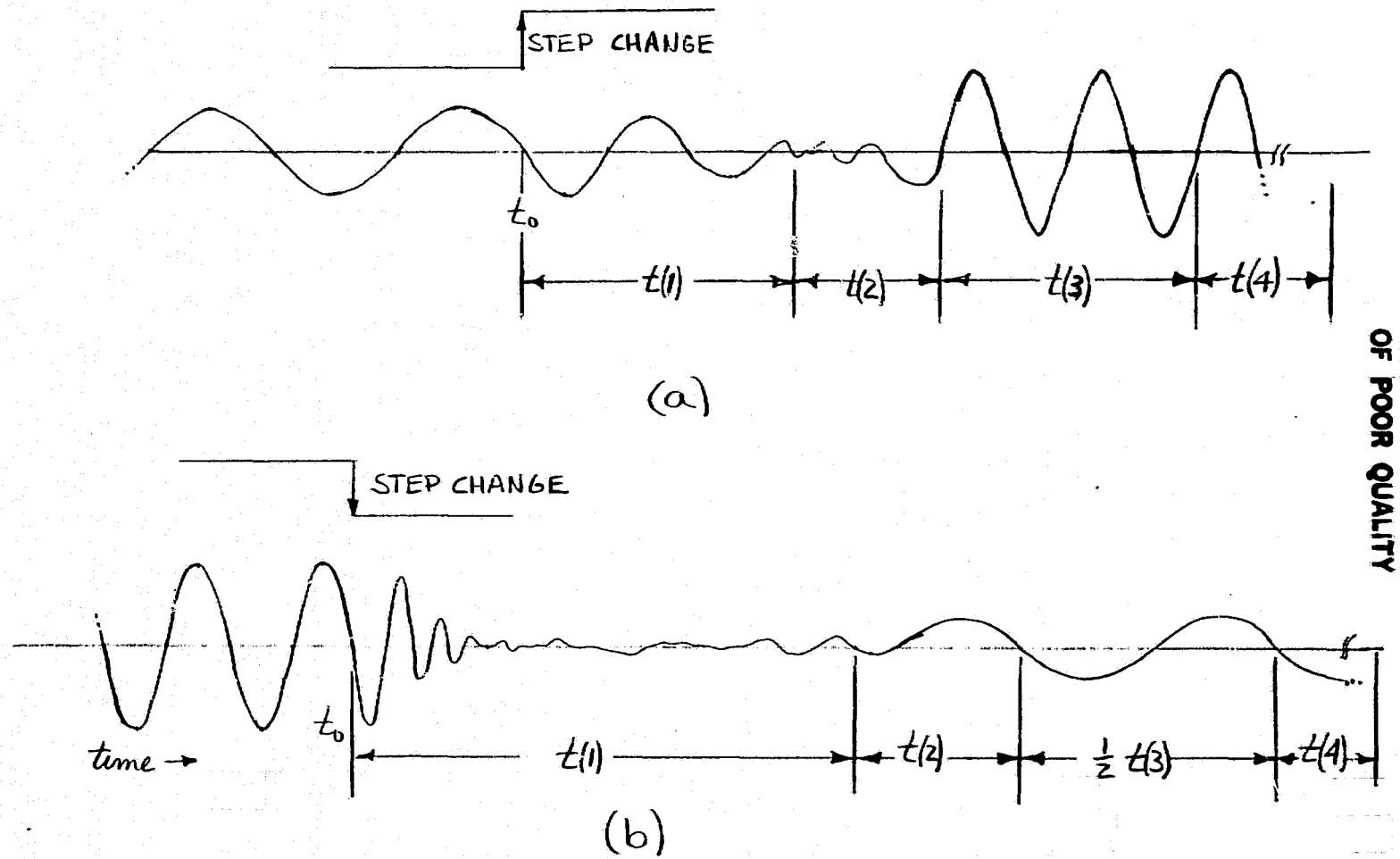

FIGURE 27 (a and b) SIGNAL OUTPUT OF VORTEX PRECESSION FLOWMETER IN RESPONSE TO STEP CHANGE (2:1) IN FLOW.

If we assume that at steady-state flowrate the frequency of precession has a normally distributed jitter about the mean frequency then we can employ statistical analysis to determine how long it will take to adequately filter the jitter and give an accurate reading of the frequency. If one assumes a 1.3% standard deviation for the degree of jitter (which has to be verified by testing later on) then the number of samples that are required to ensure less than 0.1% error of the mean with a confidence level of 95% can be calculated with a two-tailed test of variance. See appendix 10.3 for detailes of calculations.

If the flow rate is minimum, the precession frequency is about 10 Hz and the time to sample the precession frequency is the longest. About 650 samples of vortex frequency are needed. At a 10 Hz sample rate or frequency of precession, it takes 65 seconds to gather and smooth the data.

Another way to estimate the filter time constant is to find the time constant of a low-pass single pole R-C filter that attenuates noise (jitter) at and about the frequency of precession. This filtering would eventually be digital, but for now an analog representation provides for an easier analysis.

Again taking the minimum flow rate condition, where f_p =10Hz (and filter time constant is the greatest) and further assumming the noise is $\pm$1.3% of f_p (0.13 Hz) one can determine that 22.3 db attenuation of this noise is required to provide an output that is accurate to within 0.01%.

This is accomplished by placing the filter pole at 0.77 Hz. In steady-state operation the filtered output would meet the desired accuracy requirements with the given noies. A step change in flow-rate (and f_p) would require five time constants or 3.9 sec. to settle to the new value with insignificant error. See Appendix 10.3.2 for detailed analysis.

The expression for the sum of transport and period lags can be obtained by letting V_2 = average of V_1 and V_3, by letting $V_1 = 2\dot{m}/\pi\rho d^2$ in equation 6-2; by letting $V_a = V_3$ in equation 6-3 and by summing the two equations. The resulting expression gives an indication of time-response as diameter, and flow-rate are varied and is as follows:

$$t(1) + t(3) = (429.48 + 112.3)\, d(in)^3 / \dot{m} \quad (pph)$$

with sp. gr. = .80.

For d = 2.36 cm (0.93") and $\dot{m}$ = 182 kg/hr (400 PPH), t(1) + t(3) = 1.09 sec,

and for $\dot{m}$ = 9090 kg/hr (20kPPH), t(1) + t(3) = 0.22 sec.

Decreasing the diameter rapidly decreases these time lags, but to obtain .025 sec. response at 400 pph flow would require a diameter of .067cm (0.264 in). Going this small is not possible because flow velocities become extreme (Re = 1.6 X 10^6) precession frequency would hit 30K Hz, and signal pressure would go in excess of 6900 KPa (1000 psi) at maximum flow (according to the preceding graphs), not to mention adverse pressure drop. Note that the above estimates do not include the times to filter or to re-establish the vortex. Actual overall time response needs to be verified by experiment in continuing efforts.

6.3.6 Pressure Drop - At maximum flow and viscosity, pressure drop is estimated to be 11 psi by adding three factors: 1) velocity head loss of swirling flow 2) skin friction and 3) venturi action. The first predominates and according to Cahnnaud's experiments on protype meters is

$$\Delta P = 4 (\rho \, Va^2 / 2) , \qquad (6\text{-}4)$$

or four times the velocity head through the smaller diameter. For a swirl ratio of 5, this says that one fifth is regained at the deswirl vanes and four fifths is lost. It amounts to 9 psi loss. Skin friction and venturi action account for 2 psi loss, and are estimated with a model having d=2.36 cm (0.93") and having the geometry shown if Figure 28, and not having any swirler (ie, straight venturi tube).

Pressure drop increases rapidly as diameter is decreased ($P \approx 1/d^4$).

6.3.7 Tradeoffs In Design - In the preceding, basic parameters of performance are functions primarily of diameter, and mass flowrate. Table 10 summarizes the desirable and undesirable effects of decreasing diameter. In the future, when the interactions of these parameters are better understood including what limits there are on each, the design may be optimized.

6.3.8 Down Sizing (3000 pph Meter) - A 6.7 fold reduction in flow range requires first of all, a proportionally smaller diameter device to maintain Reynolds number above the lower critical value. As a result, precession frequency increases (by 6.7^2). Signal pressure may decrease slightly. Repeatability and linearity would be affected by the smaller sized transducers and perhaps manufacturing tolerances on smaller pieces. Certainly a unit with this flow range would need to be tested to verify these effects.

6.3.9 Sensor Candidates - As can be seen from Figure 26, the dynamic range of the pressure signal is 2500:1. Quartz, strain gage, and piezoelectric pressure transducers have this capability provided they are operated differentially and care is taken to minimize electrical noise. Differential operation means freeing the sensitive element from static pressures up to the proof or maximum operating pressure. With sensitivities of 100 mv/psi the expected signal voltage (r m s) would vary from 100 μV at 182 Kg/hr (400 pph) to 200 mV at 9090 Kg/hr (20,000 PPH).. Figure 29 shows such a sensor arrangement. Care must be taken in sizing the fluid passages so as not to limit frequency response by the mass of fluid column acting in conjunction with sensor elasticity.

Hot film anemometers have been used in laboratory evaluations and commercially available vortex meters. It is difficult, however, to get anemometer circuitry to operate dependably over wide ranges of environmental and functional conditions. To maintain constant sensor temperature above fuel temperature, and thereby assure sensitivity over the temperature range, fuel temperature would need to be measured via a coefficient matched probe. An explosion hazard is generated with the high currents available to heat the sensor. Reliability is always a risk with this type of sensor.

TRADEOFFS IN DECREASING DIAMETER

DESIRABLE	DECREASES TIME RESPONSE	$\left(\frac{1}{d^3}\right)$
	INCREASES SIGNAL PRESSURE	$\left(\frac{1}{d^4}\right)$
	INCREASES R_E AT LOW FLOW	$\left(\frac{1}{d}\right)$
UNDESIRABLE	INCREASES F_P (UPPER LIMIT?)	$\left(\frac{1}{d^3}\right)$
	INCREASES R_E AT HIGH FLOW POSSIBILITY OF CAVITATION	$\left(\frac{1}{d}\right)$
	INCREASES PRESSURE DROP	$\left(\frac{1}{d^4}\right)$

TABLE 9 TRADEOFFS IN DECREASING THE DIAMETER OF THE VORTEX PRECESSION.

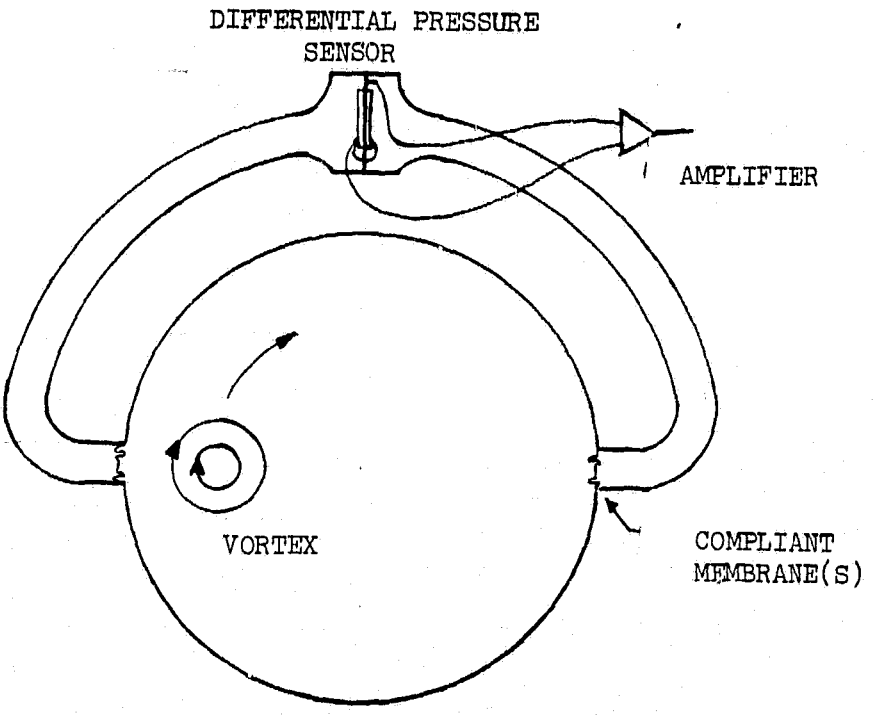

FIGURE 29 ONE CANDIDATE OF DIFFERENTIAL STATIC PRESSURE SENSOR FOR THE VORTEX PRECESSION METER.

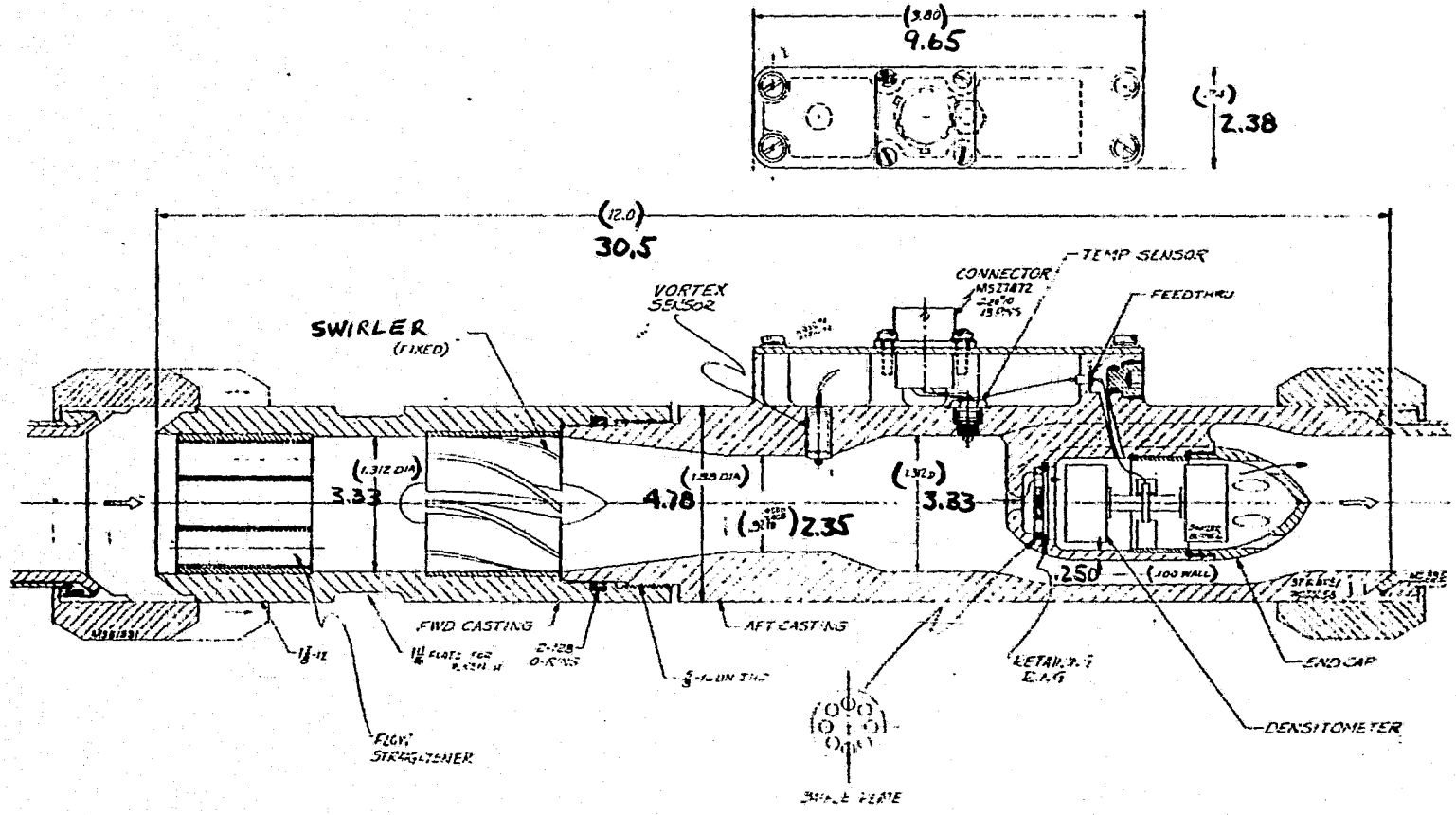

FIGURE 30 CONCEPTUAL DESIGN LAYOUT OF VORTEX PRECESSION MASS FLOWMETER

Force sensitive cantilever beams such as those developed by Krause and Fralick (Ref. 15) would be very responsive to a passing vortex but would require shielding to prevent unwanted oscillations resulting from a Von Karman vortex street shedding from the beam.

6.4 Conceptual Design Layout -

Figure 30 is a reduced copy of the conceptual design layout drawn as part of Task 6 of Phase I. The fore and aft bodies are shown as separate castings screwed together and pinned at assembly, with the swirler captured between. Flow straightening tubes are placed at the inlet to smooth out gross swirl and turbulence created by upstream pipes, but may be eliminated (along with the whole forward casting) provided tests show them to be unnecessary. A single vortex sensor is shown at the approximate best axial position.

A differential pair is most likely and would require additional material opposing that already shown for the connector and sensors. The swirler exits at 45° and uniformly accelerates fluid tangentially (parabolic shape) and generates a swirl ratio of 1. The exit angle will most likely be increased to 78° to 80° to generate swirl ratio of 5. Extensive experimentation with swirler designs will be required to gain insight to critical parameters such as swirl ratio (exit angle), blade curvature, thickness, lean angle and hub-to-tip ratio. Tangential inlets like those in Vonnegut's whistle may perform well.

The venturi contour gradually tapers to half the upstream area and expands rapidly back to the inlet area to create flow reversal. Again, optimization of this contour can be carried out only through experimentation. Downstream of the vortex section is the densitometer housing, centrally located so that the support webs act as flow straighteners. Flow through the housing is controlled by a central hole at the nose, followed by a baffle plate which slows and distributes the flow, and by holes in the aft cap section which let air bubbles out. The densitometer/viscometer itself slips into the cavity from the rear and is held in place by an end cap after the three leads are soldered to ceramic feed throughs. The temperature sensor, a flush mounting RTD, screws into the aft body inside the connector housing.

6.5 Accuracy Analysis -

Linearity of this device is not of prime consideration because the microcomputer can characterize almost any smoothly changing, single valued function. However, it is very desirable to make the device as linear as possible so that extreme accurate measurement of viscosity and temperature is not required to compensate and recover the desired accuracy. Of prime importance is repeatability. Vortex precession meters available for measurement of gas flow rates are claimed to be repeatable within $\pm$ .1% of rate. Table 11 includes this source of variability along with others to obtain an overall root-sum-square estimate for the system. Repeatability for this design is estimated at 0.15% of flow because of the increased dynamic range. The computer time base, over the temperature range, is estimated to vary $\pm$ .05%. The computer algorithm for compensating Reynolds number dependence will not be exact but can be accurate to .05% of rate by

ANALYSIS OF ACCURACY

- ASSUME 2σ LEVELS SPECIFIED
- ASSUME BIASES REMOVED IN CALIBRATION
- RANDOM ERRORS ONLY

	ERROR SOURCES	ESTIMATES %	COMMENT
Q			
	REPEATABILITY	0.150	±0.015 Hz AT LOW FLOW
	TIME BASE	0.050	±0.005 Hz AT LOW FLOW
	COMPUTER ALGORITHM	0.050	
	SAMPLING ERROR	0.100	ASSUMING 1.3% VARIATION IN F_P, 95% CONF., 1 MIN.
	VISCOSITY DEPENDENCE	0.050	ASSUMING 1% LINEARITY AND 10% VISCOSITY ERRORS
ρ	DENSITOMETER	0.122	
	RSS	0.23	

TABLE 10 SUMMARY OF CONTRIBUTING FACTORS IN ANALYSIS OF ACCURACY OF THE VORTEX PRECESSION FLOWMETER.

providing enough constants for a polynomial to follow all inflections in calibration data, or by providing enough data points so that interpolation is accurate. Sampling error and time constant are related (Section 6.3.5) and depend on the degree of variability (jitter) in the vortex signal. A statistical approach (See Appendix 10.2) indicates when the standard deviation of jitter in fp is ± 1.3%, that a 0.10% of rate accuracy is attained by averaging 600 samples.

Viscosity dependence is estimated with a linearity curve from U.S. patent 3,616,693, Figure 7. The curve shows a .5% shift in calibration for a 100% change in Reynolds number. When viscosity data ± 10% in error is used to figure Reynolds number, it will result in ± .05% of point error in calibration constant (10% X .5%). Viscosity data of this quality is expected (See Section 7.4). Lastly, the densitometer contributes .12% of point error (See Section 7.4).

All of these sources are independent and can be root-sum-squared to obtain total mass-flowmeter accuracy, as shown on the table. The vortex precession concept meets the required accuracy limit of .25% with some margin. Two contributing factors -- repeatability over the Reynolds number range and variability or jitter of the vortex signal -- were based on limited data from literature and therefore have a high risk of exceeding the above estimates. Confidence in actual capabilities must be gained through experimental work in continuing phases of development.

6.6 Specification Conformance -

Refer to Table 12 for a summary of how this conceptual design conforms to specification.

6.7 Problem Areas & Further Work For Phase II -

Table 13 is a prioritized list of problem areas for the vortex precession part of the flowmeter system. Alongside each problem area is the recommended approach to solving the problems.

Table 11 CONFORMANCE TO SPECIFICATION

	Requirement	Performance
Accuracy	±0.25% of flowrate maximum error	Meets requirement
Response Time	0.025 sec.	Exceeds Req: 1.09 sec. at min. flow; 0.022 sec. at max. flow.
Size	30.5cm (12.0") Long 11.43cm L x 7.62 cm H x 3.0 cm H side	Within evelope
Weight	Less than 5 KG	Meets requirement
Vibration	15 g	Bearingless, no rotating parts - low risk
Burst Pressure	10,000 kPa (1500 P.S.I.)	Meets Req: electrical header is the only critical area.
Fuel Temperature	-55°C to 130°C	Meets Req: parts will be designed to withstand
Pressure Drop	68 kPa (10 P.S.I.) Max.	Meets Req. with present concept. Some risk of exceeding as design matures
Failure Mode	No effect on engine performance	Meets Req: few parts in flow stream
Power	28 VDC	10 watts max. for heat transfer sensor, other types less. Temp. sensor - 50 milliwatts; Densitometer - 6 milliwatts.
Pressure Pulsations	± 2% of fuel pressure	Dependent on vortex sensor Type: Pressure sensor design will be designed for insensitivity.
Mounting and Position Sensitivity	37° flare tube; unaffected by attitude	Meets Req: no rotating parts
Overrange Capability	125% of full scale	Meets Req: swirler blades strengthened

Table 12 PROBLEM AREAS AND FURTHER WORK

1. VORTEX GENERATION	
Max. Re before cavitation Min. Re for precession Range of f_p - upper limit	o Evaluate plexiglass models with dye injection, strobe flash, high-speed movies, anemometers and pressure sensors.
Swirler design for ratio of 5-6 Geometry (area ratio, contours) Theories of operation	o Computer aided design of swirler.
2. SENSOR DESIGN	
S/N ratio Dynamic range Optimal placement	o Evaluate candidate sensors in best swirler.
3. REPEATABILITY	
.15% over range of Re	o Evaluate on best swirler/ sensor comb.
4. CALIBRATION CURVE	
Characteristics over Re What accuracy of viscosity info.	o Evaluate in lab.
5. TIME RESPONSE	
Does not meet requirements	o Confirm predictions in lab. tests

6.8 Nomenclature

D	Inlet diameter
d	Throat diameter
f_o	Frequency of base swirling flow upstream of precessing vortex
f_p	Frequency of vortex precession
k	Constant
$\dot{m}$	Mass flowrate
Psig	Pressure signal of precessing vortex
Re	Reynolds number
Re_{CR}	Critical Reynolds number
R_{on}	Rossby number
S_{tr}	Strouhal number
SP.GR.	Specific Gravity
t(1)	Transport time lag
t(2)	Re-establishment time lag
t(3)	Sampling time lag
t(4)	Filtering time lag
V	Axial velocity at inlet
V_a	Axial velocity in throat
V_t	Tangential velocity at outer radius
V_1	Axial velocity in inlet
V_2	Axial velocity in transition between inlet and throat
V_3	Axial velocity in throat
ρ	Density
ν	Kinematic viscosity
ΔP	Pressure drop

7.0 DENSITOMETER-VISCOMETER

7.1 Introduction -

The turbine and vortex precession flowmeters (Section 5.0 and 6.0) are basically volumetric and require precise density and approximate viscosity data to perform as mass flowmeters. This section covers the details of a densitometer/viscometer compatible with both type meters. General Electric currently produces a densitometer that oscillates at a frequency determined by fluid density. With the techniques to be described, viscosity data are derived from the same device.

7.1.1 Description of Densitometer - Figure 31 is a conceptual drawing of the densitometer being considered here. Two couplers joined via a spring vibrate in torsion 180° out of phase (opposite rotation at any instant). Piezoelectric crystals sandwiched between spring ends and each coupler pickoff torsional stress or drive the system into oscillation. Natural frequency decreases as coupler moment of inertia increases with increased fluid density. It is supported at the central nodal point so that no energy is transmitted to the three mounting tabs. Operational frequency is well above the normal range of environmental vibration (greater than 2K Hz). Ceramic couplers and Ni-Span-C spring, carefully heat treated, reduce its temperature sensitivity to less than 1/2% over the temperature range.

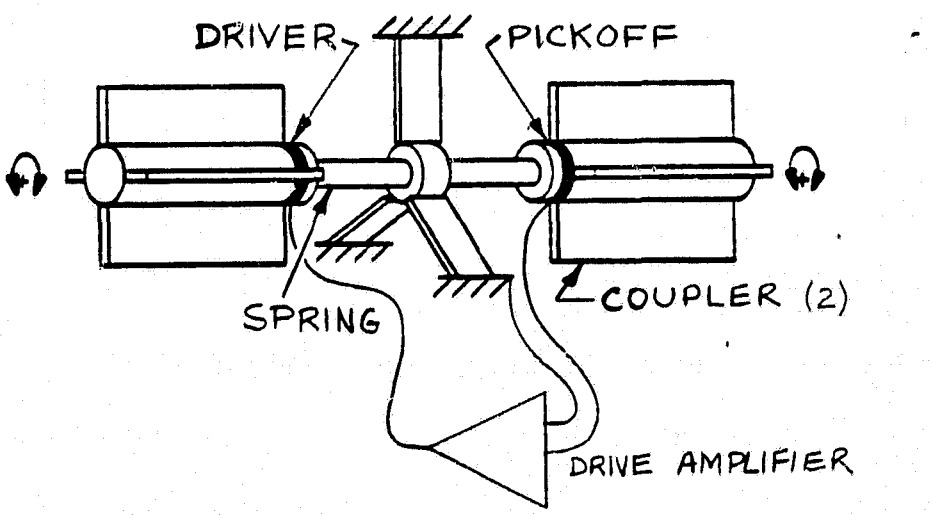

Figure 31 Densitometer Concept

The mechanical system has very low internal damping (high Q*) and is operated in a closed loop by a driving amplifier. Gain and phase characteristics of this amplifier are carefully tailored to ensure startup and resonance at the correct frequency.

Depending on fluid viscosity, the Q of the device may range from 60 to 300 and is greater than 1000 in air. High viscosity, in addition to lowering Q, tends to form a thicker boundary layer of fuel that is moved by the outer coupler surface thereby increasing coupler inertia and lowering natural frequency. To compensate for these effects (make frequency independent of viscosity), the phase of the driving amplifier is given about 45° lead. Detailed analysis of this technique is presented in Section 7.3.3.

7.2 Densitometer-Viscometer Concept -

The effect which viscosity has on the frequency response of the spring-mass system can be measured and used to determine fluid viscosity. To do this the mechanical resonator of the densitometer is retained and the simple loop-closing electronics are almost entirely replaced by more sophisticated driving and phase control circuits that provide a signal from which viscosity and density are calculated in the microcomputer. It is actually Q which is first derived from the circuit output; the relationship of viscosity to Q is measured and stored via the microcomputer algorithm. Density is calculated from the operating frequency.

A temperature sensor is provided to compensate for thermoelastic coefficient of the spring material and coefficient of thermal expansion of the coupler material. Although the spring and coupler materials are carefully selected and heat treated to minimize overall temperature sensitivity, the requirements for high accuracy dictate that any temperature sensitivity be nullified.

7.3 Analysis -

In this section an equivalent circuit analysis will be used to show how Q may be measured. The similarity of electrical and mechanical opproaches will provide insight into the technique that is to be used.

7.3.1 Electrical Equivalent Circuit - The densitometer-viscometer may be described by the differential equation,

$$J\frac{d^2\theta}{dt^2} + D\frac{d\theta}{dt} + K = \tau \qquad (7\text{-}1)$$

where:
- J = moment of inertia
- θ = angle
- t = time
- D = damping constant
- K = spring constant
- τ = torque

* Q is the reciprocal of the structural damping ratio.

The electrical circuit of Figure 32 may be described by the differential equation,

$$L \frac{d^2q}{dt^2} + R \frac{dq}{dt} + \frac{q}{C} = E \qquad (7\text{-}2)$$

where:
- L = inductance
- q = charge
- t = time
- R = resistance
- C = capacitance
- E = voltage

Equation (7-1) has the same form as that of equation (7-2). The analogous parameters are listed in Table 13.

TABLE 13

Analogous Mechanical and Electrical Parameters

Mechanical	Electrical
J moment of inertia	L inductance
θ angle	q charge
D damping constant	R resistance
K spring constant	1/C reciprocal of capacitance

Equivalency of the resistive and reactive parts of viscous impedance ($\omega L_V = R_V$) is fundamental to the concept that fluid viscosity can be ascertained by measuring Q. This equivalence is derived by Landau and Lifshitz (Ref. 16) and is further discussed by Wenger (Refs. 17 and 18). The inductive or inertial reactance is derived with the expression for boundary layer thickness on an oscillating surface: thickness $\propto \sqrt{\text{viscosity/frequency}}$.

Equations (7-1) or (7-2) and Figure 32 adequately represent a densitometer-viscometer measuring a nonviscous fluid. But when the fluid is viscous, the electrical equivalent circuit of Figure 33 is more appropriate. In Figure 33, there are three inductances. Lo represents the constant coupler inertia. L_D represents the additional inertia due to the liquid entrapped by the coupler, when the liquid is nonviscous. Lv is an addition inertia which is present when the liquid is viscous. The inertia Lv is nonlinear in that its reactance is equal to the resistance Rv arising from the viscosity of the liquid. C_o represents the spring and R_F represents the mechanical friction apart from the viscosity of the liquid being measured. By the use of the equivalent circuit of Figure 33, the operation of the densitometer-viscometer can be deduced.

C-2

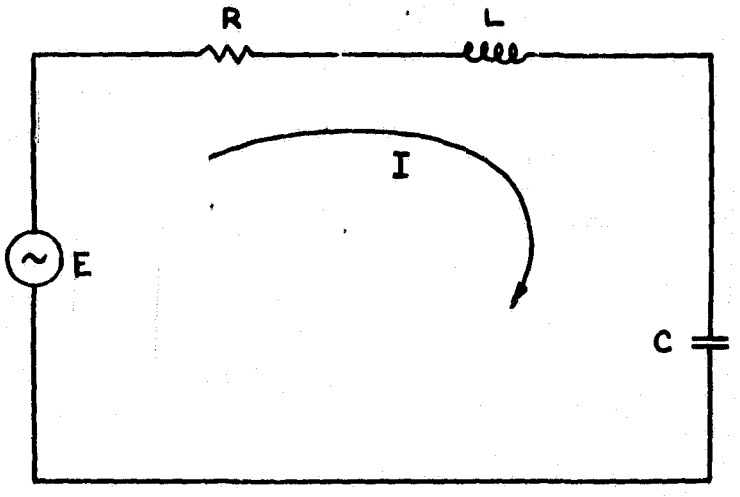

FIGURE 32 ELECTRICAL CIRCUIT

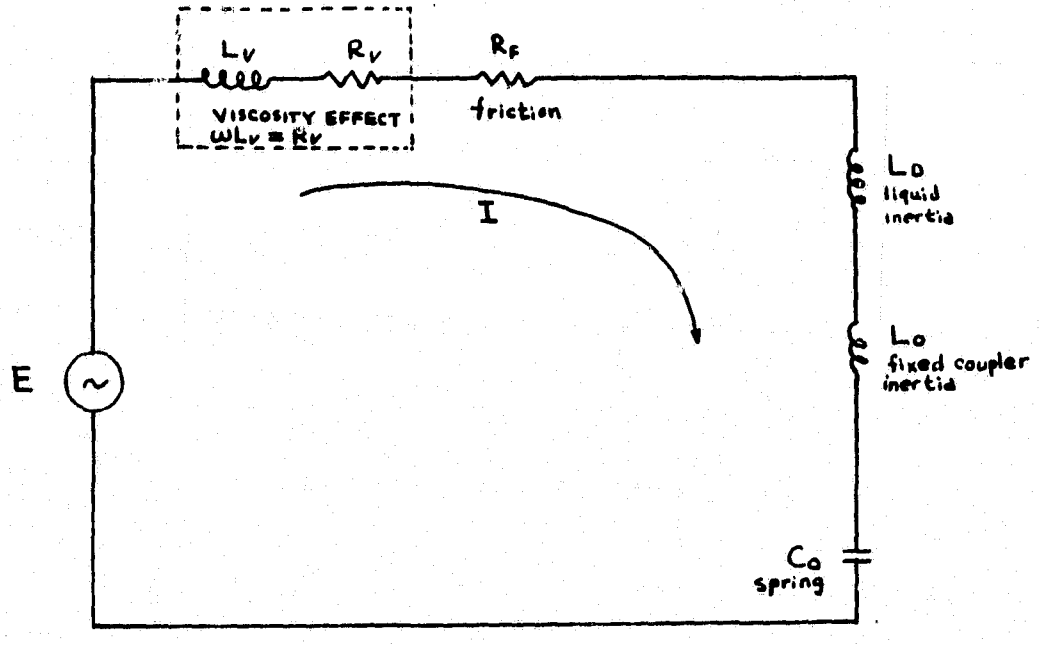

FIGURE 33 ELECTRICAL EQUIVALENT CIRCUIT OF DENSITOMETER

In its practical implementation, the mechanical friction, RF, is small enough to be neglected. In the discussion which follows, R_F is assumed initially to be zero. Then to measure the density of the liquid by means of the frequency of the excitation, one way would be to set the frequency at a value when

$$\omega (L_D + L_O) = 1/\omega C_O, \qquad (7\text{-}3)$$

so that the inductive reactance of the combined coupler and liquid inertias cancels the capacitive reactance of the spring, leaving only the impedance due to viscosity, $\mathbf{Z}_V$:

$$\mathbf{Z}_V = R_V + j\omega L_V \qquad (7\text{-}4)$$

If $wL_V = R_V$ then

$$Z_V = R_V + jR_V$$

$$Z_V = \sqrt{2}R_V \quad \angle 45^\circ$$

Since the current follows the equation

$$I = \frac{E}{\mathbf{Z}_V} = \frac{E}{\sqrt{2}\, R_V \angle 45^\circ} \qquad (7\text{-}5)$$

, or

$$I = \frac{E \angle -45^\circ}{\sqrt{2}\, R_V},$$

it lags the voltage by 45°.

The frequency where the above conditions exist (Equations 7-3, 7-4, 7-5) is then determined by measuring the phase relationship between the current and the voltage. It is the right frequency when the current lags the voltage by 45° under the assumptions taken. In any actual densitometer-viscometer, the angle may differ from 45° by a few degrees.

In order to better demonstrate how a densitometer-viscometer operates the next sections will focus on a specific spring-mass system having a resonant frequency in vacuum of 4600Hz. Since small changes in frequency determine density and viscosity, the performance equations carry nine significant figures.

7.3.2 Frequency Versus Specific Gravity - The resonance frequency of a densitometer in a nonviscous fluid (or the desired frequency in a viscous fluid) is found by.

$$F = \frac{1}{2\pi}\left(\frac{K}{I_O + I_D \times SG}\right)^{1/2} \qquad (7\text{-}6)$$

where: F = frequency
K = spring constant
I_O = coupler inertia
I_D = effective nonviscous fluid inertia of fluid with SG=1.0
SG = specific gravity

To give concrete values, equation (7-6) is given the following values:

$$F = \frac{1}{2\pi}\left(\frac{835363320.}{1 + 0.819580375 \times SG}\right)^{1/2} \qquad (7\text{-}7)$$

F is equal to 4600 Hz for a vacuum, and is equal to 3600 Hz when the fluid specific gravity is .772. Equation (7-7) is plotted in Figure 34. Over a specific gravity range of 0.6 to 1.0, the curve is linear to ±6.6 hertz, or ±0.01 specific gravity. The slope of frequency versus specific gravity at a specific gravity of 0.772 is 921 hertz per unit specific gravity.

7.3.3 Effect of Viscosity on Frequency Response - When the fluid is viscous, the effect of the viscosity is to increase the damping and inertia, so that the response to a given torque is lower and the resonance frequency is lower for increasing viscosity. In Figure 35 the effect of viscosity upon resonance frequency is shown.

Plotted is a family of four curves for fluids of the same specific gravity (SG = .772) but different viscosities. The influence of viscosity is reflected in the Q of the system with a high Q for low viscosity. The Q varies from a low value of 62 to a high of 500. The response is the current I in Figure 33 normalized to be equal to 1 at a frequency of 3600 Hz. Rf has been set to zero. That being the case, 3600 Hz is one of the half power frequencies. The maximum responses for all curves are then all equal to the square root of 2. It is evident in Figure 35 that the resonance peak frequency becomes progressively lower as the Q becomes lower (viscosity increases).

7.3.4 Effect of Viscosity on Phase Shift - In addition to the lowering of the resonance frequency with increasing viscosity the phase shift of the velocity (current) with respect to the exciting torque is also affected. Figure 36 is a plot of the phase shift of the current with respect to the excitation voltage of the circuit of Figure 33 for various Q's, again with Rf set to zero. It is seen that the higher the Q (lower viscosity) the steeper the change of phase shift versus frequency.

7.3.5 Modulation Vectors - To determine the density of fluid, it is necessary to excite the densitometer at such a frequency until a proper phase shift between the velocity and torque occurs. That frequency then gives the correct indications of the density. An alternate method would be to measure the amplitude of the response at the resonance frequency and then measure the frequency at the upper half power (or whatever ratio as appropriate) point. Of the two methods, the first is more straight forward in implementation.

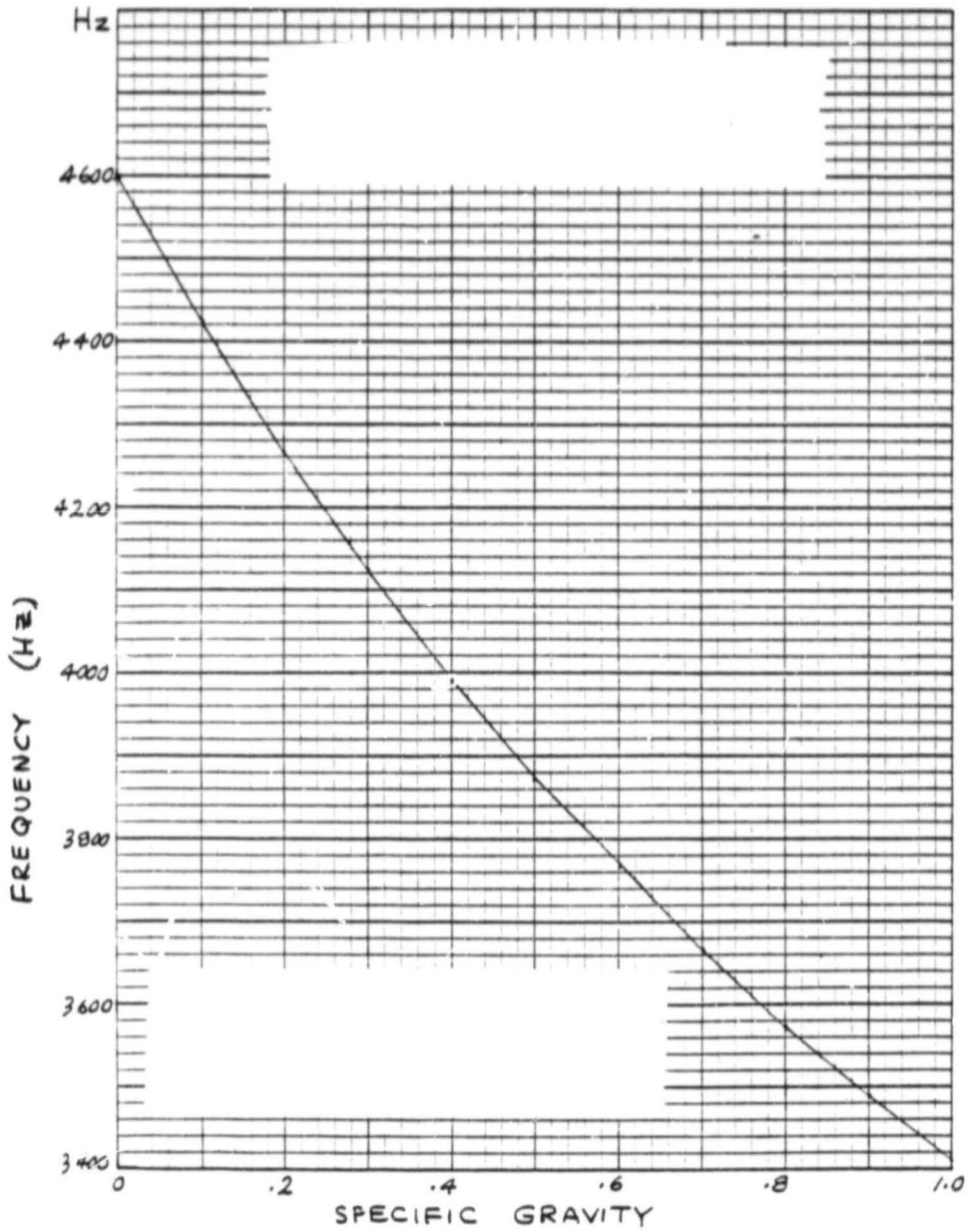

FIGURE 34 DENSITOMETER FREQUENCY
VS SPECIFIC GRAVITY

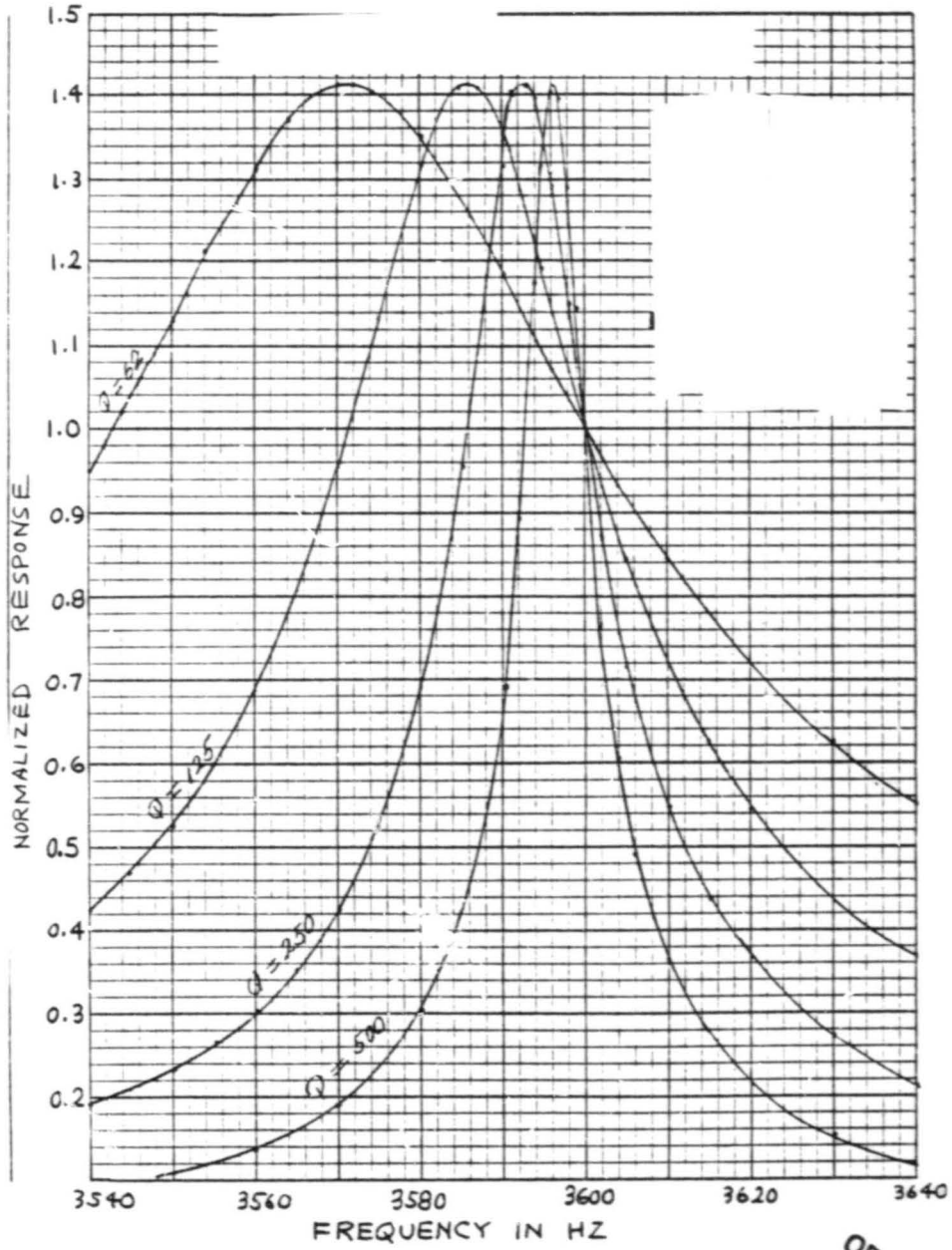

FIGURE 35 EFFECT OF VISCOSITY ON RESONANCE FREQUENCY

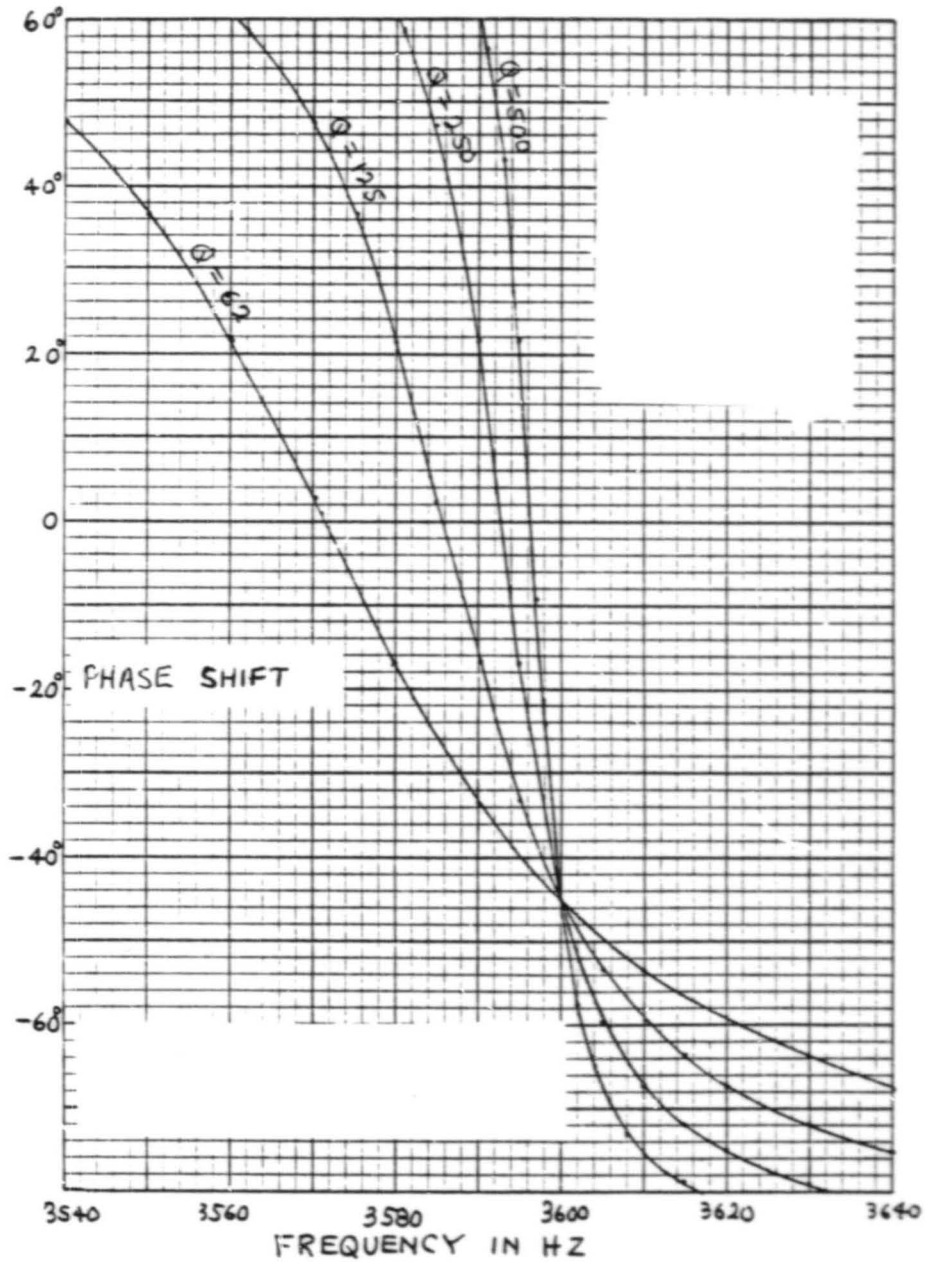

FIGURE 36 EFFECT OF VISCOSITY ON PHASE SHIFT

To determine the Q of the system, so as to determine the viscosity, one may measure the voltage E in the equivalent circuit of Figure 33 to induce a current I of a known amplitude at a prescribed phase angle between the current and voltage. An alternate method is to measure the frequency difference for a known phase difference about a nominal phase (Refs. 16, 17). The first method is simple but does require the measurement of amplitudes of excitation, a process which cannot be done as precisely as the measurement of time. The alternate method requires the operation of the system at two separate phase angles but it has the advantage of needing to measure only frequency and not amplitude measurements.

Another advantage of the alternate method can be obtained if the modulation of the phase is coupled with a modulator of the amplitude in such a way that the response of the current is constant at both operating points provided the nominal phase angle is at the correct value. Such a modulation can indeed be implemented simply. Figure 37 is a plot of the impedance of the equivalent circuit of Figure 33 on the R-X plane with frequency as a parameter. The impedance is given by equation.

$$Z = R_V + R_F + j\left[(L_O + L_D + L_V)\omega - \frac{1}{\omega C_o}\right] \qquad (7\text{-}8)$$
$$= R_T + jX_T$$

In Figure 37, R_T is a constant vector independent of frequency lying along the R-axis. The locus of the imaginary component as a function of frequency is a parallel straight line at a distant R_T to the right of the jX-axis. The impedance vector for a given frequency is a vector from the origin to a point on the straight line corresponding to that frequency. Resonance occurs when X_T equals zero and the impedance becomes R_T. The nominal operating frequency is at ω_O when

$$(L_O + L_D)\,\omega_O = \frac{1}{\omega_O C_o} \qquad (7\text{-}9)$$

In Figure 37, the impedance vector is shown as $O\text{-}\omega_O$. The impedance angle is given by

$$\Theta_O = \tan^{-1}\frac{\omega_o L_V}{R_V + R_F} \qquad (7\text{-}10)$$

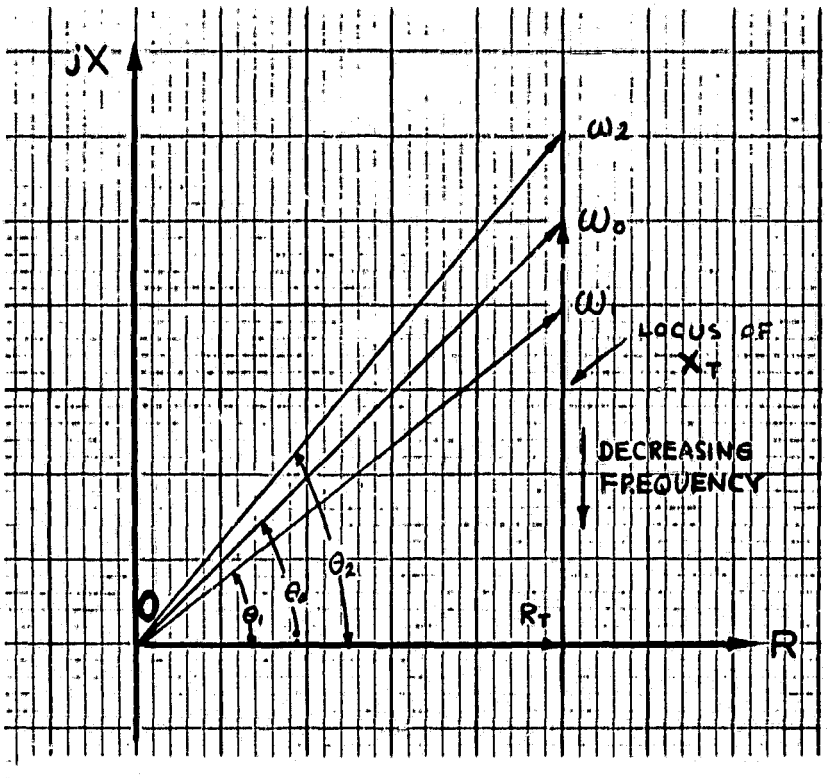

FIGURE 37 R-X PLOT OF RLC CIRCUIT

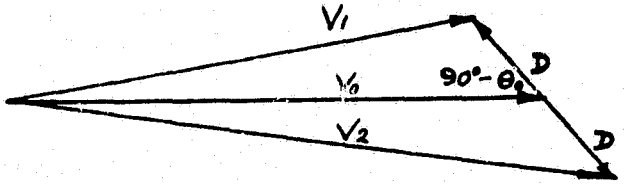

FIGURE 38 MODULATION VECTORS

Since it has been assumed that $\omega_0 L_v = R_v$, θ is less than 45° for any finite R_f and is 45° for R_f equal to zero. For a frequency lower than ω_0, such as ω_1, the impedance becomes smaller and its phase angle is also smaller. Similarly, at a higher frequency, such as ω_2, the impedance is larger and its phase angle is also larger. For frequencies near ω_0, the magnitude change of reactance, x, is very nearly linearly proportional to frequency change. If the circuit is driven at ω_1 with a voltage which is a constant with time the magnitude of the vector $0\text{-}\omega_1$, and then it is driven at ω_2 with a voltage which is equal to the same constant times the magnitude of $0\text{-}\omega_2$, then the resultant currents will remain at the same value at both frequencies. To achieve this condition it is required that to the nominal voltage another voltage, which is phase shifted by 90° , is subtracted at ω_1 and at ω_2. It happens to be true that the currents would be equal only if the modulation is about ω_0, and the average of ω_1 and ω_2 is very close to ω_0. It then becomes possible to determine whether the modulation is about the correct nominal frequency by observing the magnitudes of the currents at ω_1 and ω_2. Equal current magnitudes indicate the correct nominal frequency. Figure 38 is a diagram of voltage vectors to be used for modulating the excitation voltage of the loop. V_0 represents the voltage which should be the nominal voltage exciting the system if there were no modulation. From this voltage is subtracted another voltage, D, at an angle of 90° - to obtain V_1 (at ω_1) and added to the same voltage, D, to obtain V_2 (at ω_2).

7.3.6 Densitometer-Viscometer Oscillator Loop - In the preceding section, the analysis has been on the device being driven. In practice, the mechanics of the device together with the electronics form a sustained oscillating loop. The block diagram of such a loop is shown in Figure 39. The operation of the loop may be described initially by considering the loop consisting of the functional blocks: torquer, densitometer dynamics, pickoff, amplifier, gain control, phase control, and constant phase. Assume for the moment that at a given frequency the phase control is fixed at such a value that the total phase shift around the loop is zero or 360°, and the loop gain is equal to one. Then, the conditions are met that a steady oscillation at the given frequency is sustained without change. If now the switch S1 disconnects the (-) block and connects to the (+) block, the effect would be to change both the phase and gain of the loop. In order to sustain oscillation, the oscillation frequency is changed until the total phase shift around the loop is 0 or 360°, and the loop gain is unity. S1 is switching between + and - in accordance with a signal from the timing and control circuit. The timing and control circuit has an input from the divider which counts the oscillation cycles. At the end of N cycles it sends a pulse to the timing and control circuit. The timing and control circuit then changes the position of S1 at the receipt of the pulse. This process continues indefinitely. The output of the timing and control circuit is Ed, a squarewave which is high when S1 is connected to (-) and is low when S1 is connected to (+). It is then a squarewave with a small asymmetry, with the duration of the "high" interval longer than the "low" interval.

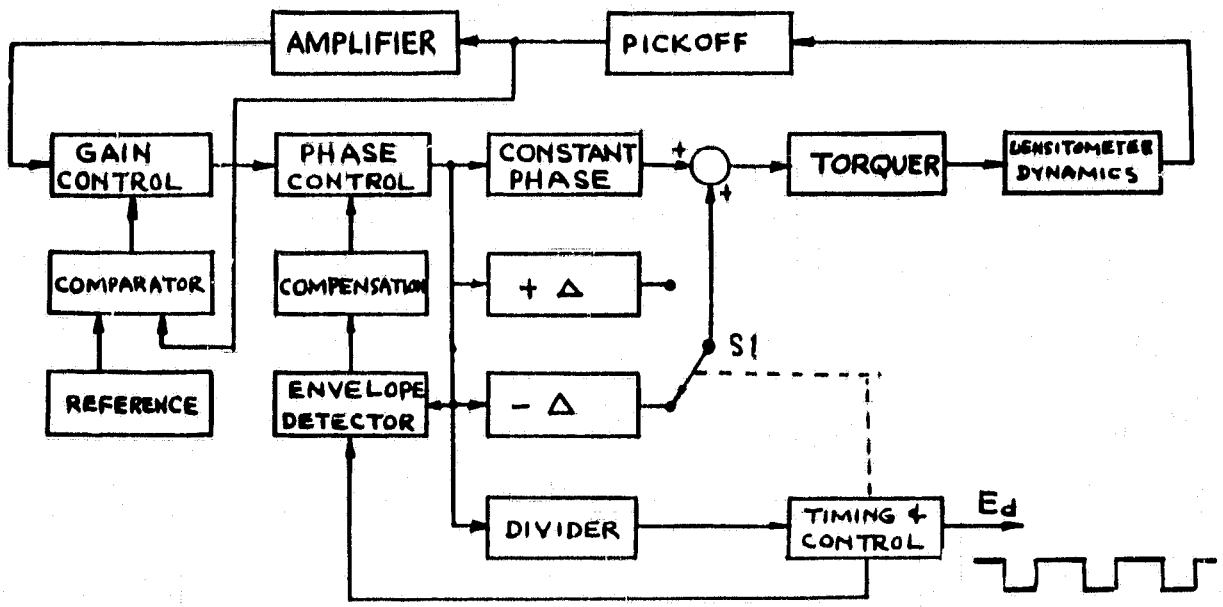

DENSITOMETER BLOCK DIAGRAM

FIGURE 39

It has been shown in Section 7.3.5 that for a proper constant phase shift, the modulation produced by alternately connecting to + and - will produce a constant loop gain if the loop is operating about the correct nominal (average) frequency. At the correct nominal frequency the envelope of the pickoff output will remain the same amplitude during both halves of the modulation cycle. If, however, the nominal frequency is not correct, then the amplitudes of the two halves will differ. Such a difference is detected by the envelope detector, which receives a reference frequency from the timing and control circuit. The output of the envelope detector is compensated for loop stability and applied to the phase control circuit. The phase control circuit shifts the phase of the loop in such a direction so as to restore equality of the amplitudes of the two halves of the modulation cycle.

The gain of the densitometer-viscometer dynamics is high for low viscosity fluid and low for high viscosity fluid. Without gain control the necessary condition of a loop gain of unity is achieved by saturation of some functions in the loop - most likely, the amplifier. Saturation will introduce phase shift as well as destroy amplitude information. To maintain linear operation the output of the pickoff is compared with a reference voltage. The output of the comparator drives the gain control circuit until the amplitude of the pickoff is equal to the reference amplitude.

7.3.7 Sensitivities - Frequency versus Specific Gravity (SG)

$$F = \frac{1}{2\pi}\left(\frac{835363320.}{1. + 0.819580375 \times SG}\right)^{1/2}$$

may be used to calculate the sensitivity of the frequency output versus changes in fluid specific gravity. The results are listed below:

Nominal Specific Gravity	Frequency Change in Hz From 1% Change of Specific Gravity	Freq. Change in Hz From 0.01 Change of Specific Gravity
0.600	6.19	10.32
0.700	6.67	9.52
0.772	6.96	9.01
0.800	7.06	8.82
0.900	7.38	8.20
1.00	7.65	7.65

Change of Frequency Versus Change of Phase - The change of the frequency of oscillation for a change of phase angle in the loop may be calculated from the impedance of the loop given by equation (7-8). The angle is given by

$$\Theta = \tan^{-1} \frac{(L_o + L_D + L_V)\,\omega - 1/\omega C_o}{R_V + R_f} \qquad (7\text{-}11)$$

The rate of change of angle versus frequency is a function of the Q of the circuit with

$$Q = \frac{\omega\,(L_o + L_D + L_V)}{R_V + R_f} \qquad (7\text{-}12)$$

The change of frequency versus phase shift and corresponing equivanlent change in density for two Q values is listed below:

Q	Frequency Change for 1° Phase Shift	Equivalent Change of SG = 0.772
	Hz	%
62	1.00	0.145
125	.56	0.072

Modulation Sensitivity - When the densitometer-viscometer is modulated in the manner described in Section 7.3.5, the oscillation frequency assumes two different values very nearly equidistant from the nominal frequency. The relationship between the frequency difference, Q and modulation factor is given by equations

$$Q = \frac{2kf_o}{(f_2 - f_1)} \qquad (7\text{-}13)$$

$$(f_2 - f_1) = \frac{2kf_o}{Q} \qquad (7\text{-}14)$$

where k = ratio of modulation component divided by the nominal excitation.
For k = 0.15, the frequency difference is 12.3 Hz at a Q of 62.

Detail calculation also shows that when the loop modulates at 1° away from the proper nominal phase, the amplitude of the velocity difference during the two halves of the modulation cycle is 0.74%.

7.3.8 Flow Velocity Effects - If flow velocity through the densitometer is too high, the resultant damping may adversely affect the determination of viscosity. Mass flowmeters have been proposed which are based on the damping effect of flow through oscillating vanes. However, initial tests on a densitometer produced no perceptable changes in Q or frequency for flow velocities up to 50cm/sec (20"/sec). In the conceptual designs of vortex precession and turbine flowmeters the flow through the densitometer is about 1% of flow rate which results in much lower velocities. Another effect of flow velocity is the time response to abrupt changes in density. At minimum flow, response takes about 42 seconds while at maximum flow rate it takes less than one second as determined by the time for one complete change of the fuel contained in the densitometer housing.

7.4 Accuracy Analysis -

Contributing factors and the RSS estimate for densitometer accuracy are summarized in Table 15 and discussed below.

Long term stability of the current densitometer is ± .1% as demonstrated by rigorous testing. Two units have been calibrated and subjected to a complete military qualification test program that included 5g sinusoidal vibration (MIL-STD-810C, Meth. 514.2, Proc. I), 15g shock, thermal shock, temperature-altitude, humidity, endurance, fuel resistance, and icing. Post-test calibration, conducted a year after the initial one, demonstrated better than ± 0.1% stability. However, these tests were run at a constant temperature so that ± 0.5% temperature sensitivity (over -54°C to +71°C range) did not contribute error. In a high-accuracy application this magnitude temperature sensitivity must be compensated out and to do this, both turbine and vortex precession meters have temperature sensors and a computer algorithm. With this implimentation a 2°C error in temperature introduces 0.008% error in density.

Calibration requires extremely accurate hydrometers traceable to National Bureau of Standards. General Electric has obtained such units good to ± 0.02% accuracy which includes variability in reading the device.

With perfect inputs (frequency and temperature) the computer algorithm can calculate within .02% of the actual calibration. This error results from imperfect match of the computer algorithm to the actual curves which have slight irregularities over the temperature, viscosity and density ranges.

A crystal controlled time base with ±100ppm stability over the temperature range (of electronics) would generate a ±0.36 Hz error in measuring the output frequency and, assuming 3600 Hz output at sp. gr. of 0.772 and a sensitivity of 6.96 Hz/1% density, would result in 0.051% error in density.

Stability of the phase control loop (Figure 39) over the temperature range (of electronics) must be within .25° so as to limit its contribution to error to less than 0.036% of density at high viscosities (Q=62).

The RSS estimate amounts to about one-quarter of the total flowmeter variability and is very likely to be obtained in hardware. One area of risk is verification of densitometer performance at temperature extremes, particularly at -55°C. Calibration at these extremes has not been performed to date due to the unavailability of highly accurate density standards which cover these temperatures. Such equipment is prerequisite to generating calibration curves to be entered into the computer program.

TABLE 14
DENSITOMETER ANALYSIS OF ACCURACY

SOURCE	ESTIMATE IN % FOR SG =0.772	
REPEATABILITY	0.100	Present Capability
TEMP. COMPENSATION	0.008	±2°C Temp. Sensor
CALIBRATION	0.020	Hydrometer Reading
CURVE FIT	0.020	Computer Algorithm
TIME BASE	0.052	±1ppm/°C Crystal
CIRCUIT STABILITY	0.036	±.25° Phase Control
RSS	0.120	

7.5 Nomenclature

C	Capcitance
C_o	Spring capacitance
D	Damping constant, Voltage
F	Voltage
F, f_o, f_1, f_2	Frequency
I_o	Coupler Inertia
I_D	Effective non-viscous inertia of fluid with SG = 1.0
J	Moment of inertia
K	Spring constant
L	Inductance
L_v	Viscous inductance
L_D	Inductance of coupled liquid
L_o	Inductance of coupler inertia
O	Origin of complex plane
Q	Quality factor indicating sharpness of resonance
q	Charge
T_R	Resistance
R_v	Viscous resistance
R_F	Internal spring resistance
R_T	Resistance of spring and viscous liquid
SG	Specific gravity
t	Time
V_o	Excitation voltage
V_1,V_2	Modulated voltage
X_T	Reactance of spring and combined inertias
Z	Impedance
Z_v	Impedance of viscosity
θ	Angle
θ_o	Impedance angle or phase shift
τ	Torque
ω	Radian frequency
ω_o	Nominal frequency
ω_1,ω_2	Operating frequencies with + and - phase

8.0 INTERFACE AND MICROCOMPUTER ELECTRONICS

8.1 Introduction -

Each of the fuel flow meters described in the preceding sections require electronics to process the signals in order to measure mass fuel flow rate. The electronics may be classified into two broad classifications - interface and microcomputer. The detailed designs of electronics remain to be done. What follows is a description of the requirements and concepts of the electronics needed. Where schematics are given, the intent is to convey an approximate form and scope rather than any specific design.

8.2 Interface Electronics -

The interface electronics comprise the power supply and all circuits which condition the sensor signals into suitable forms for the microcomputer.

8.2.1 Angular Momentum Circuits - The overall functional block diagram for the angular momentum fuel flowmeter is shown in Figure 40. The mechanical assembly shown on the left of the figure has a transient turbine. To measure the angular velocity of the transient turbine, the interface electronics (the functional block in the center of the figure) excites the variable reluctance sensor of the transient turbine with a 45 kHz voltage. The effect of the varying inductance upon the excitation voltage becomes the signal to the interface electronics. The interface electronics converts the signal into a squarewave and sends it to the microcomputer.

The mechanical assembly also has a rotor and a shroud. These together generate three timing pulses: start, rotor stop and shroud stop. These pulses are processed by zero-crossing detectors which convert the pulses into squarewaves and send them to the microcomputer.

There is a synchronous motor in the mechanical assembly which is driven by a 400 Hz voltage supplied by the interface electronics. The interface electronics are powered by 28 V dc and transforms the 28 V into other voltages needed by its own circuit and the microcomputer.

8.2.2 Turbine Circuits - The overall functional block diagram for the turbine fuel flowmeter is shown in Figure 41. The mechanical assembly shown on the left on the figure has a densitometer-viscometer, a main turbine, a sensor turbine, and a temperature sensor. The electronics for the densitometer-viscometer has been described in Section 7.3.6. The interface electronics provide excitation to the densitometer-viscometer, using its signal to form a closed loop. The output is an asymmetrical squarewave which is sent to the microcomputer.

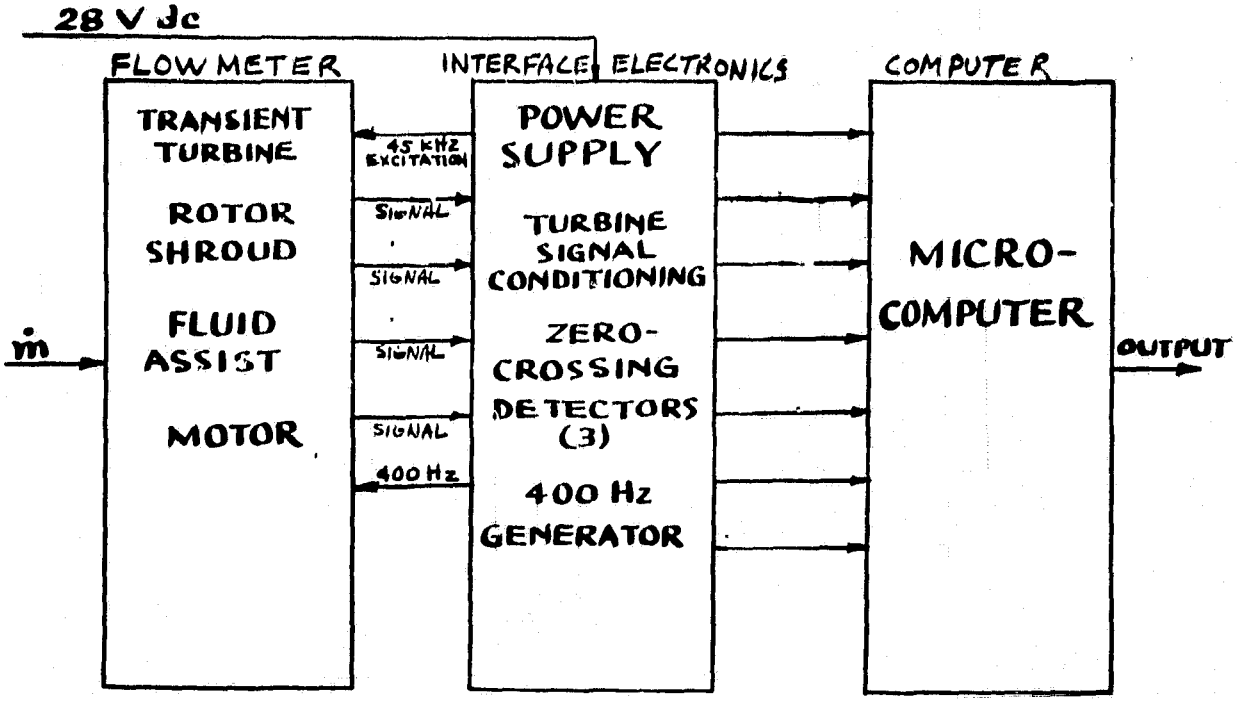

FIG. 40

ANGULAR MOMENTUM FLOWMETER

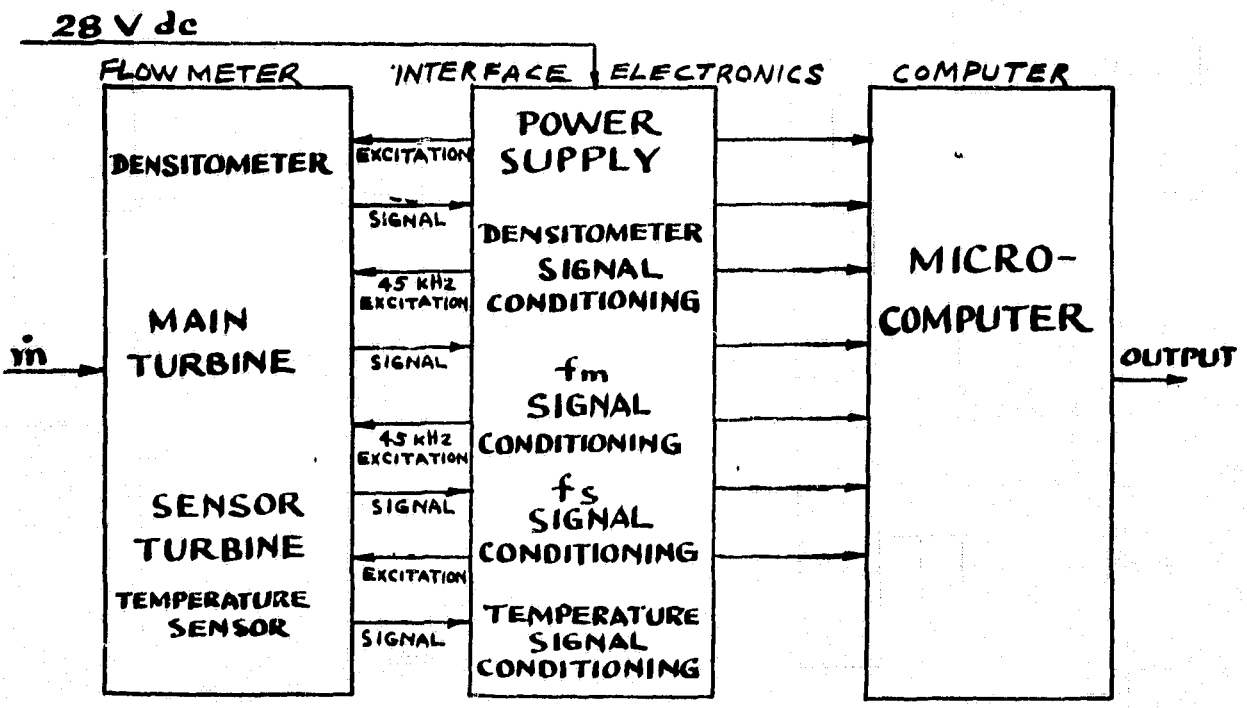

FIG. 41

TURBINE-DENSITOMETER FLOWMETER

The main turbine and sensor turbine have 45 kHz excitation voltages supplied by the interface electronics to actuate the variable reluctance sensors, and their signals are processed into squarewaves by the interface electronics and sent to the microcomputer.

8.2.3 Vortex Precession Circuits - The overall functional block diagram for the vortex precession fuel flowmeter is shown in Figure 42. The mechanical assembly shown on the left of the figure contains a densitometer-viscometer, a vortex generator, and a temperature sensor. The electronics for the densitometer-viscometer has been described in Section 7.3.6. The interface electronics provide excitation to the densitometer-viscometer, using its signal to form a closed loop. The output is an asymmetrical squarewave which is sent to the microcomputer for further processing.

The vortex generator together with its pickoff has a signal coming to the interface electronics. It is a frequency. The vortex signal conditioning amplifies and squares up the signal as output to the microcomputer for further processing.

The temperature sensor is a temperature sensitive resistor with excitation voltage from the interface electronics. The signal conditioning is the same as that described in Section 8.2.2. The output is a voltage to the microcomputer.

The interface electronics has as its primary power 28 V dc. The 28 V dc is transformed into suitable voltages by the power supply to be used by the interface circuits and the microcomputer.

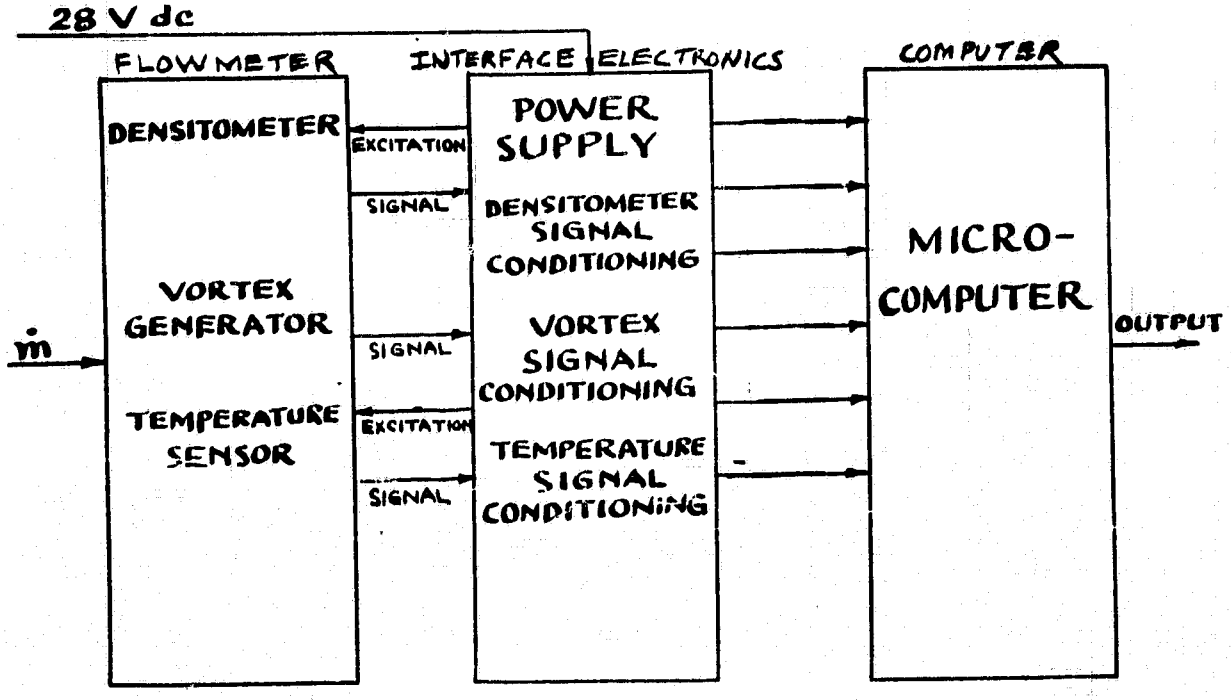

FIG 42
VORTEX PRECESSION FLOWMETER

8.2.4 Summary of Electronics Functions - The three different implementations of fuel flowmeters require nine electronics functions. None of the flowmeters requires all nine functions and some of the functions are needed more than once. The electronics functions and their uses in each type of flowmeters are listed below.

ELECTRONIC FUNCTIONS OF FLOWMETERS

Function	Angular Momentum	Turbine	Vortex Precession
Power Supply	1	1	1
Densitometer Signal Conditioning	0	1	1
45 kHz Excitation	1	2	0
45 kHz Detector	1	2	0
Zero-crossing Detector	3	0	0
Vortex Frequency Detector	0	0	1
Temperature Circuit	0	1	1
400 Hz Excitation	1	0	0
Microcomputer	1	1	1

8.2.5 Power Supply - Each flowmeter requires a power supply. The power supply design will be similar to existing designs used in several General Electric products now in production. It is a switching power supply using the flyback conversion method. Its block diagram is shown in Figure 43.

Input Diodes and EMI Filter - The input power is 28 V dc. In Figure 43 the first circuits which the input voltage encounters are the inductor and diodes. The input diodes serve the purpose of guarding against the application of a wrong polarity input voltage. The inductor limits the high frequency noise from coming in or going out, and thus serves as part of an EMI filter.

Storage Capacitors - Immediately following the EMI filter are the storage capacitors. The function of these capacitors is the attenuation of input voltage spikes and noise generated within the power supply itself. These capacitors smooth out the high frequency components of the switching converter.

5 V Regulator - A 5 V output is obtained from the storage capacitors by a simple one-transistor regulator. The 5 V is used to power the driver and PWM circuits. The regulating transistor passes current only during the start up transient. Once the switching converter reaches steady state, the 5 V current is supplied by the switching converter itself through a diode. This arrangement improves efficiency and eliminates any heat sinking requirement for the regulating transistor.

5 V Reference - The 5 V Reference is generated by an integrated circuit which also provides the functions of Error Amplifier, PWM (pulse width modulator), Shutdown circuit, and Oscillator. This reference is used to set the amplitude of the output voltages as well as the limit points for the Low Line Voltage, Over Voltage, and Current Limit monitor circuits.

Feedback Loop - The feedback loop which controls the output voltage consists of the following functional blocks: Error Amplifier, PWM, Driver, Power Switch, Transformer, Diodes and Capacitors. When input power is first applied, all the output voltages are initially zero so that the Error Amplifier sees a larger error voltage and is saturated. The output of the Error Amplifier drives the PWM to its maximum pulse-width ratio. Through the Driver and Power Switch the primary of the transformer is connected to the input voltage for the maximum duration of each period of the oscillator and then the energy stored is transferred to the secondary loads. This action proceeds until the 5.25 V voltage approaches its set value, and the error voltage decreases enough to reduce the pulse width ratio, thus cutting down the rate of energy input to the transformer. Eventually the rate of energy input is made equal to the power output at the specified output voltages and the loop settles to its equilibrium.

Monitor Circuits - There are three monitor circuits, all of which work through the shutdown circuit of the integrated circuit. The Low Line Voltage circuit monitors the input voltage and shuts down the power supply whenever the input voltage falls below a prescribed minimum value to avoid unpredictable operation of the integrated circuit. The Overvoltage circuit monitors the 15 V output. When the 15 V exceeds a prescribed maximum, the power supply is shutdown. The Current Limit circuit monitors the primary current of the transformer. When it exceeds a prescribed value, the power supply is shutdown.

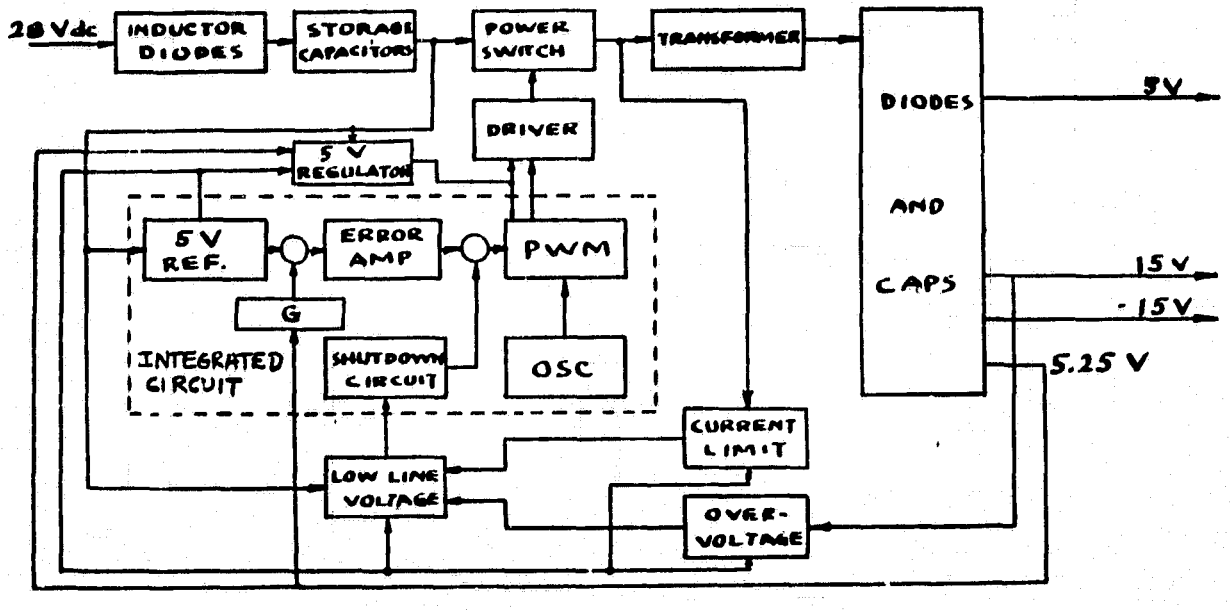

FIG. 43 POWER SUPPLY BLOCK DIAGRAM

8.2.6 Zero-crossing Detectors - There are three timing signals from the angular momentum flowmeter mechanical assembly, the reference signal T_O, the shroud signal T_S and the rotor signal T_R. The waveform of each of these signals is shown in Figure 6. The point at which time is measured is where the voltage is zero, and its slope as a function of time is negative. To minimize the number of leads, all three signals share one common return.

The schematic of all three zero-detectors is shown in Figure 44. In that figure, AR1, AR4, AR7 and AR8 are high input impedance buffer amplifiers which duplicate the sensor voltages with respect to local circuit common. The buffered voltages are then followed by differential amplifiers to achieve good common mode rejection and amplification. The outputs of the differential amplifiers then are filtered by a simple RC low pass filter to attenuate high frequency noise. AR3, AR6 and AR10 are the zero-crossing detectors.

Each detector has positive feedback when its output is negative, and because of the presence of the diodes CR1, CR2 or CR3 in the feedback path, no feedback when the output is positive. When the input signal reaches the proper zero point, the detector changes state in an accelerated rate because of the positive feedback and will remain in the new state in the presence of small deviations from zero. The state is changed again only when the input to the detectors becomes more negative (more positive in the sensor signal) than the voltage introduced by the positive feedback. When so changed, the detector is again ready to detect the next proper zero-crossing point.

8.2.7 45 kHz Excitation and Signal Detection - The 45 kHz excitation is generated simply by a NAND gate U1, which has a Schmitt trigger internally, and R1, C1. The circuit is shown in Figure 45. The frequency of oscillation is determined by R1 and C1. The output of U1 is amplified by Q1. The output of Q1 is connected to the sensor coil which has a nominal inductance of 1mH. The inductance varies at the frequency of the signal to be detected (it is changed by the presence or absence of a turbine blade). The sensor is connected to C2. The voltage across C2 varies as the sensor inductance varies. C3 is used to block the dc component of the Q1 output. Diode CR1 rectifies the ac voltage to recover the envelope waveform. AR1 is used to convert the envelope waveform into a squarewave. U2 is added to speed up the rise and fall time of the squarewave as well as to make the amplitude compatible with the digital circuits in the microcomputer.

8.2.8 Vortex Frequency Detector - The vortex frequency pickoff output is periodic with varying amplitude. The noise content is not yet defined, so the circuit of Figure 46 is intended to give some indication of circuit configuration assuming that noise is minimal. The pickoff signal is first amplified by AR1, and squared up by the combination of AR2 and U1.

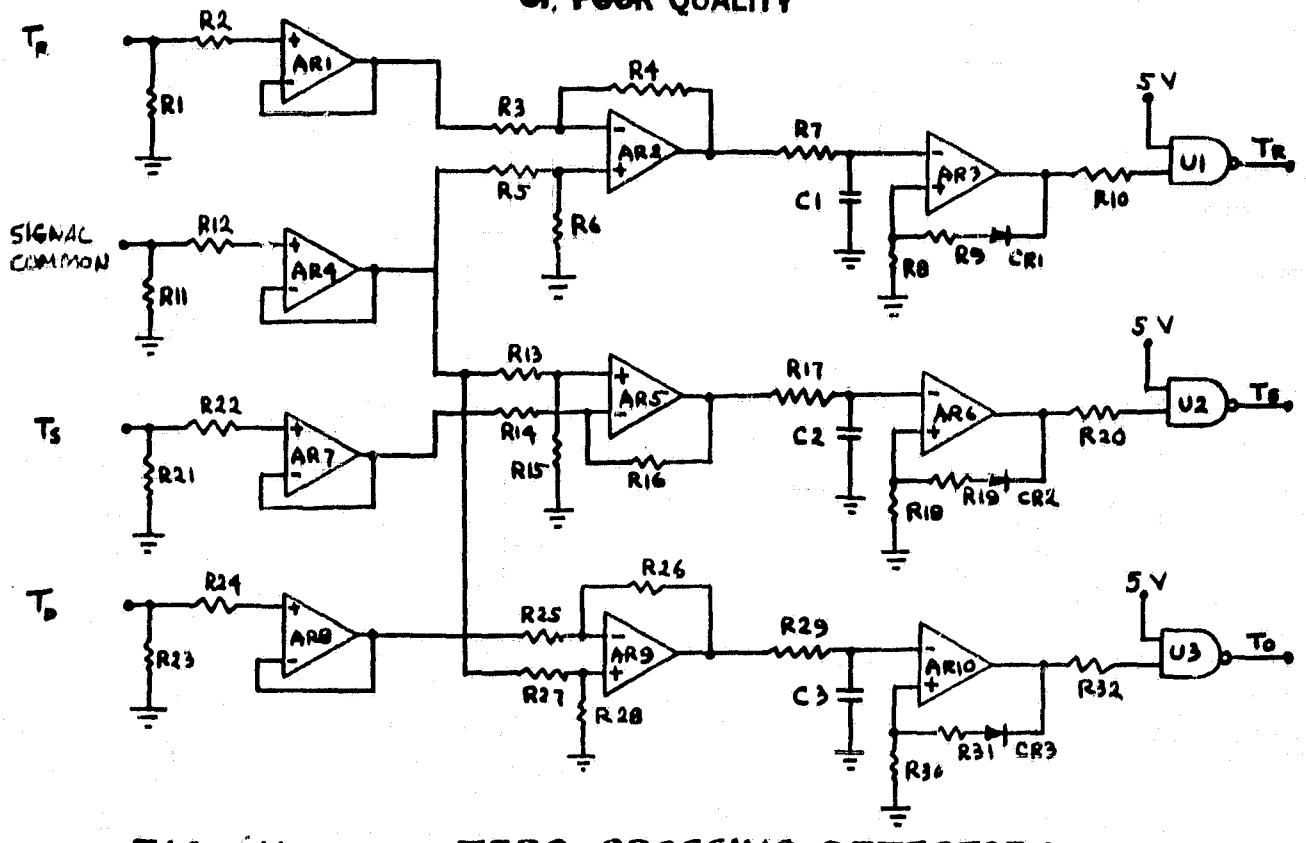

FIG. 44 ZERO-CROSSING DETECTORS

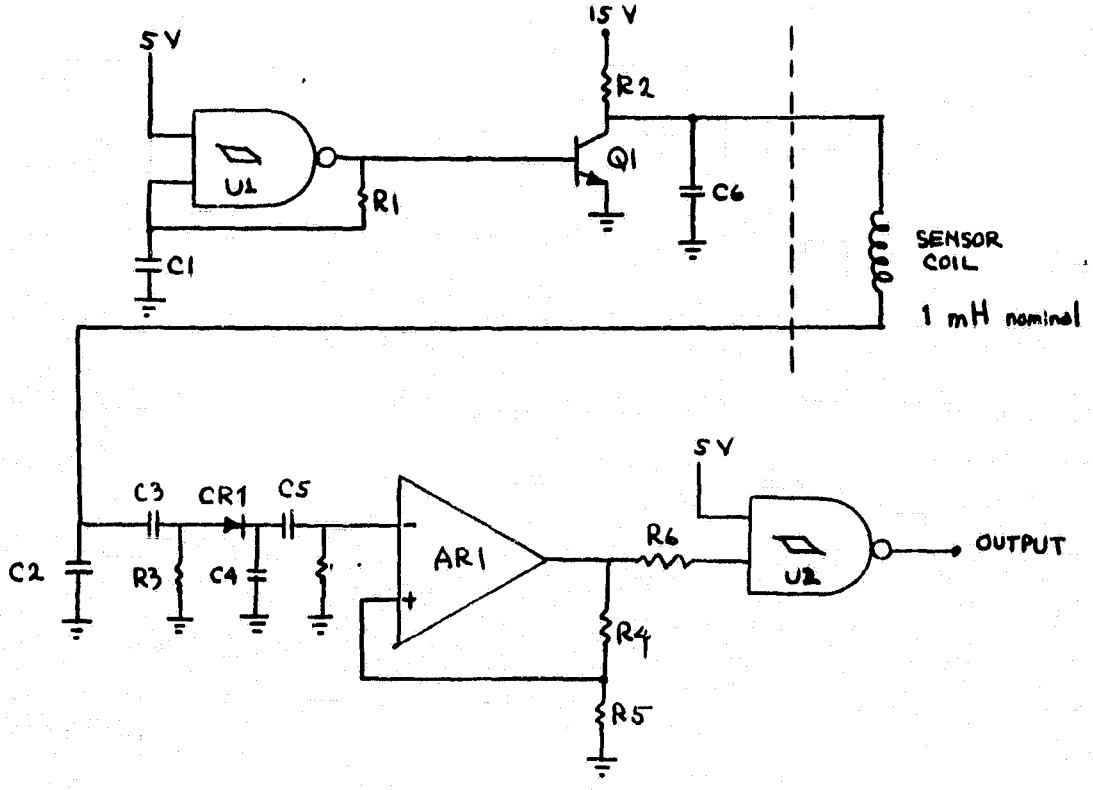

45 kHz Excitation and Signal Conditioning

FIG. 45

ORIGINAL PAGE IS
OF POOR QUALITY

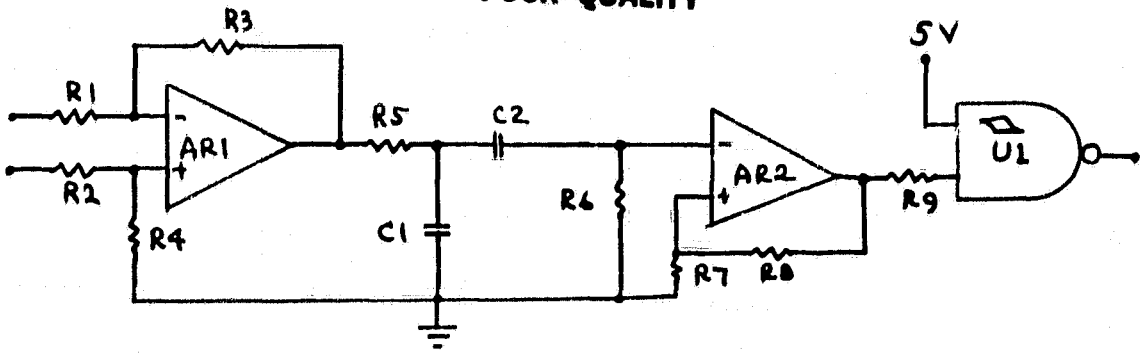

VORTEX FREQUENCY DETECTOR

FIG. 46

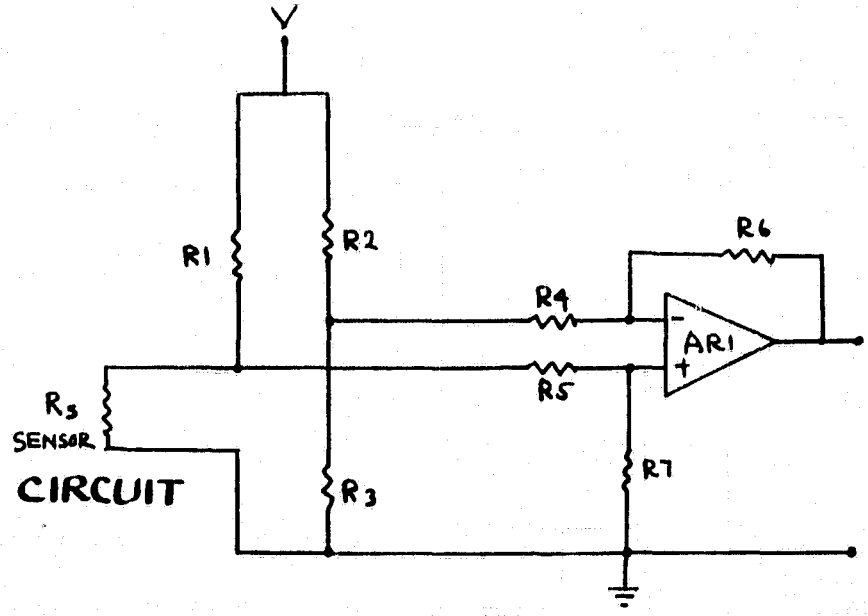

TEMPERATURE CIRCUIT

FIG. 47

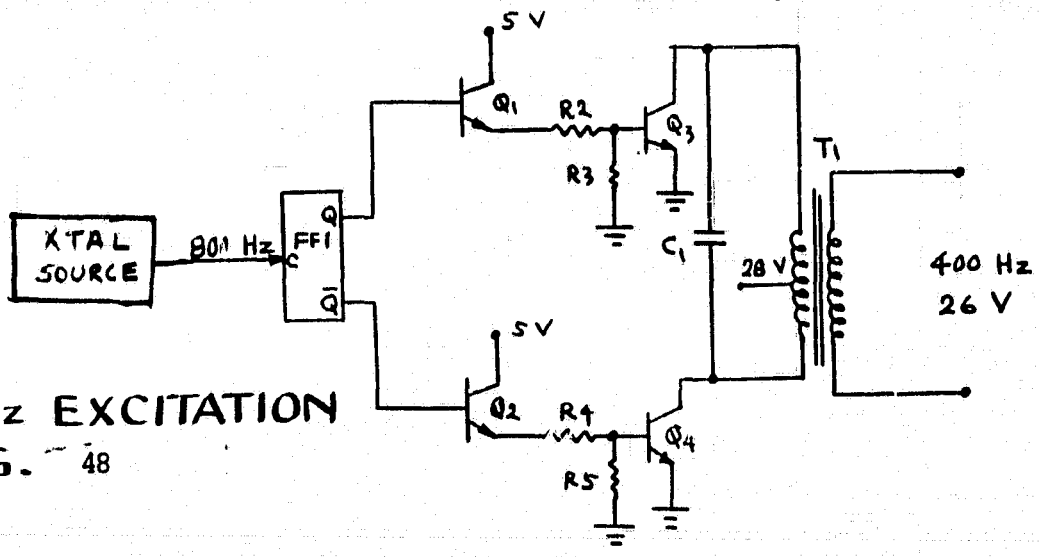

400 Hz EXCITATION

FIG. 48

8.2.9 Temperature Circuit - The schematic of the temperature circuit is shown in Figure 47. The sensor is a temperature sensitive resistance Rs which forms one leg of a bridge consisting also of R1, R2 and R3. AR1 is a differential amplifier which will have a dc voltage output proportion to the sensor temperature but with a small nonlinearity.

8.2.10 400 Hz Excitation - The synchronous motor in the angular momentum fuel flowmeter requires a 400 Hz 26 V drive. The circuit schematic is shown in Figure 48. A crystal generated 800 Hz signal is used to drive flip flop FF1. The Q and $\overline{Q}$ outputs of FF1 in turn drive transistor stages Q1, Q3 and Q2, Q4. The output is transformer coupled to the motor with C1 used to improve the power factor of the load.

8.3 MICROCOMPUTER -

In order to accurately compensate the fuel flow sensor with minimum difficulty and provide a digital output, a microcomputer based system has been selected. Given the analog inputs described in Section 8.2, two types of digital electronics are required: conditioning electronics and microcomputer electronics. They are broken out in two sub-sections below for clarity.

8.3.1 Conditioning Electronics - The fuel flow information, at the output of the interface electronics section, is encoded in the period of the incoming waveforms (temperature information is an exception and is strictly an analog voltage). The conditioning electronics must measure the period of each cycle of each input and present that information to the computer in digital format.

The technique of measuring the period of a waveform consists of timing the interval between the same point on consecutive waveforms, usually the leading edge or zero-crossing. A stable high frequency clock input is normally used as the timing standard. The challenge here is to maintain the high accuracy over the wide temperature range and period variation specified without skipping a period measurement.

Our proposed solution for the turbine-densitometer flowmeter is shown in Figure 49 as an example. The key aspects of this design are the synchronous counters and latches. The synchronous counters permit the use of a high frequency clock which is required to meet the accuracy buoget for this section of 0.025%; and the latches are used to store the previous period until the computer can retrieve the information. Without the latches, obtaining the period of each cycle would be impossible. The size of the counters and latches is a function of the accuracy required and the range of the period to be measured. In general "X" must be selected such that the following equations are true.

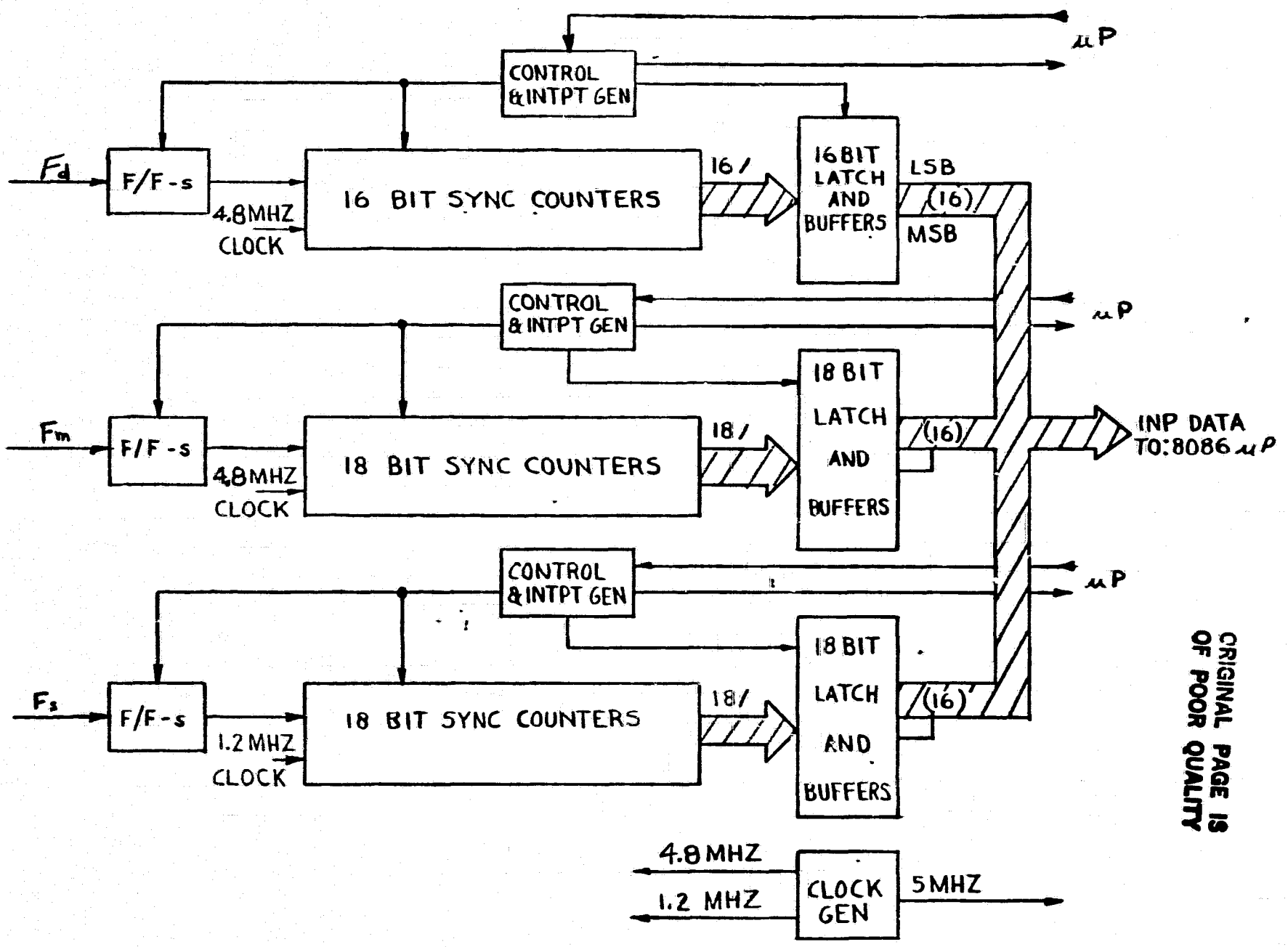

FIGURE 49 BLOCK DIAGRAM FOR PERIOD MEASUREMENT CIRCUITS

$$2^{\alpha} \geq \left(\frac{\text{Range}}{\text{Resolution}}\right) \times 100 \qquad (8\text{-}1)$$

Where - resolution is in %

- range is (max. period/min. period)

- α is number of Bits

Simplifing:

$$\alpha \geq \log\left(\frac{\text{Range} \times 100}{\text{Resolution}}\right) / \log 2 \qquad (8\text{-}2)$$

Summaries of the period measurements for each input of each sensor are presented in Tables 15, 16, 17 and 18. In addition to the period measurement circuits there is a requirement for an analog-to--digital converter (A/D) for the analog temperature input. A ten bit A/D provides the 0.1% resolution required for this input.

TABLE 15
PERIOD MEASUREMENTS FOR ANGULAR MOMENTUM FLOWMETER

	TURBINE SIGNAL	MASS FLOW PERIOD (T_r-T_o)	VISCOSITY PERIOD (T_s-T_o)
MIN FREQUENCY	43 Hz	Sample rate of 5.75 Hz from fixed rotational speed.	
MAX FREQUENCY	2580 Hz		
MIN PERIOD	388 μs	2.74 ms	732 μs
MAX PERIOD	23.3 ms	137 ms	36.6 ms
RESOLUTION*	0.1% (388 ns)	0.025% (685 ns)	0.1% (36.6μs)
MIN CLOCK FREQUENCY	2.6 MHz	1.46 MHz	27.3 kHz
MAX COUNT AT MAX PERIOD	60052	200020	1000
SIZE OF COUNTER REQUIRED (BITS)	16	18	16

* Resolution requirement is specified at max viscosity where correction for viscosity is most crucial. The resolution obtained is 10 times better than required.

TABLE 16
PERIOD MEASUREMENTS FOR TURBINE-DENSITOMETER FLOWMETER

	MAIN TURBINE	SENSOR TURBINE
MIN FREQUENCY	20 Hz	7.2 Hz
MAX FREQUENCY	1200 Hz	468 Hz
MIN PERIOD	833 us	2137 us
MAX PERIOD	50 ms	139 ms
RESOLUTION	0.025% (208 ns)	0.064% (1.37 μs)
MIN CLOCK FREQUENCY	4.8 MHz	730 kHz
MAX COUNT AT MAX PERIOD	240,000	101,500
NUMBER OF BITS COUNTER REQUIRED	18	17

TABLE 17

PERIOD MEASUREMENTS FOR VORTEX PRECESSION FLOWMETER

MIN FREQUENCY	8 Hz
MAX FREQUENCY	500 Hz
MIN PERIOD	2 ms
MAX PERIOD	125 ms
RESOLUTION	0.025% (500 ns)
MIN CLOCK FREQUENCY	2 MHz
MAX COUNT AT MAX PERIOD	250000
NO. OF BITS COUNTER REQUIRED	18

TABLE 18

PERIOD MEASUREMENTS FOR DENSITOMETER

MIN FREQUENCY	53 Hz
MAX FREQUENCY	61 Hz
MIN 1/2 PERIOD	8.0 ms
MAX 1/2 PERIOD	9.5 ms
RESOLUTION	0.003% (250 ns)
MIN CLOCK FREQUENCY	4 MHz
MAX COUNT AT MAX PERIOD	38000
NUMBER OF BITS COUNTER REQUIRED	16

8.3.2 Microcomputer Electronics - Once the input information is converted into digital format it is ready for processing by the microcomputer.

Selection of the 8086 microcomputer and appropriate support chips was based upon the following assumptions/requirements:

a) Higher Order Language (HOL) such as Fortran, Algol, Pascal, PLM, or ADA will be used.

b) A 10 ms cycle time is required to meet the 25 ms response time specified.

c) 40% spare memory and execution time will remain for future program modifications.

d) Since the input data which requires accuracy of 16 to 18 bits, a 16 bit microcomputer has been selected.

8.3.2.2 Block Diagram - The microcomputer will be of standard design utilizing an 8086 microprocessor, 5 MHz clock, two I/O port chips, 2K by 16 bit RAM, 8K by 16 bit ROM, and a Universal Synchronous/Asynchronous Receiver Transmitter (USART) for digital output. A hardware floating point multiply/divide chip is being considered and will be used if the requirement for 10 ms cycle times force the spare execution time to be less than 40%. The microcomputer block diagram, showing all of the digital electronics for clarity, is presented in Figure 50.

8.3.3 Volume and Power Estimates - The preceding designs for the microcomputer, conditioning electronics and interface electronics serve as a tentative basis for finding total volume and 28 VDC power consumption for the remote electronics package. Table 19 presents the estimates for each of the three concepts.

Table 19 ELECTRONICS VOLUME AND POWER ESTIMATES

	Interface		Microcomputer		Total	
	Volume	Power	Volume	Power	Volume	Power
FLOWMETER	CM^3	Watts	CM^3	Watts	CM^3	Watts
MOMENTUM	530	12*	600	17	1130	29
TURBINE	590	3	600	17	1190	20
VORTEX	550	2	600	17	1150	19

*INCLUDES MOTOR POWER

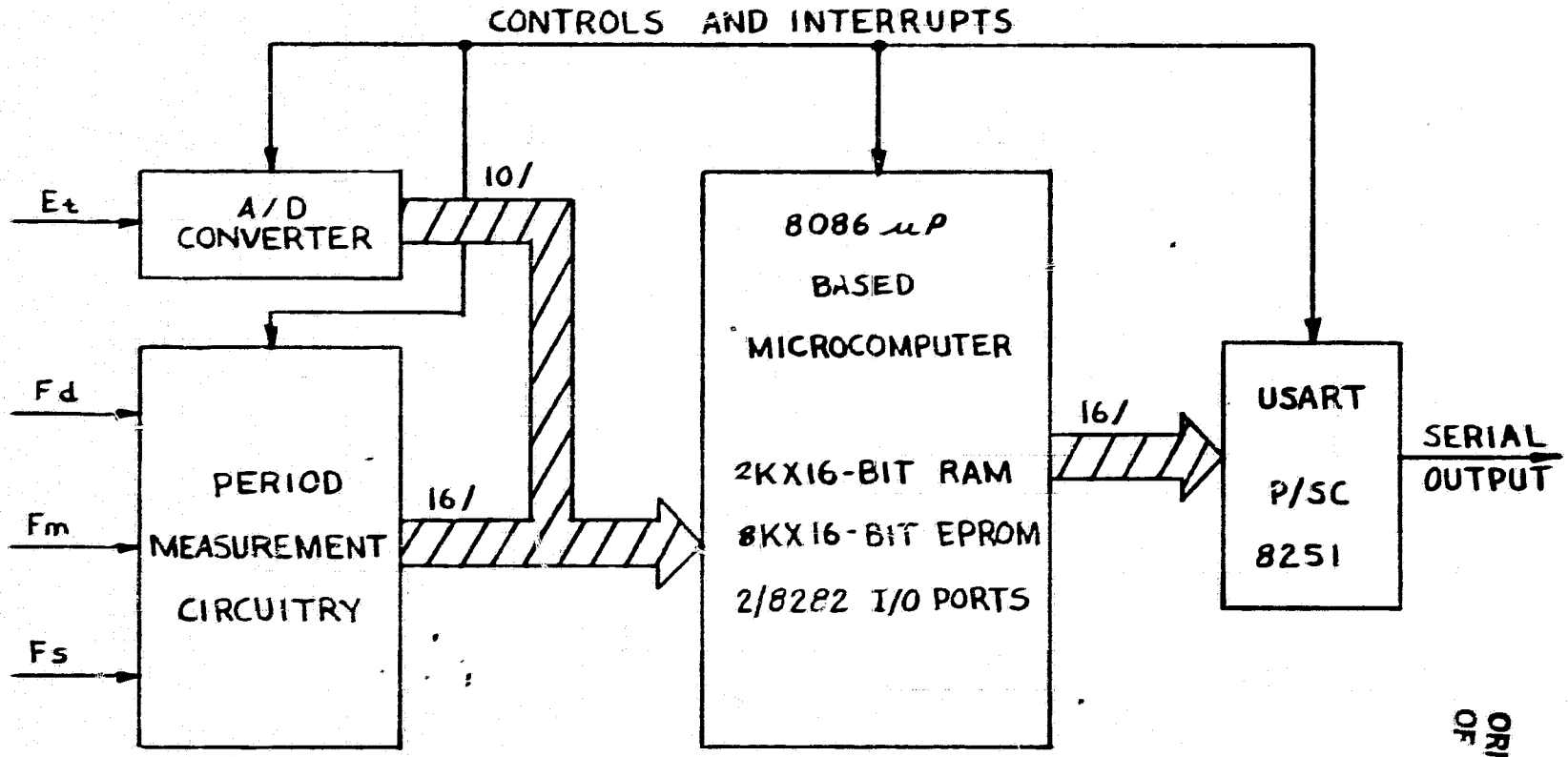

FIGURE 50 MICROCOMPUTER BLOCK DIAGRAM

8.4 Nomenclature

E_t	Temperature voltage
F_d	Densitometer frequency
F_m	Main trubine frequency
F_s	Sensor turbine frequency
LSB	Least significant bit
m	Mass flowrate
MSB	Most significant bit
T_o	Reference signal
T_R	Rotor signal
T_s	Shroud signal
X	Number of bits

9.0 SUMMARY OF RESULTS

All tasks of the Phase I contract to develop a high accuracy fuel flowmeter have been completed and are herein reported in detail. A total of 750 patents and 1500 abstracts covering various methods of measuring the mass flow of aircraft fuel have been reviewed, analyzed and pared down to three viable types. These three types: angular momentum, vortex precession and double turbine have been analyzed in detail and conceptual designs have been prepared for each. Problem areas that prevent each type from meeting the design guidelines and specifications are outlined along with the suggested approach to correcting the problem.

10.1 DESIGN GUIDELINES AND SPECIFICATIONS

1. Measurand and method of measurement - Fuel mass flow (both mass flow and total mass flow accumulated) shall be measured either directly, or by using a composite system of separately measuring volumetric flow and fuel density, or by measuring a combination of quantities from which mass flow can be calculated. For a flowmeter system that measures volumetric flow, the preferred method of measuring density is to use a densitometer rather than a correlation between density and temperature. The reason is that fuels that are within the MIL specifications can still show variations between batches that can produce uncertainties up to ±1/2 percent in density when determined by a temperature measurement. This uncertainty exceeds the contract goal.

2. Types of fuels - Fuels of interest are JP-3, JP-4, JP-5, JP-8 (Type A-1) and Type A.

3. Flow range - Typical ranges of fuel flow between engine full power and idle are between 50:1 to 100:1 depending on whether or not the engine has an afterburner. The absolute value of full scale flowrate varies with engine thrust; but for the purpose of this contract, a flowmeter with a nominal full scale of 3.2 l/s (20,000 lb/hr) and a 50:1 operating range is of primary interest. A full scale range of 0.5 l/s (3000 lb/hr) is also of interest and shall be considered.

4. Pressure - Flowmeters are subjected to high pressures because they are usually located downstream of the fuel pump. Operating pressures up to 7000 kPa (1000 psi) shall be considered. Flowmeter bodies shall be hydrostatic pressure tested to 1.5 times the maximum operating pressure.

5. Pressure drop - At maximum fuel flow the maximum pressure drop across the flowmeter shall be 68 kPa (10 psi).

6. Fuel temperature - The flowmeter shall be capable of operating over a fuel temperature span from -55°C to 130°C.

7. Ambient temperature - The flowmeter shall be capable of operating over an ambient temperature span from -55°C to 130°C.

8. Accuracy - The total error band for mass flow measurement shall be no greater than ±0.25 percent of reading. The project goal of the error band is ±0.1 percent of reading.

9. Resolution - The maximum value of resolution of fuel flow measurement at 1/50 of full scale shall be 0.25 percent.

10. Ambient pressure - The flowmeter and signal conditioning electronics are usually located in unpressurized regions of the aircraft. The units shall be capable of satisfactory operation in an external pressure environment between 100 kPa and 7 Pa (15 to 0.001 psi).

11. Vibration Characteristics - The flowmeter shall be capable of satisfactory operation in the following vibration - frequency envelope: ±1.2 mm (5 to 14 Hz), ±1 g (14 to 23 Hz), ±0.45 mm (23 to 90 Hz), and ±15 g (90 to 2 kHz).

12. Size and Weight - Because of space limitations associated with flight applications, the flowmeter shall fit within the cylindrical envelope outlined by the AN fitting nuts (MS-33656) associated with the nominal fuel line tube size for the flow range specified in paragraph 3 of Exhibit "B". A protrusion from the side of the flowmeter is acceptable but shall be no larger than a volume of the following dimensions: 3 fuel line tube diameters long, 2 fuel line tube diameters high, and 3/4 tube diameters wide. The maximum length of the flowmeter including end connections (see paragraph 19 of Exhibit "B") shall be 8 fuel line tube diameters. The maximum size of the signal conditioning, which may be located remotely from the flowmeter, shall be 1000 cm^3. The maximum weight of the flowmeter assembly including any required valves and manifolds (but not including signal conditioning) shall be 5 kg.

13. Material - Wetted parts of the flowmeter shall be compatible with the fuels listed above and at the pressures and temperatures listed above without suffering corrosion, brittleness, seal leakage, or other degrading properties.

14. Response - Time constant of the flowmeter shall not exceed 25 ms.

15. Failure mode - Because the safety of the aircraft is of paramount importance, any failure of the flowmeter shall not cut off fuel supply or otherwise interfere with proper engine performance.

16. Power - The flowmeter and signal conditioning (if required) shall operate on 28 V dc.

17. Output - The output (or outputs) of the flowmeter including signal conditioning (if required) shall be a voltage or frequency which is a single valued function of fuel mass flow or of quantities from which flow can be

computed. The output (or outputs) shall be compatible with digital processing techniques. The data processing of the output signal (or signals) is not considered part of this contract.

18. Pressure pulsations - The flowmeter performance shall be unaffected by maximum fuel line pressure fluctuations of ±2 percent of the fuel pressure for frequencies of fluctuations above 10 Hz.

19. Mounting and position sensitivity - The flowmeter shall have AN Series 37° male flared tube (MS-33656) end connections. Flowmeter performance shall be unaffected by changes in operating attitude.

20. Overrange capability - The flowmeter performance shall be unaffected after being subjected to a fuel flow of 125 percent of full scale.

21. Calibration - It is likely that insitu calibration of the flowmeter in the aircraft will not be done because of the complexity of such a procedure. However, the flowmeter, including identical flight fuel system upstream and downstream tubing sections, shall be calibrated as an assembly on a flow stand of sufficient precision to determine flowmeter accuracy.

TYPICAL CHARACTERISTICS OF AIRCRAFT DC POWER

Steady-State Voltage

During steady-state conditions, DC voltage will remain within the following limits:

DC Power Steady-State Limits

18-29.5 volts

Voltage Ripple

During steady-state conditions, the instantaneous DC voltage will not differ from the average DC voltage by more than 1.5 volts. Voltage fluctuations producing ripple may be either periodic or aperiodic. The ripple frequency will be no greater than 5000 cps.

Normal Transients

DC voltage during a normal transient will remain within the limits specified in Figure 10.1. In addition, voltage variations occurring on the DC system as a result of inductive load switching will be within the limits specified by Figure 10.2. Curve A of Figure 10.1 will apply unless otherwise specified. Switching transients per curve B of Figure 10.1 may be expected to occur up to 20 times in an hour. Transients per curve A of Figure 10.1 are less frequent, occurring during power transfer and occasionally during clearing of faults.

Abnormal Transients and Power Characteristics

During abnormal conditions, DC voltage will remain within the limits specified by Figure 10.3.

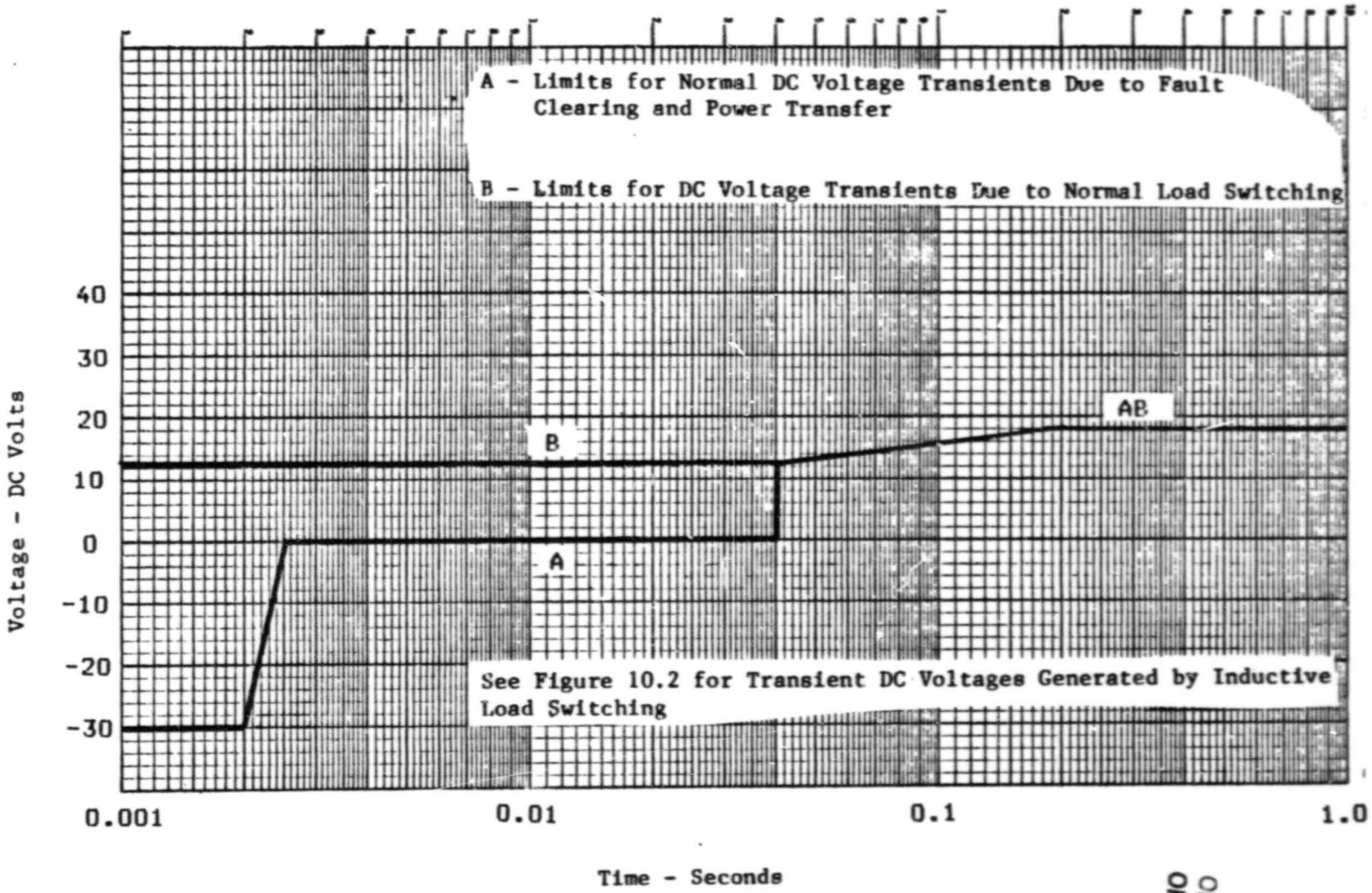

Figure 10.1 - Limits for Normal DC Voltage Transients

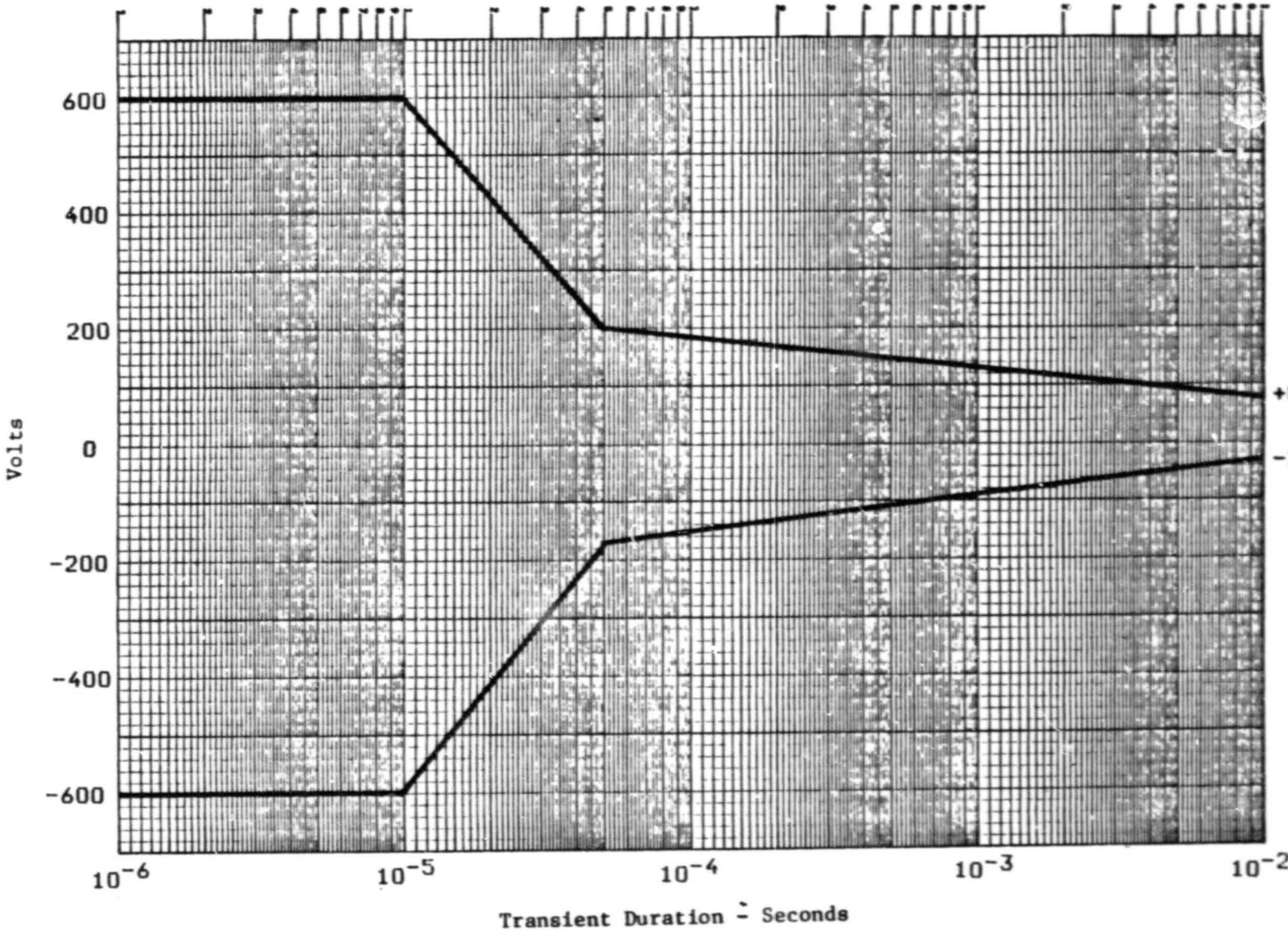

Figure 10.2 - Voltage Transient Duration Limits
(Inductive Load Switching)

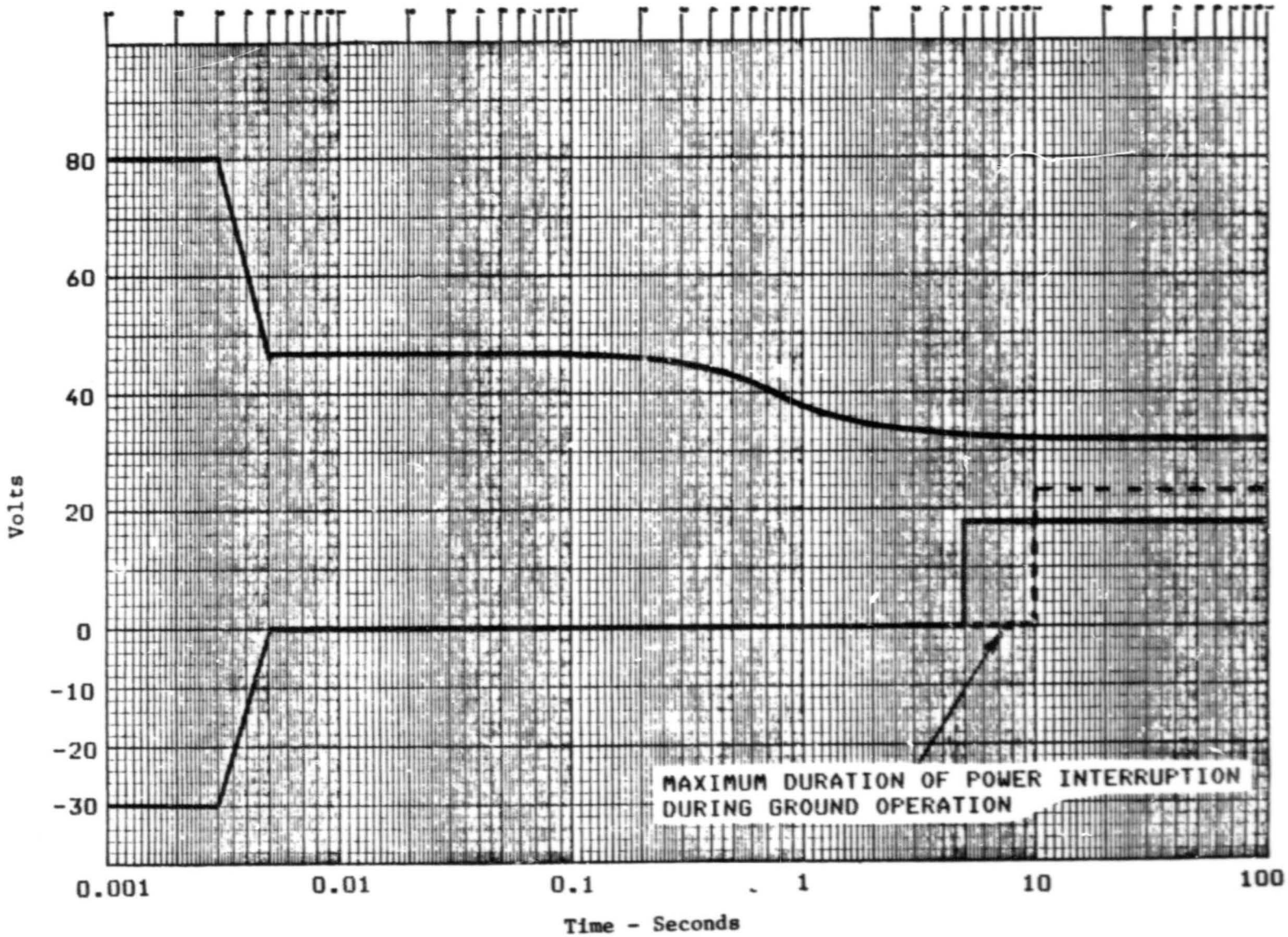

Figure 10.3 - Limits for Abnormal DC Voltage Transients

10.2 FLOWMETER TYPES AND EVALUATION

Flowmeter Type	Principle of Operation		Reasons Accept (A) /Reject (R)
I. "True" Mass Flow			
A. Momentum			
1. Angular	The torque required to change the angular velocity of a flow stream by a known amount is linearly proportional to the mass flow rate of the stream.	A	Accurate indication of mass rate of flow without density compensation.
a. Dual Element	Rotating upstream element imparts known angular velocity to fluid stream. Torque to return to zero angular velocity imparted at downstream stationary element. Various torque measuring schemes are:	-	Imperfect static balance of second element causes acceleration and position sensitivity.
i. Spring Re-strained	Spring deflection angle is measured by synchro, second harmonic pick-off, rotary transformer, position encoder, or time based pick-off.	R	Poor dynamic response relative to requirements.
ii. Closed Loop Torquer Re-strained	Electromagnetic torquer restrains turbine to null position. Current required to maintain null position is measure of mass flow.	A	Good dynamic response and linearity.
b. Single element	The torque required to angularly accelerate an irrotational flow stream to a known angular speed in a rotating impeller is measured.	-	Sensitive to upstream piping conditions. Poor time response.
i. Drive Power Measure-ment	The electrical power to drive the impeller is measured.	R	Sensitive to bearing and drive train torque.

Flowmeter Type	Principle of Operation		Reasons Accept/Reject
I. "True" Mass Flow (cont)			
ii. Reaction Torque Measurement	Reaction torque on drive gear train is measured through a spring deflection synchro system	R	Sensitive to bearing torque as well as acceleration effects (imbalance).
iii. Drive Spring Deflection	Impeller is driven through a spring, the deflection of which is a measure of drive torque. Time based optical or electromagnetic pickoff to detect angle.	A	Can be made insensitive to imbalance effects.
2. Transverse	A constant volume fluid stream is forced at right angles across another stream thereby causing a pressure drop on both. The injected stream pressure drop is proportional to the product of main stream mass flow and injected fluid volumetric rate.	R	Orifice characteristics affect calibration. Constant volume pump required to provide cross flow.
3. Oscillatory	The damping ratio of an oscillating (torsionally or linearly) spring-mass system with long straight passages through which the fluid stream passes is proportional to the fluid stream mass flow.	R	Strongly viscosity sensitive.
B. Hydrodynamic Lift			
1. Propeller	A propeller with variable pitch blades and a generator for its core is placed in the flowstream. Pitch angle is controlled so that angle of attack is held constant and generator drive torque is controlled to keep rotational speed constant. Power generated by the propeller is proportional to mass flow rate, independent of density.	R	Complex mechanization, lift coefficients vary with blade irregularities. Setting angle of attack is a complex algorithm of flow velocity.

Flowmeter Type	Principle of Operation		Reasons Accept/Reject
I. "True" Mass Flow (cont)			
2. Differential Turbine	Two turbines of unequal pitch angle are connected to each other through a torsional spring. The assembly is free to rotate. The deflection angle of the spring divided by assembly rotational speed is proportional to fluid stream mass flow.	R	Sensitivity to bearing friction.
3. Magnus Effect	A cylinder is rotated about its own axis which is at right angles to the flow stream. A lift force is generated at right angles to the flow and rotational axes which is proportional to mass flow and cylinder rotational speed.	R	Acceleration sensitive. Velocity profile sensitive.
C. Coriolis			
1. Rotating	Flow passes through a radially oriented passage which spins about an axis perpendicular to the flow passage. The coriolis force imparted by the fluid to the passage (and therefore torque to drive the passage) is proportional to the fluid stream mass flow.	R	Large radial distance and high speed required for good resolution. Large heavy package results.
2. Vibrational	A "u" shaped tube is vibrated about an axis in the plane of the u and perpendicular to its legs. The coriolis forces in each leg are in opposite directions perpendicular to the plane of the u and tend to warp it. Using time based optical pickoffs a time difference proportional to mass flow can be achieved (warp angle divided by vibration frequency).	R	Heavy base required for vibration system. Excellent for small flow rates. Vibration sensitive.

Flowmeter Type	Principle of Operation	Reasons Accept/Reject
I. "True" Mass Flow (cont)		
D. Orifice Bridge	A "wheatstone bridge" of 4 matched orifices is made with the main flow entering and exiting at opposite corners. A known small flow q is pumped between the remaining corners. The pump differential pressure is proportional to the product of q and mass flow rate	R Orifices must be identically matched. Cross flow must be precisely maintained. Orifice discharge coefficient which is non-linear with flow, enters equation with squared exponent. Very bulky due to need for positive displacement pump and parallel flow paths.
II. Volumetric		
A. Differential Pressure		R All Delta P types require density for scaling of pressure signal. Prohibitive delta P range.
1. Orifice	It is a small opening, usually round, through which the fluid flows, and is located in the main stream of a pipe channel. The pressure drop across the orifice is proportional to the square of volumetric flow rate.	R It needs long sections of upstream and downstream piping for accuracy and also the discharge coefficient is dependent on Reynolds Number
2. Venturi	It measures the static pressure difference between two points in a pipe. One point is located in the main stream and the second point is located at the converging conical section of the pipe. The pressure difference is proportional to the square of volumetric flow rate.	R Limited range and discharge coefficient depends on the Reynolds Number.
3. Nozzle	It works on the same principle as the orifice and venturi meters. The nozzle has a gradual contraction.	R It has poor performance at low range and its pressure drop recovery is very low.

Flowmeter Type	Principle of Operation		Reasons Accept/Reject
II. Volumetric (cont.)			
4. Pitot Tube	A pitot tube measures the difference between the static pressure and total pressure of a flow stream. This difference is proportional to the square of volumetric flow rate.	R	Point measurement. Profile sensitive. Prohibitive Delta P range.
5. Vortex Gradient	A vortex flow is established by tangential entry to cylindrical cavity. The radial pressure gradient is proportional to the product of density and the square of the volumetric flow rate.	R	Extreme pressure range. Potential for vapor phase at vortex core.
6. Elbow	The differential pressure between the inner and outer radii of an elbow is proportional to velocity head.	R	Prohibitive pressure range. Coefficient is Reynolds Number dependent and unpredictable in the transition region. Sensitive to upstream piping conditions.
B. Reaction Force			
1. Target	The force differential across a fixed target in the flow stream is measured by means of strain gauge or other force balance transmitter.	R	Measurement technique is very sensitive to vibration and this device is only good for point measurement in the flow tube.
2. Elbow	The reaction force on an elbow is proportional to velocity head.	R	Wide force range required. Acceleration sensitivity.
C. Fluidic			
1. Strouhal	A bluff body is placed across a fluid stream. Vortices are generated in the boundary layer on the body and shed into the downstream wake at regular intervals. The frequency of vortex shedding is proportional to the volumetric flow rate.	R	Limited applicable range and also requires long averaging time period for accuracy.

Flowmeter Type	Principle of Operation	Reasons Accept/Reject
II. Volumetric (cont.)		
2. Bistable	Fluidic oscillator type where flow is accelerated through a nozzle and the ensuing flow is caused to oscillate between two receiver ports by feedback paths which divert the flow exiting from the nozzle. The frequency of oscillation is proportioned to volumetric flow rate.	A No moving part, large dynamic range. R High pressure drop unless a part of flow is bypassed through oscillator; then flow division causes accuracy error. Requires fast response pickoff.
3. Vortex Precession	Fuel passes through a set of fixed blades at the inlet and produce a swirl to axial velocity ratio of (5 or 6): 1, and thus forms a free vortex core at the meter centerline. About three diameters down stream, the pipe expands (approx. 2:1 in area). This causes a flow reversal to form downstream, which in turn forces the vortex core off center and to attach to the wall at the point of area expansion. The vortex precesses around at a frequency proportional to volumetric flow rate. Diametrically opposed pressure sensors or heat transfer elements generate strong signals at the frequency of precession.	A Repeatability of ±.15% of rate is claimed for this technology in measuring gas volumetric flow rate, along with an operating range of 300:1 (Re) with linearity of ±10%. No moving parts is a distinct advantage for reliability. Entire flow cross-section is involved in vortex generation so the device is insensitive to inlet flow profile.
D. Ultrasonic	Sound frequencies of 100 KHz to 25 MHz are easily generated and detected by piezo-electric transducers in flow conduits. Various principles of operation are listed below.	R Basic techniques listed below measure flow velocity along a line and don't sample the entire flow profile and are thus limited in accuracy as the measured average velocity differs from the actual as the velocity profile changes.

Flowmeter Type	Principle of Operation		Reasons Accept/Reject
II. Volumetric (cont.)			
1. Delay Time	A set of transmitter/receiver transducers are fixed into opposing sides of the conduit inner surface and beam diagonally across a diameter at each other. Short duration, high frequency pulses are transmitted and received and the transit times are measured in each direction. The sum of upstream and down stream transit time gives speed of sound in fuel and the difference gives the fuel velocity.	R	Nanosecond accuracy of transit time measurement requires measurement of phase shift over the propogation path. This can be done in the laboratory, but is difficult to implement for in-flight use. Signal strength is good and no particle scatterers are needed in this scheme.
2. Doppler	A beam of ultrasound is focused at an angle 45 to 60° either upstream or downstream (or both). Particles or bubbles in the fuel reflect small amounts of energy shifted in frequency by the doppler effect. Frequency shift depends on fuel velocity, sound frequency, speed of sound in fuel and beam angle.	R	Particles of known size and concentration required for back-scatter. Low signal amplitude of back-scatter would not perform well in aircraft EMI environment.
3. Correlation	Ultrasound is transmitted diametrically across the pipe at two axial positions separated by a known distance. Passing fluid eddys modulate the upstream signal and a short time later modulate the down-stream signal. Fuel velocity is obtained by dividing the separation distance by the time between similar signal disturbances.	R	Correlation technique cannot provide precision required due to relative size of eddys and separation distances.

Flowmeter Type	Principle of Operation		Reasons Accept/Reject
II. Volumetric (cont.)			
E. Optical (also microwave)	Every optical method evaluates flow velocity at a point or line in the flow conduit from which overall volumetric rate is calculated: Q = Area x Vaverage	R	Each of the optical methods share common attributes which make them unsuited to this program: 1) Windows in the conduit are needed to pass light unobstructed. Operational life is severely limited by windows that may fog, ice, or discolor with varnish deposits. Also a safety concern exists if windows fracture. 2) Profile sensitive output. Sampling at one point or line is insufficient to provide acuracy better than 1%. 3) Particles in fuel. Particles of small know size (approximately 1 micron) and concentration are required by all of the methods. Seeding is not reliable and not recommended for flight use.
1. Doppler	Laser beams are heterodyned in a small volume in the flow, producing a fringe pattern of regularly spaced intensity. As particles pass through the pattern they reflect light which is collected optically and detected as a burst. Intensity during the burst varies at a frequency determined by fringe pattern spacing, wavelength and particle velocity. Flow velocity is calculated by averaging the frequency of a large number of bursts.	R	Size weight and electronics complexity of this technique are prohibitive.
2. Correlation	Reflected light from laser beams at two axial positions is correlated to determine the transit time of fluid in the axial direction.	R	High power required to operate lasers. The correlation technique cannot provide the required precision and time response because of the variations in eddy and suspended particle size and position and the inherent time lags.

Flowmeter Type	Principle of Operation		Reasons Accept/Reject
II. Volumetric (cont)			
3. Rotating Prism	Moving particles are viewed through a rotating prism. Rotational speed of the prism is adjusted so that the particles appear stationary. Prism speed and geometry determine the flow velocity.	R	Adjustment of prism speed to make particles stand still would be very cumbersome to mechanize.
H. Turbine			
1. Conventional	Propeller type (multi-bladed rotor) whose speed of rotation is proportional to fluid velocity.	A	Repeatable within .1%, proven reliability, plused output, less than 10 ms response.
		R	Susceptable to incoming swirl and viscosity changes.
2. Two-Rotor	Propeller type main turbine with additional down stream second, slower speed, counter rotating, sensor rotor whose function is to measure the slip in main turbine.	A	Eliminates swirl effect and minimizes viscosity effect; linearizes calibration curve.
I. Positive Displacement			
Zero Differential Pressure	A positive displacement pump with very low leakage is driven at a speed such that the sensed pressure differential across the pump is zero. Volumetric flow rate is proportional to pump speed.	R	Safety problem: if pump stops or runs at wrong speed, fuel flow will stop or very high pressures may build up.
J. Dilution			
1. Conductive 2. Radioactive	Identifiable contaminates are injected into the flow at known rates. Their down stream concentration is inversely proportional to volumetric flow rate.	R	Need accurately measured contaminant. Unsatisfactory for aircraft use.

Flowmeter Type	Principle of Operation		Reasons Accept/Reject
II. Volumetric (cont)			
F. Thermal			
1. Thomas Meter	A heater is located axially between two thermal sensors in the flow stream. At a fixed power input, the mass rate of flow is inversely proportional to the temperature difference between the sensors.	R	Calibration constant varies with fluid. Explosion hazard.
2. Tag Correlation	A pulse of heat is added to the fluid stream and detected downstream some time later. The time lag is inversely proportional to fluid velocity.	R	Poor response rate. Low resolution. Velocity profile sensitive. Explosion hazard.
3. Hot Wire/ Hot Film	The heat transfer coefficient from an electrically heated wire or film is a non-linear function of fluid mass flow (and other properties). For fixed fluid properties, the power required to maintain a constant sensor super heat is a known function of mass flow rate and velocity.	R	All of these techniques violate safety requirements for spark energy transfer to fuel (explosion hazard). Calibration constants are a function of fuel type (and even batch).
G. Electromagnetic			
1. Faraday	A conducting fluid passing through a magnetic field generates a voltage at right angles to both the field and flow axis.	R	Jet fuel is not a conductor.
2. Dielectric	The fluid stream passes between the plates of a capacitor. An alternating magnetic field is present perpendicular to both the flow axis and capacitor plates. The changing dipole moments in the fluid result in the accumulation of an anternating charge on the capacitor plates. The voltage generated is proportional to volumetric flow rate.	R	Sensitive to velocity profile. Very low signal levels are EMI sensitive. High input power required.

RELATED SENSORS - DENSITY AND VISCOSITY

Sensor Type	Principle of Operation	Reasons Accept/Reject
I Densitometer		
A. Displacement	When an object of known volume and density R is placed in a fluid, the buoyant force exerted on the object is the weight of the fluid that is displaced. Measurement techniques include level of floatation, balance of two objects with different densities.	Displacement densitometers were rejected due to positional and acceleration sensitivity.
B. Vibratory		
1. Fluid Immersed	The natural frequency of oscillation of a vibratory system in a fluid is a function of the density and viscosity of the fluid. By driving the system at a fixed phase angle between the driving function and the oscillatory motion, the effects of the fluid viscosity can be minimized and the frequency of vibration is then a function of density alone. By shifting the phase angle of the driving function between two values, the frequency shift observed is a function of viscosity of the fluid.	A The immersed vibratory densitometer was accepted as a viable design. The system has the potential of meeting .1% accuracy. Viscosity can also be determined by this densitometer.

Sensor Type	Principle of Operation		Reasons Accept/Reject
I. Densitometer (cont)			
2. Fluid Contained			
a. U-Tube	Fluid flows through a U-shaped tube. The U end of the tube is driven at its national frequency. The natural frequency is a function of the density of the fluid contained in the tube.	R	Sensitive to environmental vibration
b. Hoop	A straight section of tube is driven in its hoop mode of vibration (tube becomes egg shaped) the natural frequency is a function of the density of the fluid in the tube.	R	Rejected because the natural frequency is also a function of the mass flow in the tube and due to high driving power requirement.
C. Acoustic			
1. Acoustical Waveguide	Ultrasonic signals are sent through a waveguide submerged in a fluid. The velocity of the signals through the waveguide are inversely proportional to the density of the fluid.	R	Rejected due to poor accuracy.
2. Acoustic Impedance	Using piezoelectric crystals to send ultrasonic signals through a fluid the acoustic impedance of the fluid and the propagation velocity of a signal through the fluid are measured. These parameters will determine density by the equation. density = $\frac{\text{acoustic impedance}}{\text{propagation velocity}}$	R	Rejected due to poor accuracy and stability reported in literature.

ORIGINAL PAGE IS OF POOR QUALITY

Sensor Type	Principle of Operation		Reasons Accept/Reject
I. Densitometer (cont.)			
D. Correlation (Inference)			
1. Temperature 2. Speed of Sound 3. Dielectric	All correlation techniques of density determination measure a certain parameter of the fluid and infer the density using a predetermined relationship between the parameter being measured and the fluid density.	R	Rejected due to poor accuracy. The fuels to be measured by this device have varying relationships between density and other parameters.
E. Absorbtion of Radiation	Gamma radiation is directed through the fluid to be measured. The radiation is absorbed in proportion to the mass of the materials it passes through.	R	The repeatability of radiation densitometers has been reported to be excellent (0.01%) using long measurement times (5 sec.). This approach wasn't used due to size and weight requirements and lack of viscosity measurement capability.
F. Capacitance	The dielectric constant of a fluid is approximately proportional to its density.	R	The proportionality constant varies with fuel type and even between batches of the same type.
II Viscosity			
A. Direct			
1. Couette	Two concentric cylinders with a small annulus between them rotate at a relative angular speed. The viscous torque between the two cylinders is directly proportional to the absolute viscosity.	A	Applicable to continuous flow situation in a flowmeter. But it is susceptible to flow disturbances.
2. Capillary	Fluid flows through a capillary tube of known size. The time for a known quantity of fluid to pass through the tube is recorded. This time is proportional to the absolute viscosity.	R	Not a continuous measuring oevice and cannot be used in aircraft mass flowmeter application.

Sensor Type	Principle of Operation		Reasons Accept/Reject
II Viscosity (cont.)			
B. Vibratory (Damping)			
1. Beam/Vane 2. Tuning Fork	The degree of damping of a fixed-free or free-free oscillating spring mass system serves as a measure of fluid viscosity.	R	Both are sensitive to linear vibration in the aircraft environment.
3. Torsional	The degree of damping of a free-free oscillating torsional mass-spring-mass system serves as a measure of fluid viscosity.	A	In conjunction with a torsional vibrating densitometer viscosity may be obtained with sufficient accuracy with this approach. Torsional approach is not affected by linear vibration.
C. Acoustic Resonant Chamber	A helmholtz resonator operating in a highly overdamped mode provides accurate viscosity data.	R	Not suited to flight use because samples of fluid cannot be passed through the chamber easily, because of tight sealing.
D. Inferential	The viscosity can be very roughly inferred from a knowledge of fuel temperature and density.	R	Very strong dependence on fuel type and batch.

10.3 Sampling Error Analysis For Vortex Precession Flowmeter -

The vortex precession signal is assumed to jitter or oscillate randomly in frequency to a degree that requires filtering to recover inherent accuracy. Statistical and filter approaches are employed here to determine the filtering time required to obtain accuracy within a 0.10% of rate.

10.3.1 Statistical - Assumptions:

1) Jitter of fp is normally distributed about fp.

2) Standard deviation of jitter is 1.3% of fp.

Objective: find what number of samples, n, is needed to get 95% confidence that the mean, x, of the samples is within 0.10% of the true mean o.

Hypothesis: Ho: $\mu = \mu_0$

H1: $\mu \neq \mu_0$

Reject Ho if

$$Z_{\alpha/2} > Z > (1 - Z_{\alpha/2})$$

where $Z = \bar{x} - \mu_0 / \sigma/\sqrt{n}$

Or, accept Ho if

$$n \geq \left(\frac{\sigma Z_{\alpha/2}}{\bar{x} - \mu_0} \right)^2$$

For this investigation:

α = .05 so $Z_{x/2}$ = 1.96 (from table of normal distribution function)

σ = .013 (1.3% standard deviation)

$\bar{x} - \mu_0$ = .001 (0.1% error contribution)

Resulting in: n = 650, Required Sample Size

Time response at various flows is:

182 kg/hr , fp = 10 Hz, t(4) = 65 sec

9090 kg/hr , fp = 500 Hz, t(4) = 1.3 sec.

10.3.2 Filter Time Constant -

A stream of samples of fp in digital form can be likened to an analog voltage representation of fp, which can be filtered through a simple RC low pass filter to attenuate noise. The final implementation of the filter would of course be digital, but is more readily analyzed in analog form. Figure 1 shows a Bode plot of filter characteristics needed to fulfill the requirement of 0.1% permissible noise at fp, when the input noise is centered around fp in frequency at 1.3% amplitude. A single pole filter placed at .77 Hz provides the necessary 22.3 db attenuation at minimum flow rate (fp = 10 Hz). In steady state operation (no flow changes) the filtered output would meet desired accuracy with the given noise. A step change in flow (and fp) would require five time constants or 1.0 sec. to settle to the new output with insignificant error.

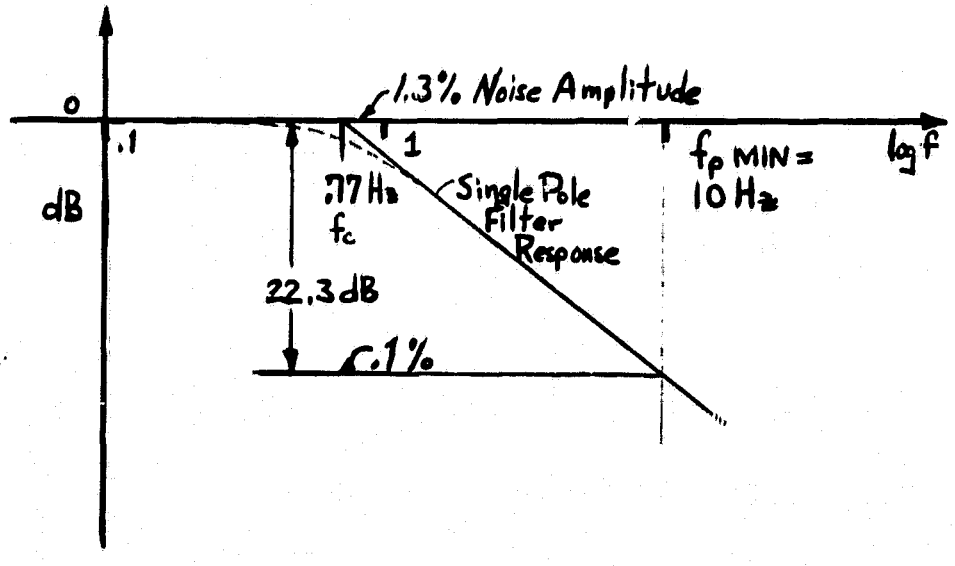

Figure 1 Single Pole Filter Response That Attenuates Jitter of fp

11.0 REFERENCES

1. Thompson, R. E. and Grey, J., "Turbine Flowmeter performance Model",J. Basic Engr., December 1970, pp. 712-722.
2. Rubin, M., Miller, R. W. and Fox, G. W., "Driving Torques In A Theoretical Model Of A Turbine Meter", J. Basic Engr., June, 1965, pp. 413-420.
3. Jepson, P. and Bean, P. G. "Effect of Upstream Velocity Profiles On Turbine Flowmeter Registration", J. Mech. Engr., Sci., Vol. 11, No. 5, 1969, pp. 503-510.
4. Lee, W. F. Z., Fisher, H. W. and Montag, D. R., "Development Of A Self Correcting and Self Checking Gas Turbine Meter", FLOW, Its Meaurement and Control In Science and Industry, Vol. 2, 1981, pp. 453-469.
5. Lee, W. G. Z., "A Study of Viscosity Effect and Its Compensation On Turbine - Type Flowmeters", J. Basic Engr., Sept. 1960, pp. 717-728.
6. Vonnegut, B., "A Vortex Whistle", J. Acoust. Soc. Am., 26, pp. 18-20.
7. U.S. Patent, 2,794,341.
8. Michelson, I., "Theory of Vortex Whistle", J. Acoust. Soc. Am., 27, 930,931 (1955).
9. Channaud, R. C., "Experiments Concerning the Vortex Whistle", J. Acoust. Soc. Am., 35, 953 (1963).
10. Channaud, R. C., "Observations of Oscillatory Motion in Certai Swirling Flows", J. Fluid Mech., 21, Part 1, pp. 117-127 (1965).
11. Channaud, R. C., Rodely, A. E., and White, D. F., "A Digital Flowmeter Without Moving Parts", A.S.M.E. technical paper No. 65-WA/FM-6 (1965).
12. Suzuki, M., "Theoretical and Experimental Studies on a Vortex Tube", Scientific Papers Of The Institute of Physical Chemistry Research, Tokyo, Vol. 54, No. 1, pp. 43-87 (1960).
13. Patent 3,279,251 including re-issue 26,410.
14. Bailey, J.S., "Two New Flowmeters Have No Moving Parts", Control Engr., Dec. 1969, pp. 73-77.
15. Krause, L. N., Fralick, G. C., "Miniature Drag Force Anemometer", Flow, Its Measurement and Control in Science and Industry, 2, pp. 117-130 (1981).
16. Landau and Lifshitz, "Fluid Mechanics", Pergamon Press, 1962, pp. 88-91.
17. Wenger, A. P., "Vibrating Fluid Densimeters: A Solution To The Viscosity Problem", IEEE Transactions On Industrial Electronics And Control Instrumentation, Vol. IECI-27, No. 3, August 1980, pp. 247-253.
18. U.S. Patent 4,177,669.

12.0 BIBLIOGRAPHY

Transverse Momentum

Li, Y. T., U.S. Patent 3,038,334, 1962.

Sipin, A. J., U.S. Patent 3,218,851, 1965.

Propeller

Goland, M., U.S. Patent 2,995,036, 1961.

Differential Turbine

Francisco, E. E., U.S. Patent 3,144,769, 1964.

Magnus Effect

Mason, H. L., U.S. Patent 2,896,450, 1959.

Rotating Coriolis

White, R. B., U.S. Patent 2,832,218, 1958.

Vibrational Coriolis

Plache, K. O., "Coriolis/Gyroscopic Flow Meter", ASME paper 77-WA/FM-4, 1977.

Orifice Bridge

Cheremisinoff, N. P., Applied Fluid Flow Measurement, Marcel Dekker, Inc., 1979, p. 136.

Differential Pressure Devices

Benedict, R. P., Fundamentals Of Temperature, Pressure, And Flow Measurements, John Wiley & Sons, New York, Second Edition, 1976.

Fluid Meters - Their Theory And Application, Report of ASME Research Committee on Fluid Meters, Sixth Edition, 1971.

Pitot Tubes

Streeter, U. L. & Wylie, E. B., Fluid Mechanics, Sixth Edition, McGraw Hill, 1975, Chapter 8, Section 2.

Elbow Meter

Hauptmann, E. G., "Take A Second Look At Elbow Meters For Flow Monitoring", Inst. Cont. Sys., Vol. 51, No. 10, pp. 47-49.

Vortex Shedding

Burgess, T. H., "Reliable Flow Measurement Using The Vortex Shedding Principle", presented at ISA conference, Oct. 1974.

Fluidic Oscillation

Ringwall, C., "A Wide Range No Moving Part Flowmeter", paper presented at ASME Fluidics Division winter annual meeting., N.Y., N.Y., December 5, 1976.

Ultrasonic

McShane, J. L., Ultrasonic Flowmeters, paper No. 2-10-214; symposium on: Flow, Its Measurement And Control In Science And Industry, Pittsburgh, 1971.

Watson, C. A., "Ultrasonic Flowmeters, Proceeding Of FLOMEKO, p. 571, 1978.

Malone, J. T., U.S. Patent 3,564,912, 1971.

Coulthard, J., U.S. Patent Re 28,686, 1976.

Yamamoto, M., U.S. Patent 3,237,453, 1966.

McShane, J. L., U.S. Patent 3,901,078, 1975.

Brown, A. E., U.S. Patent Re 28,929, 1976.

Laser Doppler

Durst, F., Melling, A. and Whitelaw, J. H., Principles And Practice Of Laser - Doppler Anemometry, Academic Press, New York, 1976.

Bates, C. J., "Flowrate Measurements Using A LDA/Computer Combination", Proc. of FLOMEKO 1978, Groningen, Neth., Sept. 11-15, 1978. North-Holland Publ. Co., New York, pp. 431-435, 1978.

Optical Correlation

Derevyanko, N. F., Latyshev, V. M., and Trokhan, A. M., "Investigating Flow Of Liquids By Means Of An Optical Correlation Method", English Translation of Izmeritel'naya Tekhnika, No. 4, pp. 34-36, April, 1969.

Rotating Prism

Kotas, T. J., LeFevre, E. J., "An Optical Technique For Measuring Velocity of A Fluid", J. Mech. Engr. Sci., Vol. 17, No. 2, pp. 65-70, 1975.

Dilution Techniques

Huang, Phelps, Hoffman, "A Theoretical Study of Quantitative Flow Measurements With Constant Infusion Of Short Lived Isotopes", Phys. Med. Biology, Vol. 24, No. 6, UCLA 1979.

Thermal Techniques

Los, J., U.S. Patent 3,187,569, 1965.

Cheremisinoff, N. P., Applied Fluid Flow, Marcel Dekker, Inc., N.Y., 1979.

Electromagnetic Flow Measurement

Rabeh, R., Baker, R. C., Hemp, J., "Induction Flow Measurement Theory For Poorly Conducting Fluids" Proceedings Of The Royal Society, London, A. 361, pp. 93-107 (1978).

Robinson, C. F., U.S. Patent 3,201,986, 1965.

Densitometers

A. Displacement

Ekman, L., U.S. Patent 3,994,174, 1976.

Lunstroth, K., U.S. Patent 4,136,551, 1979.

Reid, R., U.S. Patent 3,641,825, 1972.

B. Vibratory - Immersed

Menius, A. C. Jr., et. al., U.S. Patent 3,555,880, 1971.

C. Acoustic

Lynnworth, L. C., U.S. Patent 4,193,291, 1980.

Kritz, J., U.S. Patent 2,869,357, 1959.

D. Vibratory - Fluid Contained

Kratky, O., et. al., U.S. Patent 4,170,128, 1979.

Agar, J., U.S. Patent 4,217,774, 1980.

Agar, J., U.S. Patent 3,763,692, 1973.

Agar, J., U.S. Patent 3,983,744, 1976.

Stansfeld, J. W., U.S. Patent 4,007,627, 1977.

E. Correlation

Ishizaka, H., U.S. Patent 4,235,099, 1980.

Forster, E. O., Thomas, W. R., U.S. Patent 3,933,030, 1976.

F. Absorbtion Of Radiation

Shurtliff, R. W., "A Microprocessor - Controlled Scanning Densitometer System", Master's Thesis, University Of Idaho Graduate School, April 1980.

Kay-Ray Inc., Product Catalog, Model 3600 Density Systems

G. Capacitance

Lamphere, D. A., and Weitz, P. G., Jr., U.S. Patent 4,011,746, 1977.

Dunikowski, A., et. al., U.S. Patent 4,048,844, 1977.